PROGRESSIVE FAILURE ANALYSIS OF COMPOSITE PANELS

THESIS

Stephen Michael Spottswood, B.S.
Lieutenant, USAF

AFIT/GAE/ENY/99M-08

19990409 058

Disclaimer

The views expressed in this thesis are those of the author and do not reflect the official policy or position of the United States Air Force, the Department of Defense, or the United States Government.

PROGRESSIVE FAILURE ANALYSIS OF COMPOSITE PANELS

THESIS

Presented to the Faculty of the Graduate School of Engineering

of the Air Force Institute of Technology

Air University

In Partial Fulfillment of the

Requirements for the Degree of

Master of Science in Aeronautical Engineering

Stephen Michael Spottswood, B.S.

Lieutenant, USAF

Air Force Institute of Technology

Wright-Patterson AFB, Ohio

· March, 1999

PROGRESSIVE FAILURE ANALYSIS OF COMPOSITE PANELS

Stephen Michael Spottswood, B.S.

Lieutenant, USAF

Approved:
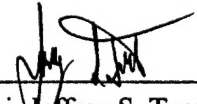
Anthony N. Palazotto

Dr. Anthony N. Palazotto
Committee Chairman

3/5/99
Date

Shankar Mall

Dr. Shankar Mall
Committee member

3/5/99
Date

Jeffrey S. Turcotte

Maj. Jeffrey S. Turcotte
Committee member

3/5/99
Date

Acknowledgments

First, and most importantly, I would like to thank my Lord and Savior Jesus Christ, who has provided me with the strength and fortitude to overcome sometimes seemingly insurmountable obstacles. With Jesus Christ as my crutch, I certainly can "...do all things".

Next, I would like to express my sincere appreciation to my faculty advisor, Dr. Anthony Palazotto, for his guidance and support throughout the course of this thesis effort. His insight, experience, patience and confidence were greatly appreciated. Dr. "P", you truly are a teacher. Equally important in the success of my endeavors were Dr. Nagesh Gummadi and Dr. Sam Naboulsi. Their experience in finite element analysis, programming and overall knowledge was generously and eagerly provided on numerous occasions. For that I thank you both. I would like to thank my sponsor, Dr. Steven Walker, AFOSR/NA, for both the support and latitude provided to me in this experience.

I would also like to express my appreciation to my father, Captain (Ret.) Stephen A. Spottswood, who has continually driven and supported his son - thanks Dad!. Finally, I would like to thank my wife, Rachel, and my daughter, Sidney Morgan, whose unwavering love, understanding, and sacrifice over the past eighteen months has been instrumental in my successful completion of this journey. The smile on my daughter's face every time I could take a break for "play-time" let me know that all was forgiven for the times when I could not leave my studies. Rachel, my nurturer, comforter and best friend, who was there for the good times and the difficult times, I thank you and I love you.

Table Of Contents

List of Figures

List of Tables

Abstract

The Air Force is interested in evaluating the performance of loading platforms that can be considered possible candidates for precision air drops. The objective of this research is to determine the physical response, including material failure, of a curved composite panel designed to resist transverse loading. The cause of the material failure, in the form of delamination, fiber and/or matrix failure, is determined through various criterion based on non-linear movement using a finite element analysis technique. The finite element analysis technique known as the simplified large displacement/rotation or SLR theory allows for large displacements but assumes small to moderate rotations. This technique characterizes a three dimensional shell structure in two dimensions, taking advantage of the small thickness relative to the shell span and width, thereby neglecting the direct transverse effects. Third order shell kinematics, defined relative to the datum or midsurface of the shell, allow for the characterization of in-plane and transverse shear effects, assuming small strain. This research initially investigated the accurate and applicable range of the SLR theory by examining the response of thin composite laminates under transverse loading. Data generated using the SLR theory both with and without the addition of progressive failure criteria, is compared with previously published experimental data, noting where the SLR theory diverges from the experimental results. The inclusion of various failure criterion, to include maximum stress, Lee, and Hashin, will provide a more realistic representation of the total physical response of the shell. The criterion are applied from initial loading, to first ply failure and further progressive composite failures. As the composite shell fails, the constitutive relations, or shell stiffness are reduced. Comparisons are also made between the SLR theory and various higher order finite element analysis

techniques. Once an approximate range of accurate physical representation is realized, progressive failure of composite sandwich shells under transverse loading are examined. Results in the form of load-deflection relations are examined, with particular attention paid to the location and type of first core failures. The physical response of both deep and shallow shells are examined with varying thicknesses to better understand the sensitivity of the SLR theory to those variables. Results of the analytic comparison with the published experimental data indicate that the SLR theory over-predicts the stiffness of the various shells for both the cases considering and not considering failure criteria. Analytic modeling is expected to result in less conservative results due to the assumption of ideal test conditions, uniform material properties and the simplifying assumptions made in the development of the SLR theory. Results generated for those cases incorporating a progressive failure criterion are slightly closer to the experimental data because of the reduced stiffness due to failure as deflection increases. Furthermore, matrix failure patterns predicted by all three criterion were similar to the experimental results. Results also indicate asymmetrical deformation modes as a result of failures. Core failures predicted in the composite sandwich analysis were similar between the failure criterion. However, results indicate that the facesheets are the dominating factor in the reduction of stiffness, as seen in the load-deflection response curves.

PROGRESSIVE FAILURE ANALYSIS OF COMPOSITE PANELS

Chapter 1 - Introduction

1.1 Motivation

As the use of sandwich composite material increases in the aerospace industry, understanding the physical response to loading is critical. ASTM defines a sandwich material as, "...a combination of alternating dissimilar simple or composite materials, assembled and intimately fixed in relation to each other so as to use the properties of each to specific structural advantages for the whole assembly" [33]. Sandwich composites are widely regarded for their high strength-to-weight-ratio, thus making them viable alternatives to isotropic as well as standard composite aerospace materials. Sandwich composites are assembled by bonding two highly dense composite laminate facesheets to a thick, low density core material. Due to the low density core, a large increase in the cross-sectional thickness results in a large increase in stiffness but only a marginal increase in weight. For example, doubling the thickness of the core of a typical graphite-epoxy sandwich composite will result in a seven fold increase in stiffness, while only a three percent increase in weight. Quadrupling the thickness of the same material will increase the stiffness by a factor of 39 times, while only increasing the weight six percent [39].

A sandwich composite material reacts to loading in the same manner as an I-beam. The composite facesheets act as the I-beam flanges, resisting both the applied and bending loads. The sandwich core, acting as miniature columns, resists transverse tension, compression and shear as well as panel buckling [33], [39]. The result is a relatively light-weight yet stiff, thick material. The

1

nature of the sandwich construction is attractive to the aerospace industry, where bending resistance and weight savings are of the utmost importance. However, sandwich construction is not new to the aerospace community. Great Britain designed and built the DeHavilland Mosquito World War II aircraft, using a plywood over balsa sandwich construction. The result was a relatively light, inexpensive, fast and incredibly successful medium bomber. So successful was the Mosquito, that their attacks became known as "Mosquito bites" and Hermann Goering, Luftwaffe Chief, wondered why he was never provided a German equivalent [2].

1.2 Background

With the advent of powerful computing technology, there has been a rapid increase in the mathematical modeling of composite plates and shells. Unlike isotropic materials, sandwich composites typically have a complex response to loading. As an example, an isotropic material's load-displacement response is linear until material yielding is reached. This yield point is typically close to the material failure point. In most if not all engineering problems considering isotropic materials, properties, such as Young's modulus, shear modulus and Poisson's ratio, are therefore assumed constant throughout this linear elastic region. On the other hand, a composite material will transition through multiple material response phases. As the composite undergoes increased loading, failures will occur as various points in the material reach their respective failure limits. These lamina failures change the characteristics of the material, resulting in a change in the material response. Assuming constant material properties in this case would only be appropriate within each linear portion of the material response curve, or in between the various material failure points. While only a simple example, it is obvious that the physical response of composite construction is complex, and it is of the utmost importance to determine where the material properties change and what those changes are.

The strength characteristics or load carrying ability of the material after it undergoes the first material failure and before final material or ultimate lamina failure is of great importance in the study of composites. There are three distinct macromechanic modes of failure associated with composite materials; fiber breakage, matrix cracking and delamination between plies. Fiber breakage occurs when the applied loading exceeds the maximum longitudinal strength of the specific fiber material. Similarly, matrix cracking occurs when the applied loading exceeds the strength of the matrix material. Delamination is a highly complex phenomenon and can occur in three forms. Delamination can occur as peeling or opening, a direct result of loading normal to the lamina. Delamination can also occur as ply shearing or tearing [6]. The inclusion of the sandwich core only increases the difficulty of capturing the material response to loading. Depending on the layup of the composite, lamina failure can occur individually or as a combination of all three of the previously mentioned forms.

Composite materials, due to the nature of multidirectional layups, may not fail completely when one or more laminas reach the material threshold. This underscores the importance of studying the progressive nature of composite laminate failure. Unlike an isotropic material, whose response can often be assumed linear until failure, a sandwich composite can continue to withstand significant loading long after the first ply failure. This first ply failure, analogous to the yield stress in an isotropic material, occurs when that lamina within the composite first reaches its respective failure limit due to the lowest applied external load. The ability of the material to withstand loading after first-ply-failure depends upon the nature of the multidirectional laminate layups. Consequently, this first-ply-failure will result in a change in the material constitutive relations, reducing the stiffness of the sandwich. This process continues until final-ply-failure, and the composite fails completely. As an example, consider two AS4-3501-6 graphite-epoxy composite center loaded arches, modeled using a higher order large displacement and large rotation finite element method.

3

The two specimens differ only in their ply layup, one in a [0/90/90/0] configuration and the other in a [90/0/0/90] configuration [12]. Because the specimens were arches, the problem is essentially one dimensional, with the arches behaving as beams. Both specimens experienced a transverse concentrated load applied at their respective centers. For the [0/90/90/0] layup, first ply failure occurred in the form of matrix cracking in the inner layers, shown as point A_1 in Fig. 1. Although final failure did not occur for this specimen, note the static instability experienced by the arch at a nondimensionalized load and displacement of 1100 and 20 respectively. From first ply failure to
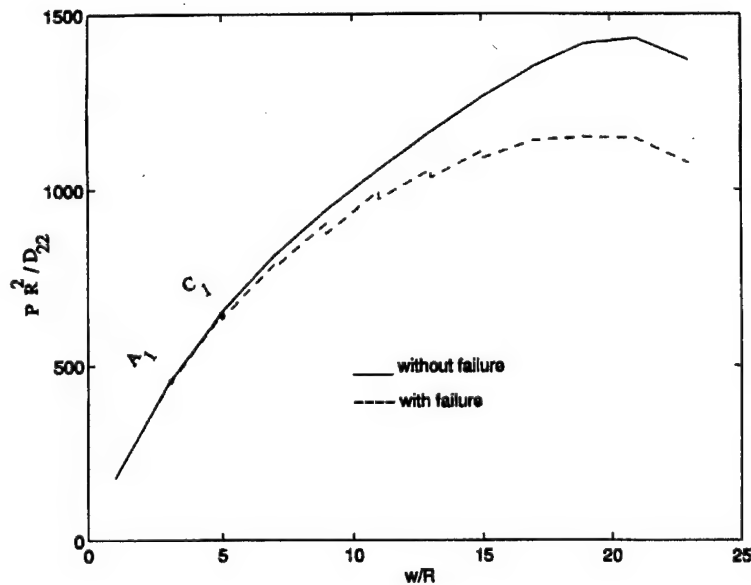
Figure 1. Load deflection characteristics of (0/90/90/0) layered shell with failure

the static instability, the load deflection curve experienced several changes in slope as failures occurred, resulting in a 20% reduction in stiffness at the instability point. In contrast, a center loaded arch made of the same material, but in a [90/0/0/90] configuration, experienced a completely different failure response as shown in Fig. 2. First ply and final ply failure occur at the same point, shown as A_2 and C_2 in Fig. 2. First ply failure occurred in the form of fiber breakage in the outer layers and final ply failure occurred in the form of matrix failure of the inner layers. The arch failed at a

4
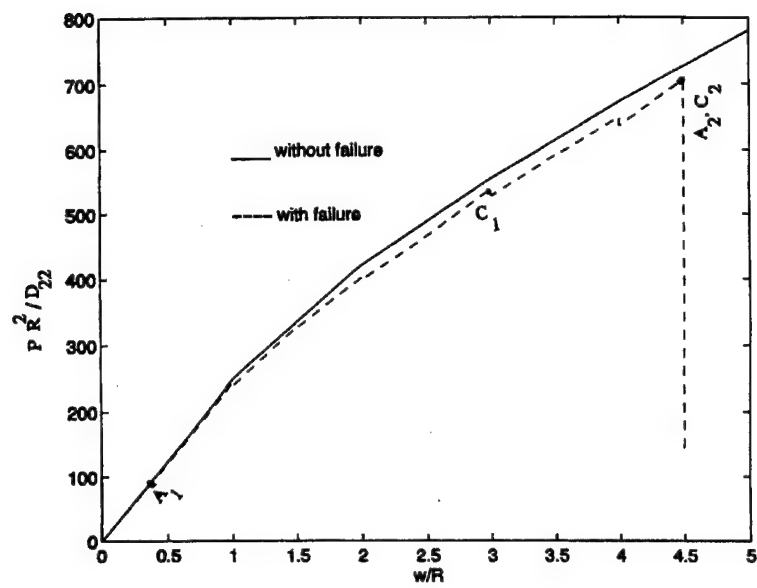
Figure 2. Load deflection characteristics of (90/0/0/90) layered shell with failure

nondimensionalized load of 700 and a maximum nondimensionalized tip deflection of 4.5. Because both first and final ply failure occurred at the same point, there was no significant change in the load deflection curve. The ability of the [0/90/90/0] composite layup to continue to withstand loading long after first ply failure, should again underscore the complex nature of a sandwich composite material and the importance of determining the physical response throughout a loading scenario.

1.3 Objective

The objective of this research is to examine and understand the physical response of a cylindrical composite and sandwich composite shell under quasi-static transverse point loading. Determining the physical response will include an analysis of the progressive damage during various loading scenarios. A third-order finite element analysis method will be utilized to model the cylindrical sandwich panels. The third-order theory models both geometric nonlinearities as well as transverse shear effects with strain continuity. Progressive damage will be analyzed through the inclusion of various failure criteria within the computer code. As a result of failure, the appropriate material stiffness properties will be reduced. The inclusion of the failure criteria will allow for the identification of the failure mode as well as the location of the failure.

1.4 Approach

The intent of this research was twofold. Initially, the purpose of the research was to gauge the accuracy and applicability of the existing higher-order finite element analysis code. The accuracy of the code refers to the precision of the results generated, and therefore the relative merits placed upon those results. The applicability refers to the shell modeling conditions allowed for by the theory utilized within the finite element code. Failure criteria was not included in this portion of the analytical investigation. Once the accuracy and applicability of the code was established, the effects of progressive ply damage were included.

6

The accuracy and applicability of the code was examined through a comparison of published experimental test data [44] with results generated using the existing finite element code. The experimental data included composite cylindrical shells under a quasi-static transverse center load. Various composite shell configurations were considered, however an exhaustive comparison effort was not undertaken. In other words, only sample shell configurations meant to represent extreme cases were modeled using the finite element code. Of primary concern were the effects of shell thickness and cylindrical radius on the total physical response. The finite element theory makes several assumptions concerning transverse shear and direct transverse effects.

The shell radius and span determine whether or not a cylindrical shell is shallow or deep. Shallow cylindrical shells tend to approach the physical response seen in plates. In other words, the load displacement response tends to remain linear until various failures are reached. Deep shells undergo large rotations and tend to exhibit extreme changes in the load displacement response due to the buckling phenomenon known as "snapping". Again, the theory utilized within the finite element code makes a simplifying assumption concerning the rotations exhibited by the shell. The effects of rotation were therefore examined by varying the radius of the specimen and comparing the results with experimentation [44].

Progressive damage in cylindrical composite and sandwich composite shells was examined through the use of several widely used failure criterion. These criterion were incorporated into the finite element code resulting in several significant abilities. Both the type and location of failure were monitored during the load history. Therefore, the first-ply-failure as well as further failures were determined. As mentioned previously, as the aerospace community increasingly incorporates composite and sandwich composite materials into critical structures, it is crucial that both the type and location of failures are determined. Due to the progressive nature of the analysis, the appropriate material constitutive relations were modified as failure occurred. The effects of

7

asymmetry due to failure were also accounted for through the addition of the appropriate elasticity arrays.

1.5 Overview

Chapter 2 presents the appropriate background necessary to accomplish this research. The SLR theory utilized in the finite element code is presented in detail. Topics covered include the SLR assumptions utilized, the resulting shell kinematics, and the conversion of the mathematical shell relations into finite element form. Next, the failure criterion utilized and a brief review of the analysis undertaken by the author are reviewed. Finally, a literature survey of both the various types of failure criterion and the methods used to model progressive failure in concert with finite element analysis is presented. The review of progressive failure analyses includes composite modeling and assumptions.

Chapter 3 includes a review of the additions made to the program. A review of the tangent stiffness relations and the method used to formulate the relations into the desired format. Also included, are the failure criterion and the resulting changes made to the constitutive relations. The final form of the progressive failure additions will be discussed as well as the reasonings and assumptions used to reach the final configuration. Also covered are the allowances and assumptions made for the sandwich core analysis.

Chapter 4 includes the results and a discussion of the analysis. Initially, the various methods, assumptions and configurations used in the analysis will be reviewed. Topics include finite element convergence, boundary conditions and symmetry or asymmetry of the shell structures. The analysis covers both the results of the initial investigation into the accuracy and applicability of the premodified code investigating composite shells and the results of the progressive failure analysis

of composite and sandwich composite shells. The results of the composite shell analysis are compared to a commercial finite element package and experimental results.

Chapter 5 presents the conclusions and a brief summary.

Elasticity relations, to include the general strain-displacement relations and the strain-displacement relations in terms of cylindrical coordinates are included in Appendix A. Appendix B presents one of the input files used to generate the changes to the elasticity arrays. Appendix C includes a guide to the SLR program and a sample input deck for reference, and Appendix D includes the STRESS subroutine, where the majority of changes were made with respect to the progressive failure analysis.

Chapter 2 - Theory and Background

Current finite element modeling has allowed researchers to determine the physical response of composite and sandwich composite shells with ever increasing accuracy. The inclusion of failure criteria has further increased the accuracy of the results by providing the researcher both the failure modes and the location of failure in composite and sandwich composite shells under load. The scope of this research was not to focus on the theory of various finite element methods, but to incorporate a progressive failure approach to a preexisting finite element code and report on the results. Therefore, the background material will cover the theory used to develop the existing code, a brief review of the various forms of failure criteria, and an overview of the past as well as current literature documenting methods and results of finite element codes with failure criteria incorporated. As the focus of this research is the addition of "progressive" failure criteria, or that criteria which continues to analyze the structure after first-ply-failure, the majority of the literature review will cover those articles addressing progressive criteria. For the sake of completeness, however, articles addressing codes utilizing first-ply-failure criteria will be reviewed briefly.

2.1 Simplified Large Displacement & Rotation Theory

This research used a pre-existing finite element code known as the Simplified Large Displacement and Rotation Theory, or SLR theory developed by Palazotto and Dennis [27]. The theory was developed in an effort to account for the through-the-thickness shear flexibility associated with the physical response of shell structures. Like a plate, a shell is characterized by a relatively small thickness as compared to the shell radius and span. The shell, however, is slightly more complex in that it is typically defined in curvilinear coordinates. By taking advantage of the small thickness, the three dimensional physical response of the shell was characterized in two dimensions or

10

the in-plane dimensions. The transverse shear effects were defined with respect to the midsurface or datum of the shell.

Due to the relatively small shell thickness, early theories completely neglected all transverse shear effects. While greatly simplifying the analysis, this resulted in limited application. Transverse shear effects are important in the study of shell structures for several reasons. Actual composite or laminated shells tend to deflect more under the influence of a transverse load than that predicted by those theories which neglect transverse shear effects and consider only the effects of in-plane stress and strain. Transverse shear also has a greater effect in laminate shell structures than in comparable isotropic shells. With the increasing use of composite and sandwich composite shell structures in the aerospace community, the over simplified theories are not adequate in their portrayal of the physical response of a laminate shell. Finally, as the shell thickness increases, the effect of transverse shear increases as well. Sandwich construction is inherently thicker than laminate shells, again, greatly increasing the need for a method to accurately model those structures.

It should be noted that the purpose of this research was not to redefine nor rederive the SLR theory in its entirety. The SLR theory is described in great detail in Ref. [27]. Only those topics which will provide a basic understanding of the SLR theory and the methodology used to characterize finite element modeling of shell structures will be reviewed. Therefore, in an effort to aid in the understanding of the SLR theory and provide the necessary background, the following subject areas will be briefly discussed; SLR assumptions, the unique kinematic and strain relations defined relative to the midsurface or shell datum, the stress-strain relations related through the generalized Hooke's Law, also known as the constitutive relations, the principals of virtual work and potential energy resulting in the appropriate equilibrium Eqns., and finally, the finite element analysis method used to solve the resulting equilibrium Eqns.. The finite element analysis review will include a discussion of the appropriate load-displacement relations and their unique form when considering

11

composite laminates, the degrees of freedom associated with a shell structure element defined in curvilinear coordinates, and the element shape functions. Unless otherwise noted, all developments related to the SLR theory were taken from Ref. [27].

2.1.1 SLR Assumptions

With the increased use and popularity of powerful computers, finite element modeling (FEM) is fast becoming the method of choice in the analysis of structures. Likewise, FEM and the theories used to develop finite element codes are increasing in sophistication. However, that increased sophistication comes at a price. While results continue to improve and the structures modeled continue to grow more and more complex, simplifications are required to allow for realistic computing and analysis time. Modeling composites, even relatively simple shells, can require extensive computing time, due to mesh refinement, the number of composite plies, and the number of degrees of freedom associated with each node. Therefore the following simplifications and/or methods were made in the development of the SLR theory. 1) Geometric nonlinearity is considered, while material linearity is assumed. Material linearity assumes the material stress-strain behavior remains linear, i.e., prior to yielding. Geometric nonlinearity allows for large displacements and small to moderate rotations. 2) The shell thickness is always considered relatively thin. Because of this assumption, the in-plane stress-strain effects will dominate the response. 3) The transverse direct stress, or σ_3, is assumed negligible. An in depth discussion on this topic can be found in [27]. 4) Transverse shear strains, ε_4 and ε_5, and therefore the transverse shear stresses, are parabolic through the thickness and vanish at the top and bottom surfaces. 5) The in-plane strains are represented by the Green's strain relations in their entirety, while the transverse shear strains are represented by the linear Green's strain terms only. This last assumption concerning the transverse shear strains, results from the relative thinness of the shell thickness, and of the dominate response of the in-plane

12

effects. 6) The governing shell relations were developed in the Lagrangian or the original coordinate system. Therefore the Green's strain tensor and corresponding 2nd Piola-Kirchhoff stress tensor are used exclusively. The calculated strains are assumed small, therefore no conversion was made between 2nd Piola-Kirchhoff and Eulerian Stresses. 7) The shell lamina are considered transversely isotropic.

The simplifying assumption concerning ε_4 and ε_5, or the use of the linear portion of the Green's strain terms, result in the compatibility Eqns. not being satisfied. For small rotations, the compatibility relations are better approximated, and for linear analysis, where the rotations and displacements are small, the compatibility relations are directly satisfied. Therefore, for general larger displacement and rotation scenarios, the transverse shear effects are not exact. However, because of the use of higher order kinematic relations and the entire Green's strain relations for in-plane effects, the mid-surface or shell datum load-displacement results are assumed to be accurate and will model the important shell collapse or buckling characteristics.

2.1.2 Kinematics and Strain Developments

Referencing Fig. 3 for convention, the following kinematic relationships were developed by Palazotto and Dennis [27] for an arbitrary shell geometry:

$$u_1 (\xi_1, \xi_2, \zeta) = u (1 - \zeta/R_1) + \zeta\psi_1 + \zeta^2\phi_1 + \zeta^3\gamma_1 + \zeta^4\theta_1$$

$$u_2 (\xi_1, \xi_2, \zeta) = v (1 - \zeta/R_2) + \zeta\psi_2 + \zeta^2\phi_2 + \zeta^3\gamma_2 + \zeta^4\theta_2$$

$$u_3 (\xi_1, \xi_2) = w \tag{1}$$

where ξ_1, ξ_2, and ζ are the respective curvilinear coordinates, R_α are the respective radii of curvature, ψ_α are the rotations of the normals, ϕ_α, γ_α, θ_α are unknown coefficients determined by forcing

13

the transverse shear stresses to zero at the top and bottom surfaces of the shell, and u, v, and w are the associated datum or midsurface displacements as shown in Fig. 3, [27]. The following Eqns.
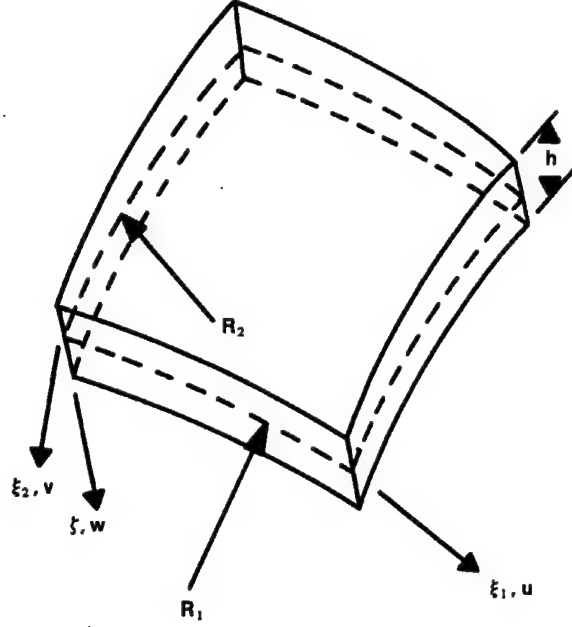
Figure 3. Surface and shell coordinate system.

are the Green's strain relations for transverse shear in curvilinear coordinates taken from Ref. [36]:

$$
\begin{aligned}
\gamma_{13} &= \frac{1}{2}\left(h_3\frac{\partial u_3}{\partial y_1} + h_1\frac{\partial u_1}{\partial y_3} - u_1\frac{\partial h_1}{\partial y_3} - u_3\frac{\partial h_3}{\partial y_1}\right) \\
&\quad + \frac{1}{2}\left(\frac{\partial u_1}{\partial y_3} - \frac{u_3}{h_1}\frac{\partial h_3}{\partial y_1}\right)\left(\frac{\partial u_1}{\partial y_1} + \frac{u_3}{h_3}\frac{\partial h_1}{\partial y_3} + \frac{u_2}{h_2}\frac{\partial h_1}{\partial y_2}\right) \\
&\quad + \frac{1}{2}\left(\frac{\partial u_3}{\partial y_1} - \frac{u_1}{h_3}\frac{\partial h_1}{\partial y_3}\right)\left(\frac{\partial u_3}{\partial y_3} + \frac{u_1}{h_1}\frac{\partial h_3}{\partial y_1} + \frac{u_2}{h_2}\frac{\partial h_3}{\partial y_2}\right) \\
&\quad + \frac{1}{2}\left(\frac{\partial u_2}{\partial y_1} - \frac{u_1}{h_2}\frac{\partial h_1}{\partial y_2}\right)\left(\frac{\partial u_2}{\partial y_3} - \frac{u_3}{h_2}\frac{\partial h_3}{\partial y_2}\right) \qquad (2a) \\
\gamma_{23} &= \frac{1}{2}\left(h_3\frac{\partial u_3}{\partial y_2} + h_2\frac{\partial u_2}{\partial y_3} - u_2\frac{\partial h_2}{\partial y_3} - u_3\frac{\partial h_3}{\partial y_2}\right) \\
&\quad + \frac{1}{2}\left(\frac{\partial u_2}{\partial y_3} - \frac{u_3}{h_2}\frac{\partial h_3}{\partial y_2}\right)\left(\frac{\partial u_2}{\partial y_2} + \frac{u_3}{h_3}\frac{\partial h_2}{\partial y_3} + \frac{u_1}{h_1}\frac{\partial h_2}{\partial y_1}\right) \\
&\quad + \frac{1}{2}\left(\frac{\partial u_3}{\partial y_2} - \frac{u_2}{h_3}\frac{\partial h_2}{\partial y_3}\right)\left(\frac{\partial u_3}{\partial y_3} + \frac{u_2}{h_2}\frac{\partial h_3}{\partial y_2} + \frac{u_1}{h_1}\frac{\partial h_3}{\partial y_1}\right)
\end{aligned}
$$

14

$$+\frac{1}{2}\left(\frac{\partial u_1}{\partial y_2}-\frac{u_2}{h_1}\frac{\partial h_2}{\partial y_1}\right)\left(\frac{\partial u_1}{\partial y_3}-\frac{u_3}{h_1}\frac{\partial h_3}{\partial y_1}\right) \tag{2b}$$

where h_α are the scale factors, and for cylindrical coordinates, y_1, y_2 and y_3 are described by the cylindrical variables, r, θ, and z respectively. The physical strains can then be calculated using the following Eqn. [27]:

$$\varepsilon_{ij} = \frac{\gamma_{ij}}{h_i h_j} \tag{3}$$

Using only the linear components of Eqn. 2a, and solving for the physical strains using Eqns. 1 and 3, the following relations for the transverse shear strains result:

$$\varepsilon_4 = \frac{1}{h_2}\left(u_{3,2}+h_2 u_{2,3}-u_2 h_{2,3}\right)$$

$$\varepsilon_5 = \frac{1}{h_1}\left(u_{3,1}+h_1 u_{1,3}-u_1 h_{1,3}\right) \tag{4}$$

If one substitutes Eqn. 1 into Eqn. 3, forces the transverse shear strains to be zero at the top and bottom shell surfaces, and solves for the appropriate coefficients, the results become the following third order general shell kinematics:

$$u_1\left(\xi_1,\xi_2,\zeta\right) = u\left(1-\zeta/R_1\right)+\zeta\psi_1+\zeta^3 k\left(\psi_1+\frac{w_{,1}}{\alpha_1}\right)$$

$$u_2\left(\xi_1,\xi_2,\zeta\right) = v\left(1-\zeta/R_2\right)+\zeta\psi_2+\zeta^3 k\left(\psi_2+\frac{w_{,2}}{\alpha_2}\right)$$

$$u_3\left(\xi_1,\xi_2\right) = w \tag{5}$$

15

where $k = -4/(3h^2)$, h is the shell thickness, $w_{,\lambda}$ refer to the differentiation or slopes of the respective axes, and α_λ are calculated from elements of the surface metric tensor, used in the transformation between the Cartesian and cylindrical coordinate systems characterizing the shell's curvature. For further detail on curvilinear coordinates see Ref. [36]. In the expressions for u_1 and u_2, the ψ_λ terms which are multiplied by ζ represent the rigid body rotation of the shell's cross-section. The terms in the expressions for u_1 and u_2, which are multiplied by ζ^3 represent the "shear rotation" of the shell's cross-section, or β_i, i.e. $\beta_1 = (\psi_1 + w_{,1}/\alpha_{,1})$. β represents the rotation in which a normal to the shell cross-section no longer remains normal after deformation. In other words, the shear rotation allows for the calculation of varying transverse shear strains. The algerbraic summation of β and ψ_λ results in $w_{,\lambda}$. For small rotations, this is an accurate assumption, however, as the rotations become larger, the assumption loses accuracy and the shell behaves stiffer than in reality. Kinematics that do not allow for shear rotation, resulting in constant transverse shear strains, require a shear correction factor to address the associated error. It should be pointed out that the SLR FEM approach produces a through-the-thickness strain continuity. The by-product of this continuity is to produce in a general composite layup a transverse shear stress function which is discontinuous. The approach of assuming strain continuity is an approach which allows for the inclusion of transverse strain without undue analytic development.

With the kinematic expressions of Eqn. 5, the strain relationships can be developed. Inserting Eqn. 5 into Eqn. 4, and neglecting the third-order terms, results in the following expressions for transverse shear strain in contracted notation:

$$
\begin{aligned}
\varepsilon_4 &= \frac{1}{h_2}\left(w_{,2} + \alpha_2\psi_2\right)\left(1 - \frac{4\zeta^2}{h^2}\right) \\
\varepsilon_5 &= \frac{1}{h_1}\left(w_{,1} + \alpha_1\psi_1\right)\left(1 - \frac{4\zeta^2}{h^2}\right)
\end{aligned}
\tag{6}
$$

16

Similarly, the in-plane strain relations, are found by solving the Green's strain-displacement relations found in [27] and [36], using Eqn. 5. These in-plane strain relations in cylindrical coordinates, derived in [27], can be found in Appendix A1. The 18 displacement terms for the previously mentioned strain relations are as follows:

$$d^T = \left(u \; u_{,1} \; u_{,2} \; v \; v_{,1} \; v_{,2} \; w \; w_{,1} \; w_{,2} \; w_{,11} \; w_{,22} \; w_{,12} \; \psi_1 \; \psi_{1,1} \; \psi_{1,2} \; \psi_2 \; \psi_{2,1} \; \psi_{2,2} \right) \qquad (7)$$

where the u term was added for completeness even though it is not included in the strain-displacement relations of Appendix A2.

2.1.3 Stress-Strain Relations

The stress-strain or constitutive relations for an orthotropic material in contracted notation, are as follows [6]:

$$
\begin{bmatrix} \sigma_1 \\ \sigma_2 \\ \sigma_3 \\ \sigma_4 \\ \sigma_5 \\ \sigma_6 \end{bmatrix} =
\begin{bmatrix}
C_{11} & C_{12} & C_{13} & 0 & 0 & 0 \\
C_{12} & C_{22} & C_{23} & 0 & 0 & 0 \\
C_{13} & C_{23} & C_{33} & 0 & 0 & 0 \\
0 & 0 & 0 & C_{44} & 0 & 0 \\
0 & 0 & 0 & 0 & C_{55} & 0 \\
0 & 0 & 0 & 0 & 0 & C_{66}
\end{bmatrix}
\begin{bmatrix} \varepsilon_1 \\ \varepsilon_2 \\ \varepsilon_3 \\ \varepsilon_4 \\ \varepsilon_5 \\ \varepsilon_6 \end{bmatrix}
\qquad (8)
$$

where the $C'_{ij}s$ are the components of the stiffness matrix, relating stress to strain. Assuming an approximate state of plane stress, i.e., neglecting the effects of σ_3, results:

$$
\begin{bmatrix} \sigma_1 \\ \sigma_2 \\ \sigma_6 \\ \sigma_4 \\ \sigma_5 \end{bmatrix} =
\begin{bmatrix}
Q'_{11} & Q'_{12} & 0 & 0 & 0 \\
Q'_{12} & Q'_{22} & 0 & 0 & 0 \\
0 & 0 & Q'_{66} & 0 & 0 \\
0 & 0 & 0 & Q'_{44} & 0 \\
0 & 0 & 0 & 0 & Q'_{55}
\end{bmatrix}
\begin{bmatrix} \varepsilon_1 \\ \varepsilon_2 \\ \varepsilon_6 \\ \varepsilon_4 \\ \varepsilon_5 \end{bmatrix}
\qquad (9)
$$

where the $Q'_{ij}s$ are the reduced stiffness matrix components. Finally, since each layer can be orientated at some angle relative to the shell coordinate system, Eqn. 9 must be resolved into the shell coordinates for each layer. Therefore the following relation results for each shell layer:

$$
\begin{bmatrix} \sigma_1 \\ \sigma_2 \\ \sigma_6 \end{bmatrix}^k = \begin{bmatrix} \overline{Q}_{11} & \overline{Q}_{12} & \overline{Q}_{16} \\ \overline{Q}_{12} & \overline{Q}_{22} & \overline{Q}_{26} \\ \overline{Q}_{16} & \overline{Q}_{26} & \overline{Q}_{66} \end{bmatrix}^k \begin{bmatrix} \varepsilon_1 \\ \varepsilon_2 \\ \varepsilon_6 \end{bmatrix}
$$
$$
\begin{bmatrix} \sigma_4 \\ \sigma_5 \end{bmatrix}^k = \begin{bmatrix} \overline{Q}_{44} & \overline{Q}_{45} \\ \overline{Q}_{45} & \overline{Q}_{55} \end{bmatrix}^k \begin{bmatrix} \varepsilon_4 \\ \varepsilon_5 \end{bmatrix} \tag{10}
$$

where k denotes the properties calculated at each layer, $\overline{Q}_{ij}$ (i,j = 1,2,6) and $\overline{Q}_{mn}$ (m,n = 4,5) are the reduced stiffness components for the kth layer, and σ_i, ε_i and σ_j, ε_j are measured with respect to the shell coordinates.

2.1.4 Shell Potential Energy

The expressions of equilibrium for a shell structure are realized by analyzing the potential energy of that conservative system. A conservative system is one in which the work done by the internal strains and externally applied forces is path independent or, in other words, independent of deformation. The principal of stationary potential energy states that the admissible configurations of a conservative system, that satisfy the equilibrium Eqns. make the potential energy stationary with respect to relatively small variations in displacement [3]. An admissible configuration, with respect to finite elements, implies that the structural configuration satisfies both internal compatibility and the essential boundary conditions. Internal compatibility does not allow for discontinuities or "kinks" in the structure. Fig. 4 from Ref. [3] shows examples of both types of violations. Essential boundary conditions in finite elements are the prescribed degree of freedom variables. The potential energy of a conservative system or structure is composed of two parts; 1) the internal strain

18

energy due to elastic deformation, and 2) the potential of externally applied loads to accomplish work. Therefore, the potential energy is written in the following form:

$$\Pi_p \;=\; U + V \tag{11}$$

where U is the internal strain energy of the system and V is the potential energy of externally applied loads. In general, the internal strain energy is defined as:

$$U \;=\; \frac{1}{2}\int_V \varepsilon^T \sigma \, dV \tag{12}$$

Using Eqn. 10, the stress in Eqn. 12 can be represented as a function of the shell strains and transformed stiffness relations, $\overline{Q}_{ij}$ (i,j = 1,2,6) and $\overline{Q}_{mn}$ (m,n = 4,5). Therefore, applying Eqns. 10 and 12 as well as the in-plane and shear strain terms developed in [27], results in the following internal strain energy for a general shell:

$$
\begin{aligned}
U_1 \;=\; \frac{1}{2}\int_\Omega \int_h \big(& \overline{Q}_{11}(\varepsilon_1^0 + \zeta^p \kappa_{1p})^2 + \overline{Q}_{22}(\varepsilon_2^0 + \zeta^p \kappa_{2p})^2 \\
& + 2\overline{Q}_{12}(\varepsilon_1^0 + \zeta^p \kappa_{1p})(\varepsilon_2^0 + \zeta^r \kappa_{2r}) + \overline{Q}_{66}(\varepsilon_6^0 + \zeta^p \kappa_{6p})^2 \\
& + 2\overline{Q}_{16}(\varepsilon_1^0 + \zeta^p \kappa_{1p})(\varepsilon_6^0 + \zeta^r \kappa_{6r}) \\
& + 2\overline{Q}_{26}(\varepsilon_2^0 + \zeta^p \kappa_{2p})(\varepsilon_6^0 + \zeta^r \kappa_{6r})\big) d\zeta d\Omega
\end{aligned}
\tag{13a}
$$
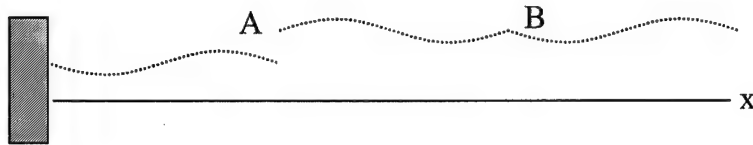
Figure 4. violations of A) essential boundary conditions and B) internal compatibility

19

$$U_2 = \frac{1}{2} \int_\Omega \int_h (\overline{Q}_{44}(\varepsilon_4^0 + \zeta^2 \kappa_{42})^2 + \overline{Q}_{55}(\varepsilon_5^0 + \zeta^2 \kappa_{52})^2$$

$$+ 2\overline{Q}_{45}(\varepsilon_4^0 + \zeta^2 \kappa_{42})(\varepsilon_5^0 + \zeta^2 \kappa_{52}))\mathrm{d}\zeta \mathrm{d}\Omega \tag{13b}$$

where U_1 and U_2 are the in-plane and transverse shear contributions to the internal strain energy respectively, and together they combine to make up the total internal strain energy, or U. Both the in-plane and transverse strain energy terms are integrated over the shell midsurface, or Ω, and through the thickness, or h. In Eqn. 13a, the ε_i^0 ($i = 1, 2, 6$) terms define the in-plane strains at the mid-surface. The κ_{jp} ($j = 1, 2, 6 \ \& \ p = 1, 2, 3, 4, 5, 6, 7$) terms are functions of the shell displacements and curvilinear scale factors. The ζ^r term ($r = 1, 2, 3, 4, 5, 6, 7$) refers to the ply layer coordinate with respect to the shell mid-surface. The ε_m^0 ($m = 4, 5$) terms in Eqn. 13b, define the transverse strains at the midsurface. The κ_{n2} ($n = 4, 5$) terms, again, are functions of the shell displacements and curvilinear scale factors. The exact terms in their entirety are defined in Ref. [27]. It should be pointed out that given the typical variance in fiber orientation for the lamina in a composite panel, the stiffness terms, or the $\overline{Q}_{ij}$ and $\overline{Q}_{mn}$ terms ($i, j = 1, 2, 6 \ m, n = 4, 5$) are generally different for each ply. Expanding Eqn. 13a and integrating through the thickness, or in the ζ direction, allows one to express the in-plane internal strain energy in terms of the elasticity arrays, or:

$$U_1 = \frac{1}{2} \int_\Omega (u_1 + u_2 + u_3) \, \mathrm{d}\Omega \tag{14}$$

where:

$$u_1 = \int_h \varepsilon_j^0 \varepsilon_i^0 \overline{Q}_{ij} \mathrm{d}\zeta$$

$$= \varepsilon_j^0 \varepsilon_i^0 A_{ij} \tag{15a}$$

20

$$u_2 = \int_h 2\varepsilon_j^0 \overline{Q}_{ij} \kappa_{ip} \zeta^p \mathrm{d}\zeta$$

$$= 2\varepsilon_j^0(\kappa_{i1}B_{ij} + \kappa_{i2}D_{ij} + \kappa_{i3}E_{ij} + \kappa_{i4}F_{ij}$$

$$+\kappa_{i5}G_{ij} + \kappa_{i6}H_{ij} + \kappa_{i7}I_{ij}) \tag{15b}$$

$$u_3 = \int_h \kappa_{jp}\kappa_{ir}\overline{Q}_{ij}\zeta^{p+r}\mathrm{d}\zeta$$

$$= \kappa_{j1}\kappa_{i1}D_{ij} + 2\kappa_{j1}\kappa_{i2}E_{ij} + (2\kappa_{j1}\kappa_{i3} + \kappa_{j2}\kappa_{i2})F_{ij}$$

$$+2(\kappa_{j1}\kappa_{i4} + \kappa_{j2}\kappa_{i3})G_{ij} + (2\kappa_{j1}\kappa_{i5} + 2\kappa_{j2}\kappa_{i4} + \kappa_{j3}\kappa_{i3})H_{ij}$$

$$+2(\kappa_{j1}\kappa_{i6} + 2\kappa_{j2}\kappa_{i5} + \kappa_{j3}\kappa_{i4})I_{ij} + (2\kappa_{j1}\kappa_{i7}$$

$$+2\kappa_{j2}\kappa_{i6} + 2\kappa_{j3}\kappa_{i5} + \kappa_{j4}\kappa_{i4})J_{ij}$$

$$+2(\kappa_{j2}\kappa_{i7} + 2\kappa_{j3}\kappa_{i6} + \kappa_{j4}\kappa_{i5})K_{ij} + (2\kappa_{j3}\kappa_{i7}$$

$$+2\kappa_{j4}\kappa_{i6} + \kappa_{j5}\kappa_{i5})L_{ij} + 2(\kappa_{j4}\kappa_{i7} + \kappa_{j5}\kappa_{i6})P_{ij}$$

$$+2(\kappa_{j5}\kappa_{i7} + \kappa_{j6}\kappa_{i6})R_{ij} + 2\kappa_{j6}\kappa_{i7}S_{ij} + 2\kappa_{j7}\kappa_{i7}T_{ij} \tag{15c}$$

where $i, j = 1, 2, 6$ and $p, r = 1, 2, 3, 4, 5, 6, 7$. The following elasticity arrays introduced in the previous Eqns.:

$$[A_{ij}, B_{ij}, D_{ij}, E_{ij}, F_{ij}, G_{ij}, H_{ij}, I_{ij}, J_{ij}, K_{ij}, L_{ij}, P_{ij}, R_{ij}, S_{ij}, T_{ij}] \tag{16}$$

are defined in the subsequent Eqn., as functions of the thickness parameter, ζ:

$$\int_h \overline{Q}_{ij} \left[1, \zeta, \zeta^2, \zeta^3, \zeta^4, \zeta^5, \zeta^6, \zeta^7, \zeta^8, \zeta^9, \zeta^{10}, \zeta^{11}, \zeta^{12}, \zeta^{13}, \zeta^{14}\right] \mathrm{d}\zeta \tag{17}$$

Similarly, the internal transverse shear strain term, U_2, can be written as:

$$U_2 = \frac{1}{2} \int_\Omega (\varepsilon_m^0 \varepsilon_n^0 A_{mn} + 2\varepsilon_n^0 \kappa_{m2} D_{mn} + \kappa_{n2}\kappa_{m2}F_{mn})\mathrm{d}\Omega \tag{18}$$

21

where:

$$[A_{mn}, D_{mn}, F_{mn}] \quad = \quad \int_h \overline{Q}_{mn} \left[1, \zeta^2, \zeta^4\right] d\zeta \tag{19}$$

As a means of presenting the elasticity arrays in an understandable format, consider the following development of the classical plate theory using the following strain relation:

$$\{\varepsilon\} \quad = \quad \{\varepsilon^0\} + z\{\kappa\} \tag{20}$$

where ε is the laminate strain in the composite panel, defined as a function of ε^0, or the reference plane strain at the mid-surface of the panel, z, or the "through-the-thickness" coordinate, and κ, or the components referred to as curvature [35]. For an orthotropic lamina in a state of plane stress, the stress-strain constitutive relationships defined for the orthotropic laminate $x - y$ system is as follows:

$$\{\sigma_{xy}\} \quad = \quad \left\{ \begin{array}{c} \sigma_x \\ \sigma_y \\ \tau_{xy} \end{array} \right\}_k = \left[\begin{array}{ccc} \overline{Q}_{11} & \overline{Q}_{12} & \overline{Q}_{16} \\ \overline{Q}_{12} & \overline{Q}_{22} & \overline{Q}_{26} \\ \overline{Q}_{16} & \overline{Q}_{26} & \overline{Q}_{66} \end{array} \right]_k \left\{ \begin{array}{c} \varepsilon_x \\ \varepsilon_y \\ \gamma_{xy} \end{array} \right\}_k \tag{21}$$

where k refers to an individual lamina. In an effort to relate laminate deformation to the forces and moments within the composite, Eqn. 20 is substituted into Eqn. 21 and integrated through the thickness or "z" direction, resulting in the following expression:

$$\left[\begin{array}{c} M \\ N \end{array} \right]_k \quad = \quad \left[\begin{array}{cc} A & B \\ B & D \end{array} \right]_k \left\{ \begin{array}{c} \varepsilon^0 \\ \kappa \end{array} \right\}_k \tag{22}$$

22

where N and M are the resultant force and moment vectors acting per unit length, and A, B and D are the resulting elasticity arrays, again functions of the through-the-thickness variable "z" and are defined as:

$$(A_{ij}; B_{ij}; D_{ij}) = \int_{-h/2}^{h/2} \overline{Q}_{ij}^{k}(1, z, z^2)dz \tag{23}$$

where $m, n = 4, 5$. The A_{ij}, B_{ij} and D_{ij} elasticity arrays define the extensional, coupling and bending laminate stiffness of the panel, respectively. More specifically, A_{ij} relates in-plane loads to in-plane stresses, B_{ij} relates in-plane loads to curvatures and moments to in-plane strains, and D_{ij} relates moments to curvature. The greater number of elasticity arrays in the SLR theory, introduced in Eqns. 14 and 18 result from the assumed nonlinearity of the kinematic relationships, or the inclusion of higher order "ζ" terms, where ζ is again referring to the SLR composite shell geometry. Those higher-order terms lead to the elasticity arrays, E_{ij} through T_{ij}. It should be noted that the modeling of symmetric composite laminates effectively reduces the number of elasticity arrays by half, since terms multiplying an odd power of ζ are zero when integrated through the thickness. When originally formulated, the SLR theory included only those terms multiplied by even powers of ζ, or the A_{ij}, D_{ij}, F_{ij}, H_{ij}, J_{ij}, L_{ij}, R_{ij}, and T_{ij} arrays. This assumption allowed for the modeling of symmetric laminates only. One of the modifications made to the SLR code, which will be described shortly, is the inclusion of those arrays defined by odd powers of ζ. As the laminates fail under loading or the prescribed displacement increment, asymmetrical failure may occur. For example, a ply in the positive ζ direction may fail in compression, while the corresponding symmetric laminate may not fail, thus resulting in an originally symmetric laminate no longer remaining so. For accurate modeling and to account for all scenarios, the additional elasticity terms should be considered. However, if an originally balanced laminate remains so

23

during deformation and failure, then the previously mentioned arrays, or those arrays multiplied by odd powers of ζ, will be reduced to zero.

Eqns. 11, 14, 18 as well as the strain displacement relations of Appendix A2, define the total potential energy of the cylindrical shell structure. The variation of the resulting potential energy would result in coupled, nonlinear partial differential Eqns. representing the equilibrium of the structure. Finite element analysis, through the discretization of a structure and the resulting "finite" number of Eqns., can be used to solve those equilibrium Eqns.. Discretization refers to the representation of the shell structure in terms of discrete elements connected at nodes. The summation of the elemental energy would result in the total potential for the structure. The potential energy of the shell, written in terms of general discretized elements is shown in the following:

$$\Pi_p = \frac{q^T}{2}\left(K + \frac{N_1}{3} + \frac{N_2}{6}\right)q - q^T R \tag{24}$$

where q represents the nodal values of displacement, K represents an array of constant stiffness coefficients, N_1 represents an array of stiffness components that are linear with respect to the displacement, N_2 represents an array of stiffness components that are quadratic with respect to the displacements and R represents the applied nodal loading. Together, K, N_1 and N_2 make up K_T or the tangent stiffness. Applying the principal of stationary potential energy, thereby minimizing the previously mentioned expression with respect to the displacements, results in the following expression:

$$\begin{aligned}
\delta\Pi_p &= \delta q^T \left[\left(K + \frac{N_1}{3} + \frac{N_2}{6}\right)q - R\right] = 0 \\
&= \delta q^T F(q) = 0
\end{aligned} \tag{25}$$

24

and finally, the equilibrium equations are expressed as:

$$F(q) = 0 \tag{26}$$

A Taylor series expansion of Eqn. 26 in terms of q, is accomplished to solve the equilibrium expressions:

$$(K + N_1 + N_2)\Delta q = -F(q) \tag{27}$$

In other words, small variations in q, or Δq, are inputs into Eqn. 26, and the resulting forces, or $F(q)$, are iterated upon using a Newton-Raphson solution technique until convergence is reached. In the SLR program, convergence is based upon calculated displacements and a user specified convergence limit, typically 0.1% [27]. A required condition in the SLR development of the shell potential energy was that the stiffness arrays of Eqns. 24, 25 and 27, or the tangent stiffness arrays, were formulated in such a way from the internal strain energy relations, as to simplify the manipulation of the potential energy expression. In other words, it was desired that the tangent stiffness arrays, or K, N_1 and N_2 stiffness terms, remain unchanged after the first variation of the potential energy, or Eqn. 25, and again, after the Taylor series expansion of Eqn. 27. This formalism in the development of the tangent stiffness terms was desired for several reasons. First, it simplified both the variation and resulting linearization of Eqn. 26 by decreasing the number of algerbraic manipulations required. Second, the amount of code required to solve Eqn. 27 in a finite element program is greatly reduced, as the tangent stiffness array remains unchanged requiring their calculation only

25

once. The resulting technique employed by Ref. [27] to facilitate this simplification, and the resulting repeatable and symmetric form of the tangent stiffness components denoted as, $\widehat{K}$, $\widehat{N}_1$ and $\widehat{N}_2$ are discussed in subsequent sections.

The detail that the author went into discussing the desired form of the tangent stiffness matrices was necessary, as one of the modifications to the SLR program involved adding the additional elasticity arrays, defined as odd functions of ζ. As shown in the development of the potential energy and linearization expressions, the elasticity arrays are integral components of the tangent stiffness terms. Palazotto and Dennis [27] formulated the tangent stiffness components in such a way as to allow those arrays to be repeatable and symmetric throughout the potential energy formulation and resulting linearization. As discussed earlier, this was desired, as it allowed for fewer algerbraic computations as well as reducing the amount of computer code and computing time. The steps required for the repeatability of the tangent stiffness arrays are as follows. First, the strain-displacement terms of Appendix A2 were separated into linear and nonlinear functions of the displacement gradient vector or d, as shown in the following Eqn.:

$$
\begin{aligned}
\varepsilon_i^0 &= {}_0L_i^T\, d + \frac{1}{2}d^T\, {}_0H_i\, d \\
\kappa_{ip} &= {}_pL_i^T\, d + \frac{1}{2}d^T\, {}_pH_i\, d
\end{aligned}
\tag{28}
$$

where ${}_pL_i$ are column arrays representing linear displacement terms, ${}_pH_i$ are symmetric matrices representing the nonlinear displacement terms ($j = 0, 1, 2, \ldots, 7$, $i = 1, 2, 6$ $and\ p = 1\ to\ 7$) and the displacement gradient vector is defined in Eqn. 7. Again, note that there are only 17 unique displacement terms in the strain relations of Appendix A2, however, the additional term "u" was added to the displacement gradient vector for completeness. Neither the ${}_jL_i$ or ${}_jH_i$ arrays are functions of the displacement gradient vector d, but rather contain only constants. The ${}_jL_i$ and

26

$_jH_i$ constant arrays are shown in their entirety in [27]. As a means of describing the reasoning behind the separation of the strain terms into the linear and nonlinear components, consider ε_1^0 from Appendix A2 written in the method just described:

$$\varepsilon_1^0 = u_{,1} + \frac{1}{2}(u_{,1}^2 + v_{,1}^2 + w_{,1}^2)$$

$$\varepsilon_1^0 = {_0}L_1^T d + \frac{1}{2}d^T {_0}H_1 d \qquad (29)$$

where $_0L_1^T$:

$${_0}L_1^T = [0, 1, 0, 0, \ldots, 0]$$

and

$$
{_0}H_1 = \begin{bmatrix}
0 & 0 & 0 & 0 & 0 & 0 & 0 & 0 & \cdots & 0 \\
0 & 1 & 0 & 0 & 0 & 0 & 0 & 0 & \cdots & 0 \\
0 & 0 & 0 & 0 & 0 & 0 & 0 & 0 & \cdots & 0 \\
0 & 0 & 0 & 0 & 0 & 0 & 0 & 0 & \cdots & 0 \\
0 & 0 & 0 & 0 & 1 & 0 & 0 & 0 & \cdots & 0 \\
0 & 0 & 0 & 0 & 0 & 0 & 0 & 0 & \cdots & 0 \\
0 & 0 & 0 & 0 & 0 & 0 & 0 & 0 & \cdots & 0 \\
0 & 0 & 0 & 0 & 0 & 0 & 0 & 1 & \cdots & 0 \\
\vdots & \vdots & \vdots & \vdots & \vdots & \vdots & \vdots & \vdots & & \vdots \\
0 & 0 & 0 & 0 & 0 & 0 & 0 & 0 & \cdots & 0
\end{bmatrix}
$$

The benefit of expressing the strain-displacement relations in this manner is in the ease of manipulation, since all terms are represented as 18 x 18 arrays. Rewriting the in-plane strain relations of Appendix A2 in terms of $_jL_i$ and $_jH_i$ results in the following energy expression, or the energy terms due to ε_1, ε_2 and ε_6:

$$U_1 = \frac{1}{2}\int_\Omega d^T \left(\tilde{K} + \tilde{N}_1 + \frac{1}{4}\tilde{N}_2\right) d\, d\Omega \qquad (30)$$

where

27

$$\widetilde{K} = A_{ij}\,{}_0L_i\,{}_0L_j^T + 2B_{ij}\,{}_0L_i\,{}_1L_j^T + D_{ij}(2\,{}_0L_i\,{}_2L_j^T + {}_1L_i\,{}_1L_j^T)$$

$$+E_{ij}(2\,{}_0L_i\,{}_3L_j^T + 2\,{}_0L_i\,{}_3L_j^T) + F_{ij}(2\,{}_0L_i\,{}_4L_j^T + 2\,{}_1L_i\,{}_3L_j^T$$

$$+{}_2L_i\,{}_2L_j^T) + G_{ij}(2\,{}_1L_i\,{}_4L_j^T + 2\,{}_2L_i\,{}_3L_j^T) + H_{ij}(2\,{}_2L_i\,{}_4L_j^T$$

$$+{}_3L_i\,{}_3L_j^T) + 2I_{ij}\,{}_3L_i\,{}_4L_j^T + J_{ij}\,{}_4L_i\,{}_4L_j^T \tag{31}$$

$$\widetilde{N_1} = A_{ij}\,{}_0L_i\,d^T\,{}_0H_j + B_{ij}({}_0L_i\,d^T\,{}_1H_j + {}_1L_i\,d^T\,{}_0H_j) + D_{ij}({}_0L_i\,d^T\,{}_2H_j$$

$$+{}_2L_i\,d^T\,{}_0H_j + {}_1L_i\,d^T\,{}_1H_j) + E_{ij}({}_0L_i\,d^T\,{}_3H_j + {}_3L_i\,d^T\,{}_0H_j$$

$$+{}_1L_i\,d^T\,{}_3H_j + {}_3L_i\,d^T\,{}_1H_j + {}_2L_i\,d^T\,{}_2H_j) + G_{ij}({}_0L_i\,d^T\,{}_5H_j$$

$$+{}_1L_i\,d^T\,{}_4H_j + {}_2L_i\,d^T\,{}_3H_j + {}_4L_i\,d^T\,{}_1H_j + {}_3L_i\,d^T\,{}_2H_j)$$

$$+H_{ij}({}_0L_i\,d^T\,{}_6H_j + {}_1L_i\,d^T\,{}_5H_j + {}_2L_i\,d^T\,{}_4H_j + {}_3L_i\,d^T\,{}_3H_j$$

$$+{}_4L_i\,d^T\,{}_2H_j) + I_{ij}({}_0L_i\,d^T\,{}_7H_j + {}_1L_i\,d^T\,{}_6H_j + {}_2L_i\,d^T\,{}_5H_j$$

$$+{}_3L_i\,d^T\,{}_4H_j + {}_4L_i\,d^T\,{}_3H_j) + J_{ij}({}_1L_i\,d^T\,{}_7H_j + {}_2L_i\,d^T\,{}_6H_j$$

$$+{}_3L_i\,d^T\,{}_5H_j + {}_4L_i\,d^T\,{}_4H_j) + K_{ij}({}_2L_i\,d^T\,{}_7H_j + {}_3L_i\,d^T\,{}_6H_j$$

$$+{}_4L_i\,d^T\,{}_5H_j) + L_{ij}({}_3L_i\,d^T\,{}_7H_j + {}_4L_i\,d^T\,{}_6H_j) + P_{ij}\,{}_4L_i\,d^T\,{}_7H_j \tag{32}$$

$$\widetilde{N_2} = A_{ij}\,{}_0H_i\,d\,d^T\,{}_0H_j + B_{ij}\,{}_0H_i\,d\,d^T\,{}_1H_j + D_{ij}({}_0H_i\,d\,d^T\,{}_2H_j$$

$$+{}_1H_i\,d\,d^T\,{}_1H_j) + E_{ij}({}_0H_i\,d\,d^T\,{}_3H_j + 2\,{}_1H_i\,d\,d^T\,{}_2H_j) + F_{ij}({}_0H_i\,d\,d^T\,{}_4H_j$$

$$+2\,{}_1H_i\,d\,d^T\,{}_3H_j + {}_2H_i\,d\,d^T\,{}_2H_j) + G_{ij}({}_0H_i\,d\,d^T\,{}_5H_j + 2\,{}_1H_i\,d\,d^T\,{}_4H_j$$

$$+2\,{}_2H_i\,d\,d^T\,{}_3H_j) + H_{ij}({}_0H_i\,d\,d^T\,{}_6H_j + 2\,{}_1H_i\,d\,d^T\,{}_5H_j + 2\,{}_2H_i\,d\,d^T\,{}_4H_j$$

$$+{}_3H_i\,d\,d^T\,{}_3H_j) + I_{ij}({}_0H_i\,d\,d^T\,{}_7H_j + 2\,{}_1H_i\,d\,d^T\,{}_6H_j + 2\,{}_2H_i\,d\,d^T\,{}_5H_j$$

$$+2\,{}_3H_i\,d\,d^T\,{}_4H_j) + J_{ij}(2\,{}_1H_i\,d\,d^T\,{}_7H_j + 2\,{}_2H_i\,d\,d^T\,{}_6H_j + 2\,{}_3H_i\,d\,d^T\,{}_5H_j$$

$$+ 2_4 H_i\, d\, d^T\, {}_4 H_j) + K_{ij}(2_2 H_i\, d\, d^T\, {}_7 H_j + 2_3 H_i\, d\, d^T\, {}_6 H_j + 2_4 H_i\, d\, d^T\, {}_5 H_j)$$

$$+ L_{ij}(2_3 H_i\, d\, d^T\, {}_7 H_j + 2_4 H_i\, d\, d^T\, {}_6 H_j + {}_5 H_i\, d\, d^T\, {}_5 H_j)$$

$$+ P_{ij}(2_4 H_i\, d\, d^T\, {}_7 H_j + 2_5 H_i\, d\, d^T\, {}_6 H_j) + R_{ij}(2_5 H_i\, d\, d^T\, {}_7 H_j$$

$$+ {}_6 H_i\, d\, d^T\, {}_6 H_j) + S_{ij} 2_6 H_i\, d\, d^T\, {}_7 H_j + T_{ij}\, {}_7 H_i\, d\, d^T\, {}_7 H_j \tag{33}$$

Taking the variation of the the $\widetilde{K}$, $\widetilde{N}_1$ and $\widetilde{N}_2$ terms of Eqns. 31-33 will not yet result in the repeating stiffness arrays sought after. One final step is required, to replace the form of the RHS of Eqns. 31-33 with the following format yields the desired repeating formalism. Therefore, for $\widetilde{K}$:

$$\frac{1}{2} \int_\Omega d^T\, C_{ij}\, {}_p L_i\, {}_p L_j^T\, d\, d\Omega \ \text{(no sum on } p) = \text{no change}$$

$$\frac{1}{2} \int_\Omega d^T\, 2 C_{ij}\, {}_p L_i\, {}_r L_j^T\, d\, d\Omega = \frac{1}{2} \int_\Omega d^T\, C_{ij}\, ({}_p L_i\, {}_r L_j^T + {}_r L_i\, {}_p L_j^T)\, d\, d\Omega \tag{34}$$

where C_{ij} refers to any of the elasticity arrays within $\widetilde{K}$. For $\widetilde{N}_1$:

$$\frac{1}{2} \int_\Omega d^T\, C_{ij}\, {}_p L_i\, d^T\, {}_r H_j\, d\, d\Omega$$

$$= \frac{1}{6} \int_\Omega d^T\, C_{ij}\, ({}_p L_i\, d^T\, {}_r H_j + d^T\, {}_p L_i\, {}_r H_j + {}_r H_i\, d\, {}_p L_j^T)\, d\, d\Omega \tag{35}$$

where C_{ij} refers to any of the elasticity arrays within $\widetilde{N}_1$. Finally, for $\widetilde{N}_2$:

$$\frac{1}{8} \int_\Omega d^T\, C_{ij}\, {}_p H_i\, d\, d^T\, {}_p H_j\, d\, d\Omega = \frac{1}{12} \int_\Omega d^T\, C_{ij}({}_p H_i\, d\, d^T\, {}_p H_j$$

$$+ \frac{1}{2} d^T\, {}_p H_j\, d\, d^T\, {}_p H_i)\, d\, d\Omega \ \text{(no sum on } p)$$

$$\frac{1}{8} \int_\Omega d^T\, C_{ij}\, {}_r H_i\, d\, d^T\, {}_p H_j\, d\, d\Omega = \frac{1}{8} \int_\Omega \frac{d^T}{3} C_{ij}({}_r H_i\, d\, d^T\, {}_p H_j$$

$$+\frac{1}{2}d^T \,_rH_i \, d \, d^T \,_pH_j + \,_pH_i \, d \, d^T \,_rH_j + \frac{1}{2}d^T \,_pH_i \, d \, d^T \,_rH_j)d \, d\Omega \qquad (36)$$

where C_{ij} refers to any of the elasticity arrays within $\widetilde{N}_2$. Therefore, the in-plane energy expression, or Eqn. 30 can now be written as:

$$U_1 \;=\; \frac{1}{2}\int_\Omega d^T \left(\widehat{K} + \frac{\widehat{N}_1}{3} + \frac{\widehat{N}_2}{6}\right) d \, d\Omega \qquad (37)$$

The transverse shear terms were handled in a similar manner and are described in detail in Ref. [27].

Finally, given the preceding tangent stiffness terms, the tangent stiffness terms of Eqn. 24 can be represented as:

$$\begin{aligned}
K &= \int_\Omega D^T \widehat{K} \, D \, d\Omega \\
N_1 &= \int_\Omega D^T \widehat{N}_1 \, D \, d\Omega \\
N_2 &= \int_\Omega D^T \widehat{N}_2 \, D \, d\Omega
\end{aligned} \qquad (38)$$

where D^T represents the array of shape functions or interpolating functions in natural coordinates and their derivatives used to approximate the displacement gradient vector, or Eqn. 7. The shape functions for the specific finite elements used in this analysis will be developed in the subsequent section.

2.1.5 Finite Element Formulation

The finite element formulation is a numerical procedure that approximates the displacements and therefore the loads, strains and stresses of a structure by analyzing the structure's discretized domain [3]. To discretize a structure is to model that structure as an assemblage of finite elements.

30

The term finite is specifically used to distinguish the reference element from a differential element. The finite element process approximates those discretized displacements through the use of interpolating functions, also called shape functions. The potential energy of the structure as described in the previous section, is formulated in terms of the discrete displacements. In other words, the individual nodal displacements and therefore the nodal strains for each element make up the total potential energy for the structure. Thus the total structure, or continuum displacement can be written as a function of algerbraic expressions through the use of the interpolating functions. The unknowns, or nodal displacements are then solved using a finite element analysis technique. Typically, as a finite element mesh is refined, the results of the analysis approaches the exact solution as long as several requirements are met. In the formulation of the SLR theory and resulting finite element method, the following six requirements were enforced: 1) each element must satisfy continuous displacement within that element, 2) each element must represent a constant strain condition, 3) the rigid body terms, or the ψ_i ($i = 1, 2$) and u, v, w terms were incorporated into the displacement functions, 4) each element must ensure compatibility is met, see Fig. 4, 5) each element should not have preferred directions, i.e. it should be geometrically invariant.

For the purposes of this research, 8-node, 36-degree-of-freedom (dof) elements were utilized for all scenarios. Fig. 5 displays the node numbering and the degrees-of-freedom for each node, element geometry, as well as the cylindrical displacement variables, x and s [27]. There are seven degrees-of-freedom (dof) at each corner node: u, v, w, $w_{,1}$, $w_{,2}$, ψ_1 and ψ_2. In addition, there are four "mid-nodes" with the degrees-of-freedom, u and v. In the initial development of the SLR finite element theory, a 28 degree-of-freedom element was proposed. This approach is appropriate for flat plate analysis, however the in-plane u and v displacements for a cylindrical shell are coupled to the transverse displacements to a much greater degree in shell analysis due to the nonzero shell curvature. For this reason, the mid-node displacement variables, u and v were added,

31
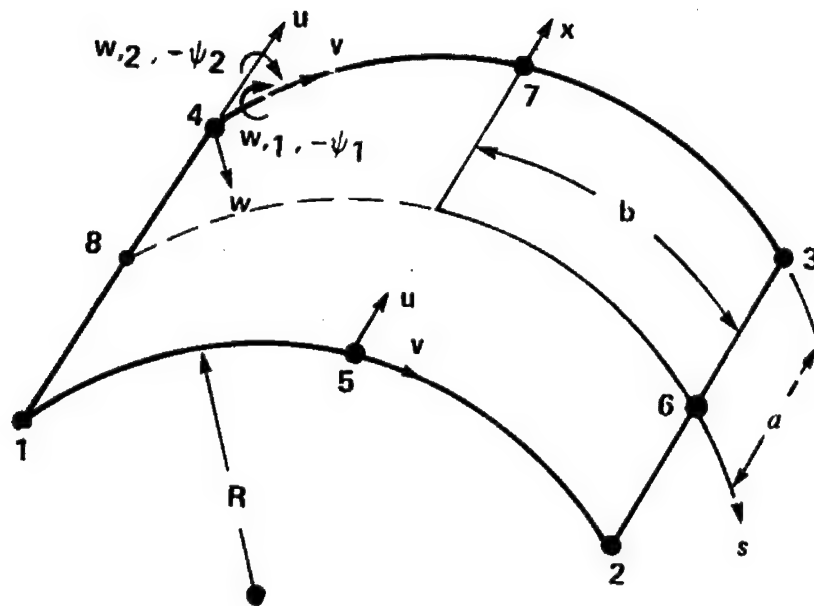
Figure 5. 36-degree of freedom rectangular shell element. Corner nodes have 7 degrees of freedom, midside nodes have 2 degrees of freedom.

resulting in the 36 degree of freedom element. C^0 continuity was required for the displacement degrees of freedom u, v, ψ_1 and ψ_2 and C^1 continuity was required for the displacement degrees of freedom w, $w_{,1}$ and $w_{,2}$. Therefore, bilinear Lagrangian shape functions were used for ψ_1 and ψ_2, quadratic Lagrangian shape functions were used for u and v due to the addition of the mid-nodes, and cubic Hemitian shape functions were used for w, $w_{,1}$, and $w_{,2}$. Fig. 6 displays a rectangular shell element in terms of the natural coordinates ξ and η, where $\xi = x/a$ and $\eta = s/b$ [27]. The
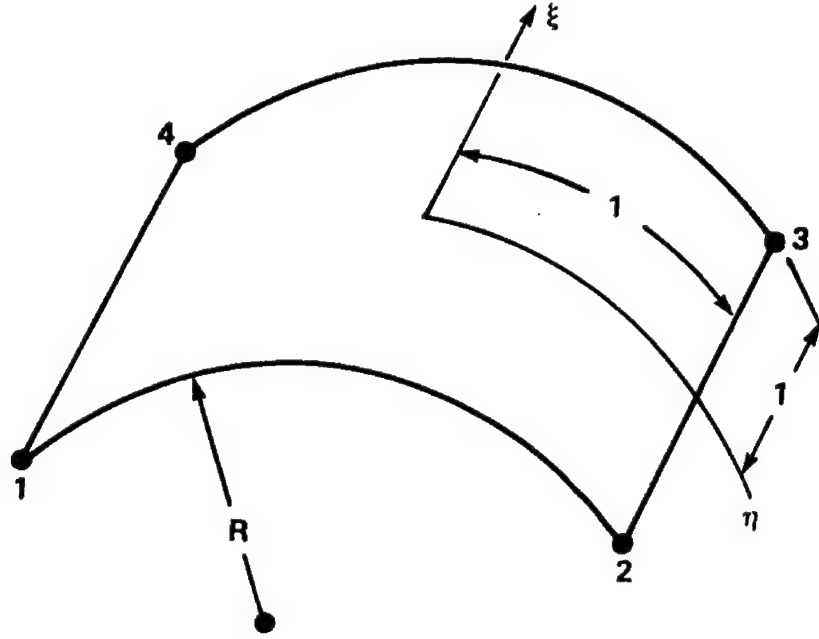
Figure 6. Rectangular shell element in natural coordinates.

following expression is the bilinear Lagrangian shape function for dof ψ_1 and ψ_2 in terms of natural coordinates:

$$\aleph_k \;=\; \frac{1}{4}\left(1 + \xi_k\xi\right)\left(1 + \eta_k\eta\right) \tag{39}$$

where for the kth node, $q_k^T = \{\psi_1 \; \psi_2\}$. For the displacement degrees of freedom u and v for the kth node, the quadratic Lagrangian shape functions in terms of natural coordinates are shown in the

33

following:

$$\Im_k = \frac{1}{4} \left(1 + \xi_k \xi\right) \left(1 + \eta_k \eta\right) \left(\xi_k \xi + \eta_k \eta - 1\right), \ k = 1,2,3,4$$

$$\Im_k = \frac{1}{2} \left(1 - \xi^2\right) \left(1 + \eta_k \eta\right), \ k = 6,8$$

$$\Im_k = \frac{1}{2} \left(1 - \eta^2\right) \left(1 + \xi_k \xi\right), \ k = 5,7 \tag{40}$$

where nodes 1 through 8 are displayed in Fig. 5. Finally, the cubic Hermitian shape functions for dof w, $w_{,1}$ and $w_{,2}$ are defined as follows:

$$\begin{aligned}
\Re_k &= \frac{1}{8} \left(1 + \xi_k \xi\right) \left(1 + \eta_k \eta\right) \left(2 + \xi_k \xi + \eta_k \eta - \xi^2 - \eta^2\right) \\
&\quad \left(\frac{a}{8}\right) \xi_k \left(1 + \xi_k \xi\right)^2 \left(\xi_k \xi - 1\right) \left(1 + \eta_k \eta\right) \\
&\quad \left(\frac{b}{8}\right) \eta_k \left(1 + \xi_k \xi\right) \left(\eta_k \eta - 1\right) \left(1 + \eta_k \eta\right)^2
\end{aligned} \tag{41}$$

where for the kth node, $q_k^T = \{w \ w_{,1} \ w_{,2}\}$. Using the 18 degree of freedom displacement gradient vector of Eqn. 7, the displacement gradient vector for the 36 dof shell element can now be written in the following matrix form, including the shape functions and the shape function derivatives in terms of natural coordinates:

$$\begin{aligned}
d\left(\xi, \eta\right) &= Dq \\
&= \begin{bmatrix} Q_1 & 0 & 0 & \cdots & Q_4 & 0 & 0 & Q_5 & \cdots & Q_8 \\ 0 & H_1 & 0 & \cdots & 0 & H_4 & 0 & 0 & \cdots & 0 \\ 0 & 0 & N_1 & \cdots & 0 & 0 & N_4 & 0 & \cdots & 0 \end{bmatrix} \begin{Bmatrix} q_1 \\ \vdots \\ q_4 \\ q_5 \\ \vdots \\ q_8 \end{Bmatrix}
\end{aligned} \tag{42}$$

where

$$q_k^T = \{u\ v\ w\ w_{,1}\ w_{,2}\ \psi_1\ \psi_2\}_k,\ k = 1, 2, 3, 4$$

$$q_k^T = \{u\ v\}_k,\ k = 5, 6, 7, 8 \tag{43}$$

and

$$Q_k = \begin{bmatrix} \Im_k & 0 \\ \Im_{k,\xi} & 0 \\ \Im_{k,\eta} & 0 \\ 0 & \Im_k \\ 0 & \Im_{k,\xi} \\ 0 & \Im_{k,\eta} \end{bmatrix} \tag{44}$$

$$H_k = \begin{bmatrix} \Re_{k1} & \Re_{k2} & \Re_{k3} \\ \Re_{k1,\xi} & \Re_{k2,\xi} & \Re_{k3,\xi} \\ \Re_{k1,\eta} & \Re_{k2,\eta} & \Re_{k3,\eta} \\ \Re_{k1,\xi\xi} & \Re_{k2,\xi\xi} & \Re_{k3,\xi\xi} \\ \Re_{k1,\eta\eta} & \Re_{k2,\eta\eta} & \Re_{k3,\eta\eta} \\ \Re_{k1,\eta\xi} & \Re_{k2,\eta\xi} & \Re_{k3,\eta\xi} \end{bmatrix} \tag{45}$$

$$N_k = \begin{bmatrix} \aleph_k & 0 \\ \aleph_{k,\xi} & 0 \\ \aleph_{k,\eta} & 0 \\ 0 & \aleph_k \\ 0 & \aleph_{k,\xi} \\ 0 & \aleph_{k,\eta} \end{bmatrix} \tag{46}$$

With the development of the discretized shell domain and stiffness relations complete, a transformation from natural to global coordinates, or a transformation from the coordinates in Fig. 6 to Fig. 5 is required. The transformation is presented in the following expression:

$$d(x, s) = \Gamma d(\xi, \eta) \tag{47}$$

where Γ is the inverse of the Jacobian matrix that relates the two coordinate systems. Having accomplished the transformation, the linearized, incremental/iterative relations of Eqn. 27 can now be represented as:

$$\sum_{k=1}^{n} \left(\int_{\Omega_e} D^T \left(\widehat{K} + \widehat{N}_1 + \widehat{N}_2 \right) D\ d\Omega_e \right)_k \Delta q$$

35

$$= -\sum_{k=1}^{n} \left[\int_{\Omega_e} D^T \left(\widehat{K} + \frac{\widehat{N}_1}{2} + \frac{\widehat{N}_2}{3} \right) D \, d\Omega_e \right]_k q + R \qquad (48)$$

where Ω_e represents the two dimensional domain of each element, n is the total number of elements in the mesh, Δq and q represent the global displacement arrays assembled from the individual element displacement vectors, and R represents the global load array. The integration in Eqn. 48 is accomplished using Gaussian quadrature. Solutions to Eqn. 48 are found when the RHS of the Eqn. satisfies the user specified convergence criteria.

2.2 Failure Criteria

Why is failure criteria important? Strength prediction in fiber composite materials is critical when designing a structure. Failure in the structure will occur when the applied loading in the form of stress exceeds the load carrying threshold or ability of the structure. It is an expensive and often impossible process to experimentally analyze every possible design. Therefore, failure criterion have been established to predict the load carrying abilities of anisotropic composite structures. The idea of analytically predicting the residual strength of a structure utilizing failure criteria is not new. In fact, the process has been in practice for several centuries. The use of failure criteria in the design process requires several considerations [10]. First, the material constants used in the analysis must be easily determined. In order to apply a failure criterion, experimental studies are carried out to determine the composite ply strengths in the principal material directions. Composite failure theories relate those principal strength properties, or material constants, to the stresses in the composites. Failure theories must also be applied within appropriate boundaries. Appropriate boundaries implies several things. The failure criteria must accurately predict behavior, or provide results with known error for conservative design purposes. Failure criteria must also be applied appropriately with regards to the type of structure and loading. Structures are rarely exposed

36

to single axis loading, and the typical multi-ply and multioriented nature of composites leads to complex multiaxis loading. Some failure theories relate various stress components, i.e., relating shear and normal stress components, while other criterion simply compare the material directed stresses to the principal material properties. Finally, failure criteria in the design process must be simple to apply, i.e., complex mathematical formulae are not practical for general use.

Each failure criteria describes a failure envelope, beyond which, the criterion predicts the material will fail. As seen in Fig. 7 taken from [6], which depicts a failure envelope using the maximum stress theory, if the applied stresses $\sigma_1$or σ_2 exceed the material strength limits, F_{1T}, $-F_{1C}$ or F_{2T}, $-F_{2C}$ respectively, then the material will fail.
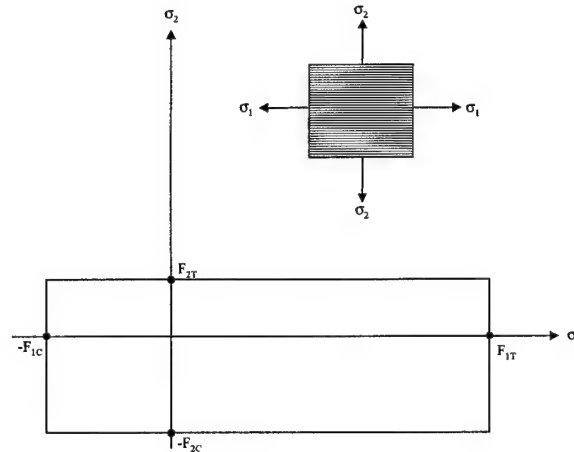
Figure 7. Failure envelope for unidirectional lamina under biaxial normal loading (maximum stress theory)

There are numerous forms of failure criterion. Specifically, failure criterion can be classified as either non-interactive or interactive [43]. Non-interactive failure criteria, like the maximum stress and maximum strain theories, are typically used for brittle isotropic materials. In other words, there is no attempt to take into account the multiple stress interactions when the structure experiences a biaxial state of stress [6]. Interactive, to include quadratic failure criteria, are so

37

named for the assumption that stresses do interact under biaxial loading. These criteria are typically used for ductile isotropic materials experiencing yielding. Both non-interactive and interactive failure criterion have been applied to fiber reinforced composite materials. Given an understanding of the assumptions used to formulate various criteria, their use provides a powerful tool in the composite design process. There are numerous macroscopic failure theory surveys available in the literature, and [35], [43] and [26] are several that provide a fairly exhaustive review of the current failure criteria in use. There are also new criteria being developed constantly [1], [47].

2.2.1 Fiber Failure Criteria

There were three criterion used in this research: the Hashin, Lee and maximum stress theories. For all of the various failure modes considered, the chosen failure criterion allowed for the ability to distinguish between the failure mode. The following inequality relationships were used to analyze the state of stress, assuming fiber failure had occurred:

Maximum stress crtierion:

$$\sigma_{11} \geq \sigma_{FN}$$

Lee criterion [9]:

$$\left(\sigma_{12}^2 + \sigma_{13}^2\right)^{\frac{1}{2}} \geq \sigma_{FS}$$

Hashin criterion [9], [14]:

$$\left(\frac{\sigma_{11}}{\sigma_{FN}}\right)^2 + \frac{\left(\sigma_{12}^2 + \sigma_{13}^2\right)}{\sigma_{FS}^2} \geq 1 \tag{49}$$

where "11", "12" and "13" indicate the fiber, matrix and in-plane directions with respect to the material axis, σ_{FN} is the allowable fiber normal strength and σ_{FS} is the allowable fiber strength in shear. The maximum stress criteria differs from the Lee and Hashin criteria in that it considers

only the direct stress contribution. The Lee criteria considers only the shear components of stress and the Hashin criteria is a combination of direct and shear stress contributions.

2.2.2 Matrix Failure Criteria

Matrix failure can be divided into two categories, failure in tension and failure in compression. The inequalities used to analyze the state of stress in the composite structure for matrix failure in tension are expressed in the following:

Maximum stress crtierion:

$$\sigma_{22} \geq \sigma_{MNT}, \ (\sigma_{22} > 0)$$

Lee criterion [9]:

$$\left(\sigma_{12}^2 + \sigma_{23}^2\right)^{\frac{1}{2}} \geq \sigma_{MS}$$

Hashin criterion [9], [14]:

$$\frac{1}{\sigma_{MNT}^2} (\sigma_{22} + \sigma_{33})^2 + \frac{1}{\sigma_{MS}^2} \left(\sigma_{23}^2 - \sigma_{22}\sigma_{33}\right) +$$
$$\frac{1}{\sigma_{FS}^2} \left(\sigma_{12}^2 + \sigma_{13}^2\right) \geq 1, \ (\sigma_{22} + \sigma_{33}) > 0 \tag{50}$$

where σ_{MNT} is the allowable matrix strength in normal tension and σ_{MS} is the allowable matrix strength in shear. The following were the expressions used for matrix failure in compression:

Maximum stress crtierion:

$$\sigma_{22} \geq \sigma_{MNC}, \ (\sigma_{22} < 0)$$

Lee criterion [9]:

$$\left(\sigma_{12}^2 + \sigma_{23}^2\right)^{\frac{1}{2}} \geq \sigma_{MS}$$

39

Hashin criterion [9], [14]:

$$\frac{1}{\sigma_{MNC}^2}\left[\left(\frac{\sigma_{MNC}}{2\sigma_{MS}}\right)^2 - 1\right](\sigma_{22}+\sigma_{33}) + \frac{1}{4\sigma_{MS}^2}(\sigma_{22}+\sigma_{33})^2 +$$
$$\frac{1}{\sigma_{MS}^2}(\sigma_{23}^2 - \sigma_{22}\sigma_{33}) + \frac{1}{\sigma_{FS}^2}(\sigma_{12}^2 + \sigma_{13}^2) \geq 1, \ (\sigma_{22}+\sigma_{33}) < 0 \qquad (51)$$

where σ_{MNC} is the allowable matrix strength in normal compression. It should be noted that σ_{33} was neglected in the formulation of the SLR theory, resulting in a reduction of the Hashin criteria.

2.2.3 Delamination

Finally, the last failure mode considered in this research was delamination. The inequalities used to express the state of stress assuming delamination had occurred were the following:

Maximum stress criterion

$$\sigma_{13} \geq \sigma_{DS} \ or \ \sigma_{23} \geq \sigma_{DS}$$

Lee criterion [9]:

$$\left(\sigma_{13}^2 + \sigma_{23}^2\right)^{\frac{1}{2}} \geq \sigma_{DS}$$

Hashin criterion [9]:

$$\left(\frac{\sigma_{33}}{\sigma_{ZN}}\right)^2 + \frac{\sigma_{12}^2 + \sigma_{13}^2}{\sigma_{DS}^2} \geq 1 \qquad (52)$$

where σ_{ZN} is the allowable transverse normal strength, and σ_{DS} is the allowable delamination strength in shear. It should be noted that σ_{33} was neglected as a result of assumptions made in the SLR theory, therefore the delamination considered in this research was based solely on transverse shear stresses.

40

There are currently two areas of research in the study of failure in composite structures. Failure criteria can be used to determine first ply failures as well as further progressive failure, or failure after the first ply failure has occurred. Progressive failure analysis incrementally reduces the strength of the composite structure using various techniques. As alluded to earlier, composite materials, can retain significant strength after first-ply-failure. It is therefore beneficial to analyze composite structures both for first-ply-failure and for the failures that follow. For the aforementioned reasons, a means of analyzing progressive failure is extremely important in the analysis of composite structures. There are many avenues available to engineers to aid in this investigation. Some methods use statistical analyses, micromechanics or fracture mechanics approaches to predicting lamina damage progression [46]. Finite element analysis also provides engineers a ready platform for the study of failure in composite materials. Failure criteria has been included in many finite element methods used to analyze composite structures for both first-ply-failure and last ply failure.

First ply as well as progressive failure analysis was the true scope of this research, so little time was spent researching first ply failure only. Reddy and Pandey [30] incorporated failure criteria into a first order or classical shear deformation finite element method in order to examine first ply failure utilizing various criteria. Multiple ply layups, specimen geometries and plate element configurations were considered. Maximum stress, maximum strain, Hoffman, Tsai-Wu and Tsai-Hill criteria were compared for all configurations considered. The finite element method solved for the stresses in each element of each ply from an initially applied load. Once the failure criteria was satisfied for a given load, or first ply failure was reached, the load was reduced by 20% and the stresses and failure analysis were recalculated in order to better predict the load responsible for first ply failure. The iterative procedure was continued until the difference between any two load increments was less than 1%. Output data includes the failure load, type and location of first

41

ply failure. Results of the study indicate that the criteria investigated yield the same results for in-plane loading. For the cases of transverse loading, the interactive and non-interactive failure criterion results diverge.

Reddy and Reddy [31] investigated first ply failure using a first order shear deformation theory and various failure criteria. Linear and non-linear (von-Karman) loads were computed and compared for several loading conditions, to include in-plane and transverse loading. The failure criteria investigated included both independent and polynomial failure criteria. The independent criteria includes maximum stress and maximum strain. The polynomial failure criteria includes the polynomial maximum stress, polynomial maximum strain, Tsai-Hill, Hoffman's and Tsai-Wu criteria. The non-linear loads and first failure were calculated using an iterative procedure similar to Ref. [30]. Results indicate that the failure loads predicted by the various criteria varied a maximum of 35% for the linear analysis and by a maximum of 50% for the non-linear analyses. There were significantly more differences in the results calculated for linear and non-linear cases while under transverse loading than for cases involving in-plane loading.

Calculating the loads and stresses in a composite specimen prior to failure is not difficult. Even comparing those stresses to various failure criteria and determining the first ply failure is a relatively straightforward procedure. However, post-failure analysis of composite laminates is an extremely complex process and has therefore been studied using various simplifying approaches. Those simplifying approaches are made in an effort to handle the strength reduction after first ply failure and all additional failures. Various strength reduction procedures include removing stiffness properties or ultimate strengths in some incremental form [34]. The following is a short, and by no means complete compilation of various progressive failure analyses incorporated within finite element methods.

Sandhu et al. [29] developed a progressive-ply-failure program for structures with stress concentrations. The finite element method utilized was also compared with several experimental procedures incorporating stress concentrators with good results [22]- [28]. The finite element method was based upon a modular program that allowed the user to specify the element type, failure criteria and post failure ply unloading method. Constant strain elements were used along with the Total Strain Energy failure criteria developed by R. S. Sandhu [37] and two post failure unloading methods. The unloading procedures included a gradual method where the affected element moduli were reduced by a percentage and the incremental loading continued. When the stresses in an element were reduced to zero due to failure, the moduli were then assigned a nominally small value. The second procedure, or rapid unloading immediately reduced the affected element moduli to nominally small values. In both cases, if failure had occurred, the loads and therefore the stresses were recalculated after the moduli had been reduced in order to calculate any secondary failures. The procedure was repeated until no further failure occurred. The gradual unloading procedure yielded good results for multi-directional lamina, but overestimated the strength in unidirectional specimens. As expected, the rapid unloading scheme resulted in more conservative lamina strength calculations for all specimens.

Tolson and Zabaras [42] developed a progressive finite element method incorporating Maximum stress, Hoffman, Tsai-Wu, Lee and Hashin failure criteria in the study of composite plates. In the use of the Maximum stress, Lee and Hashin failure criteria, the failure mode was readily determined. For the Hoffman and Tsai-Wu failure criteria, the various proportions of direct and transverse fiber and matrix contributions were examined to determine the mode of failure. Once the failure mode was determined, the appropriate stiffness relations were modified. As the calculated loads and therefore the stresses exceed the failure criteria, the appropriate element stiffness relations were reduced. After a failure has been reached and the appropriate stiffness reduced, the

43

lamina stresses are recalculated with the new global stiffness relations in order to calculate further material failures. The sequence continued until no more failure occurs at the prescribed load. Final ply failure was assumed to have been reached when all lamina moduli have been reduced to zero at a given (x,y,z) coordinate. Results indicate that the Lee criteria gave the best results, with first ply failure and last ply failure enveloping the true structural limitations.

Hwang and Sun [17] analyzed laminated composite panels under uniaxial tension using a three dimensional finite element method. Failure criterion, in the form of the Tsai-Wu theory, was used to investigate three forms of failure; fiber breakage, matrix cracking and delamination. The first ply failure load is solved for using an iterative mixed field technique to solve the linear portions of the finite element Eqns.. A Newton-Raphson iterative technique was employed to solve the nonlinear finite element Eqns. for the progressive analysis. Progressive analysis is accomplished using stiffness reduction as failures occur. Analytic results indicate reasonably good correlation with experimental results for both notched and unnotched tensile specimens.

Gummadi and Palazotto used a geometrically nonlinear finite element method based upon the total Langragian approach to investigate progressive failure in laminated beams and arches [13] and composite cylindrical shells [12]. The finite element method allowed for both large displacements and large rotations. Finite element discretization was based upon twelve degree of freedom elements. The load carrying abilities of various structures were considered after first ply failure. Failure relations based upon 2nd Piola Kirchoff stresses and large strains were considered. In the investigation of beams and arches three failure criterion were utilized in the analysis: Lee, Hashin and maximum stress. Results indicated significant residual strength after first ply failure. Failure modes included fiber breakage, matrix cracking and delamination for all but the Hashin failure theories. Progressive loading calculated using Hashin criteria were the most conservative. Hashin, Lee and maximum stress failure criteria were again examined in the analysis of composite

44

cylindrical shells. Changes to the elasticity relations allowed for the analysis of asymmetrical failure. Results indicated significant load carrying capability after first ply failure for certain lamina considered.

Lee [21] developed a three dimensional finite element method for the analysis of failure in layered fiber reinforced composite lamina. His algorithm allows for the calculation of element stresses, failure modes, damage accumulation and lamina ultimate strength. Three damage modes were considered, fiber breakage, matrix failure and delamination. With the occurrence of failure, total reduction of the appropriate stiffness relations was accomplished. Numerical analysis was accomplished on various specimen configurations under several loading cases. Results indicate limitations in the program. Due to the relative coarseness of the meshes considered, delamination while logically expected, was never experienced. Given the early nature of the study and limited computing resources, trade-offs in finite element studies were necessary.

Eason and Ochoa [9] developed a shear deformable element for ABAQUS[R], capturing three dimensional states of stress and damage progression in composites. This allows an ABAQUS[R] user to analyze damage progression in a composite structure through a readily available commercial finite element package. The user defined element allows for the analysis of damage progression by comparing the calculated stresses to several failure theories. The failure modes considered for the research were fiber breakage, matrix cracking and delamination. Subroutines allowed the user to choose from Hashin, Greszczuk, maximum stress, Lee and Ochoa criterion for each mode of failure. Stiffness reduction took place as the stresses calculated at the element Gaussian points exceeded the failure criteria on a ply-by-ply basis. Analysis of composite plates with a center-through hole or center delamination yielded good results when compared with experimentation. Excellent correlation was also observed between the user defined element and the ABAQUS[R] shell element (S8R5).

45

Moas and Griffin [25] developed a methodology for the analysis of progressive damage in thin structures undergoing large deformations based on a finite element theory that accounts for geometric and material nonlinearitites. An iterative solution process based upon the Newton-Raphson technique converges to an updated load, and therefore the stresses. The stresses are then compared with the maximum strain or Tsai-Wu failure criteria. An experimental investigation, examining a six foot diameter arch, representative of a rotorcraft stiffener, provided a direct comparison with the analytical solution. The finite element method accurately predicted the arch failure point and the residual stiffness after failure for both the maximum strain and Tsai-Wu failure criteria.

Sleight, et al [38] devised a progressive failure analysis method based upon classical theory using C^1 plate and shell elements. Again, a Newton-Raphson solution technique was employed to solve the nonlinear Eqns. for either an applied load or displacement situation. Hashin, Christensen and maximum strain failure criteria were compared with the converged stresses. If the stresses were calculated to cause failure, either an instantaneous or gradual reduction technique was employed. Analytical analyses were carried out on two specimens which are common in experimental studies. Results indicate good comparison with experimental data and the overprediction of the final failure load for all criterion considered.

Kim and Hwang [19] used a penalty finite element method to analyze the progressive failure of pin-loaded laminated composites to predict the failure strengths and failure modes. Pin loaded composites are becoming increasingly important in aerospace structures. Three failure modes were considered for the pin-loaded analysis; tension, shear-out and the bearing mode. The tension and shear-out modes were taken to be caused by tensile and shear stresses respectively, and the bearing failure mode caused by compressive stresses. Therefore, the two failure mechanisms considered for this research, or fiber breakage and matrix cracking, were analyzed using Hashin failure criteria.

46

When failure occurred, the appropriate stiffness terms were reduced to zero. For the plane stress cases considered, results indicate excellent correlation with experimental data.

Kim and Hong [18] incorporated macroscopic failure criteria into a two dimensional finite element method in an effort to analyze progressive failure in composite laminates with stress concentrators. Fiber and matrix failure modes as well as appropriate stiffness reduction were considered using fiber bundle failure and a shear lag analysis respectively. Results indicate good results for flat composite laminates without a hole. Analytical results for laminates with a hole yielded the state of stress, ultimate strength, the extant of damage and matrix crack density.

Tan and Perez [41] also considered the progressive failure analysis of a composite laminate with a hole under compressive loading. In-plane failure modes in the form of fiber breakage and matrix cracking were evaluated using a lamina based fiber failure criteria and the Tsai-Wu criteria respectively. Stiffness reduction took place using stiffness degradation factors, "D_i" which were treated as material constants during the analysis. If matrix failure occurred at a particular load increment, the element stiffness was reduced and the load was incremented. If, on the other hand, fiber failure occurred, the element stiffness was reduced, the stress distribution was recalculated resulting in a recheck of fiber failure. The procedure was continued until fiber failure was no longer detected, and the next load increment was examined. Results in the form of failure mechanisms and ultimate strengths compared reasonably well with experimental results.

Tan [40] developed a progressive failure finite element method to analyze damage progression, stress-strain states and ultimate strength in composite laminates under tensile loading containing openings in the form of a central hole. Unique in this study of progressive failure analysis, was the inclusion of environmental effects in the form of thermal residual stresses and the stresses due to moisture content. Similar to the author's previous research, fiber and matrix in-plane failure modes were considered using Tsai-Wu failure criteria. Again the constant stiffness degradation factors,

47

"D_i" were used to reduce element stiffness. If matrix failure occurred, new element stiffness relations were calculated using the stiffness degradation factor. Subsequent failures at that load were not considered. If fiber failure occurred, element stiffness reduction was accomplished and subsequent failures were considered before the load was incremented. Experimental comparisons indicate good correlation with stress-strain states, ultimate strengths and damage progression.

Youngchan, Davalos and Barbero [20] developed a progressive failure model for laminated composite beams using a beam finite element considering layer-wise constant shear. Maximum stress and Tsai-Wu failure criteria were used to evaluate fiber breakage and matrix cracking. The element stiffness relations were reduced using degradation factors. The degradation factors were chosen using parametric studies and by analytic comparison with experimental results. If either fiber or matrix failures were discovered, element stiffness reduction took place using the degradation factors and then subsequent failures were checked for prior to a new load increment being accomplished. Good results based on stiffness degradation and failure criteria were achieved in the prediction of progressive failure and ultimate load, although the ultimate displacement varied as much as 30% from experimental results.

Reddy, Dakshina Moorthy and Reddy [32] analyzed progressive failure in composite plates using various independent and polynomial failure criteria incorporated into a three dimensional finite element method. The authors considered stiffness reduction directly proportional to structural discretization. In other words, instead of reducing an element's stiffness to zero irrespective of the element size, a gradual reduction method was used. Therefore, the element stiffness was reduced incrementally until no further failures occurred at a particular loading. Parametric studies were accomplished using various gradual stiffness reduction percentages.

For the present research, progressive failure criterion was incorporated into the SLR theory for the purpose of studying failure characteristics of composite lamina and sandwich composite

48

structures. As will be explained in greater detail in further chapters, stresses were determined at the Gaussian points within the elements of the discretized plate or shell structure. The stresses were then compared with the previously mentioned failure criterion of Eqns. 49-52. If the various failure criterion were determined to have been satisfied, in other words if the boundaries of the state of stress had been exceeded, then a reduction in stiffness was made. Since the chosen failure criterion allowed the user to distinguish between various failure modes, the appropriate constitutive coefficients were reduced to a nominal value within the respective ply, on an element-by-element basis. Once the constitutive relations were modified, equilibrium was again reached for the same load condition in order to investigate subsequent failures. When further failures no longer occurred, the displacement increment process continued.

Chapter 3 - SLR Modifications

There were several major modifications made to the SLR finite element method. First, the tangent stiffness relations were expanded to include the possible effects of asymmetrical failure. Next, the failure criteria of Eqns. 49 through 52 was added to the SLR program. Coincident with the addition of the failure criteria, the element constitutive relations were modified to allow for stiffness reduction as failure occurred. Throughout the modification process, various updates were incorporated into the program in order to facilitate the previously mentioned changes.

3.1 Elasticity Arrays

As mentioned in Chapter 2, the SLR method was originally formulated to analyze only symmetric plate and shell structures. For the case of composites, this is a satisfactory assumption if symmetric laminates are the primary focus of the research. However, with the inclusion of failure criteria, symmetry may no longer be an accurate assumption. A composite laminate or sandwich composite plate or shell can experience varying stresses throughout the thickness. This variance in stress can be further aggravated as the thickness of the composite structure increases and failures result. As failures occur in a composite structure, asymmetry can result if a ply fails on either the top or bottom surface and the corresponding symmetrical ply does not fail. For that reason, the SLR program required modification to include the elasticity arrays in the stiffness matrices.

Having explained the need to include the elasticity arrays, and described in detail the procedure undertaken to arrive at the desired repeatability of the elasticity arrays and hence the tangent stiffness arrays, the B_{ij}, E_{ij}, G_{ij}, I_{ij}, K_{ij}, P_{ij}, and S_{ij} arrays were added to the appropriate tangent stiffness terms in the SLR program. Incorporating the elasticity arrays into the tangent stiffness Eqn. resulted in literally hundreds of 18x18 arrays, given the required matrix format. Subsequently, a means was needed to carry out the manipulation given time and resource constraints.

50

Therefore, the symbolic mathematical manipulator, MATHEMATICA, was chosen for the process. Using the MATHEMATICA program and the relations for the repeatable tangent stiffness arrays of Eqns. 31-33, with the respective changes noted in Eqns. 34-36, the necessary development was carried out.

The MATHEMATICA program was specifically chosen due to the sheer size of the arrays incorporated in the previously discussed elasticity relations. MATHEMATICA allowed the author to assemble the literally hundreds of element-independent arrays with relative ease and furthermore, express the output in Fortran format for immediate inclusion into the SLR program. The B_{ij}, E_{ij}, G_{ij} and I_{ij} arrays were added to the $\widehat{K}$ stiffness matrix, and the B_{ij}, E_{ij}, G_{ij}, I_{ij}, K_{ij} and P_{ij} arrays were added to the $\widehat{N}_1$ stiffness matrix. Because of the sheer size of the arrays and the resulting thousands of lines of code, only the first four arrays, or the B_{ij}, E_{ij}, G_{ij} and I_{ij} were included in the $\widehat{N}_2$ stiffness matrix. Even without the last three elasticity arrays, or K_{ij}, P_{ij}, and S_{ij}, included in $\widehat{N}_2$, the total lines of code added to the SLR program exceeded 25,000. The input file used to generate the changes made to the $\widehat{K}$ stiffness matrix is included in Appendix B.

3.2 Failure Criterion

The importance of failure criteria in the design process can not be overstated. When used properly and conservatively, failure criteria can provide an engineer a powerful tool used in the design process. The proper addition of failure criteria into a finite element method can lend realism to a structural analysis. For many composite structural analyses, finite element methods are the only means of investigating the structural response other than an experimental investigation. This is due to the complex nature of a composite structure with multiple plies, arrayed in multiple orientations. Therefore, the addition of failure criteria into a finite element method investigating composite struc-

tures can give designers a multitude of information in a reasonable amount of time and for limited resources.

3.2.1 Assumptions

There were several assumptions made during the addition of failure criteria as a result of SLR assumptions, material property limitations, or for general simplification purposes. As described in Chapter 2, the SLR theory makes several assumptions regarding the thickness of the structure and the resulting kinematics, the effect of the transverse shear strains relative to the in-plane strains and stresses, and the importance of the transverse direct stress. Finally, a discussion will be made with respect to several general finite element method simplifications.

The SLR theory takes advantage of a shell's relative thinness with respect to the width or span of the panel. Therefore, the SLR kinematics describe the transverse displacements relative to the midsurface of the shell. Because of this simplification, the transverse location of the Gaussian points and therefore the location of the stress calculations is carried out at the midsurface of each lamina. All stress calculations, including those used to calculate delamination failure, also occur at the midpoint of each ply or lamina. Therefore the stresses are considered to be intraply as opposed to interply, or at the interface between two plies.

Because of the previous assumption, i.e., a thin panel in an approximate state of plane stress, the transverse direct stress, σ_z, is taken to be zero. This implies that the in-plane stress-strain effects will dominate the response. Palazotto and Dennis [27] accounted for this assumption by showing that σ_z was small when compared to the transverse shear stresses in thin plates and shells. This assumption, however, loses accuracy as thickness increases, i.e., as more plies are considered or for sandwich panels, and the problem essentially becomes three dimensional. Furthermore, this leaves the transverse shear calculations as the only means of calculating any form of transverse fail-

52

ure. Also, the transverse shear strain-displacement relations were assumed linear, and the resulting transverse shear stress was parabolic through the thickness. The combination of the zero transverse direct and parabolic transverse shear stress assumptions will affect the accuracy of the progressive failure calculations. While these assumptions may not have a significant affect on thin, composite analyses, this may have a great affect on composite sandwich analysis. Remember, sandwich composite panels rely on the sandwich core to provide significant transverse shear resistance, while the facesheets provide the majority of the bending resistance. These assumptions leave the parabolic transverse stress calculations as the only means of approximating core failure.

The SLR theory considers geometric nonlinearity, while material linearity is assumed. Material linearity assumes the material stress-strain behavior remains linear prior to yielding. Geometric nonlinearity and therefore the SLR theory allows for large displacements, but only small to moderate rotations. The displacements and ultimately the stresses calculated from the SLR kinematics lose accuracy for larger midsurface rotations, as the slope $w_{,1}$ can not by itself accurately represent the elastic curve. The result is a response that is stiffer than in reality. Specifically, when investigating composite shells, which as will be shown later can undergo significant rotations, the small angle assumption loses accuracy.

A final assumption of the SLR theory is the use of Green's strains and 2nd Piola Kirchoff stresses. The failure criteria as written in Eqns. 49, 50, 51 and 52 require the use of the Eulerian stresses. There was no conversion undertaken between the 2nd Piola Kirchoff stresses and Eulerian stresses, thereby assuming that the strains considered in this analysis were small.

3.2.2 Program Logic

The SLR program was separated into three components, the pre-processor, processor and the post-processor, as shown in Fig. 8. The pre-processor has several functions. First the program
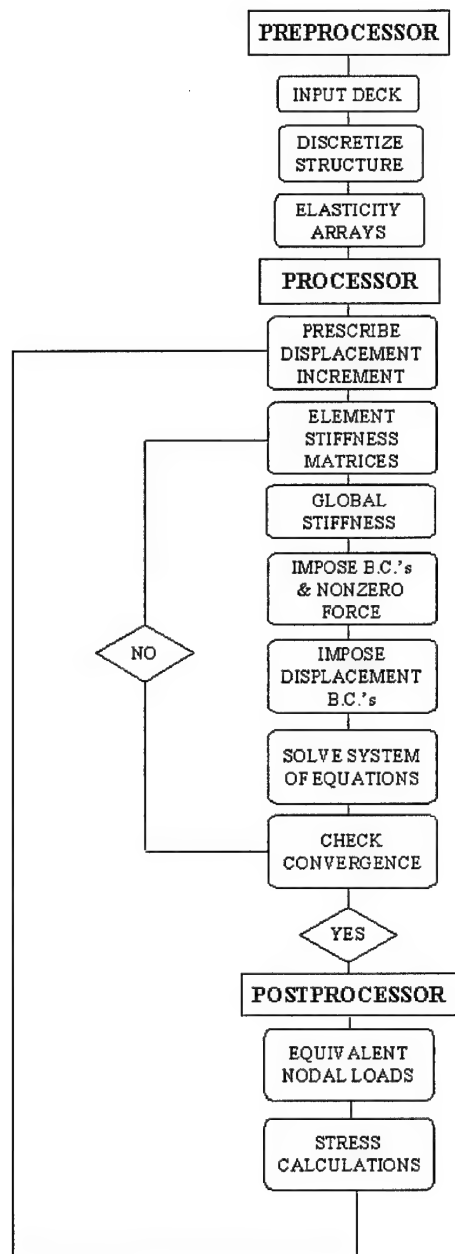
Figure 8. SLR program flowchart without failure criteria

54

receives an input file from the user. Included in the input file, are the panel geometry, element type and size, prescribed displacements and forces, number of plies and orientation, and material properties. The pre-processor takes geometric inputs, discretizes the structure, and calculates elasticity arrays. The processor portion of the program solves the algerbraic system of Eqns. (Eqn. 27), using the Newton-Raphson solution method and the user specified convergence criteria. First, the processor prescribes a displacement, and using the previously calculated elasticity arrays, the elemental stiffness is calculated. The element stiffness is summed over the discretized structure in order to attain the global stiffness. The importance of the desired repeatability in the tangent stiffness should now be readily apparent. Once the global stiffness is calculated, the boundary conditions, prescribed forces and displacement boundary conditions are imposed. Next, the previously mentioned system of equations is solved, resulting in an updated displacement vector. If convergence has not been reached, the process is repeated until convergence is achieved. If, on the other hand, convergence has been reached, the program shifts to the post-processor. The job of the post-processor is to calculate the nodal loads and elemental stresses. Once the loads and stresses are calculated, a new displacement increment is prescribed.

The majority of the modifications made to the SLR program took place in the STRESS subroutine of the post-processor. A guide to the SLR program along with a sample input deck are included in Appendix C, and the STRESS subroutine is included in Appendix D. The STRESS subroutine, as the name implies, calculates the stresses in the discritized structure. Once the SLR program achieves equilibrium with respect to the displacements, the STRESS subroutine is called for each element in the structure. Stresses are calculated at the four outermost Gaussian points of each element. There are two nested loops used to calculate the stress in every element. Starting with the first element, at the top layer or most negative distance in the transverse direction, the stress is calculated at the each of the outer four Gaussian points. The stresses are then calculated

through the thickness towards the bottom most layer. Once the stresses at each Gaussian point for all lamina at that particular element are calculated, the procedure is repeated for all elements in the structure.

3.2.3 Failure and Stiffness Reduction

Failure criteria was added to the post-processor segment of the program as shown in Fig. 9. The stresses calculated at the four outermost Gaussian points were transformed into the material axis system and compared with the user specified failure criteria, where fiber, matrix and delamination failure were examined. Failure was assumed to occur at the end of each displacement increment. For that reason, the displacements were kept relatively small. If the elemental transformed stresses exceeded the respective failure criteria at a given "n" ply, then a stiffness reduction was accomplished. For the purposes of this research, a total reduction method was implemented. For each Gaussian point that failed, the appropriate stiffness components of that particular element ply were reduced by 25%. When all Gaussian points in an element failed, the stiffness was reduced to a residual value, again on a ply basis. Initial analysis indicated that to reduce the elemental stiffness to zero instead of a residual value resulted in computational difficulties. As mentioned previously, the choice of the maximum stress, Hashin and Lee failure criteria allowed for the prediction of the type of failure. Leaving a residual value allowed the analysis to continue until significant strength was lost in the lamina. Once the elemental stiffness reduction took place, a new equilibrium configuration was considered without prescribing a new displacement. This allowed for the calculation of subsequent failures as a result of the initial failure and resulting lamina stiffness reduction. The result of this technique was seen as a load drop for a displacement control analysis, or a displacement drop for a load control analysis. When no further failures occurred, a new displacement increment was prescribed and the analysis continued.

56
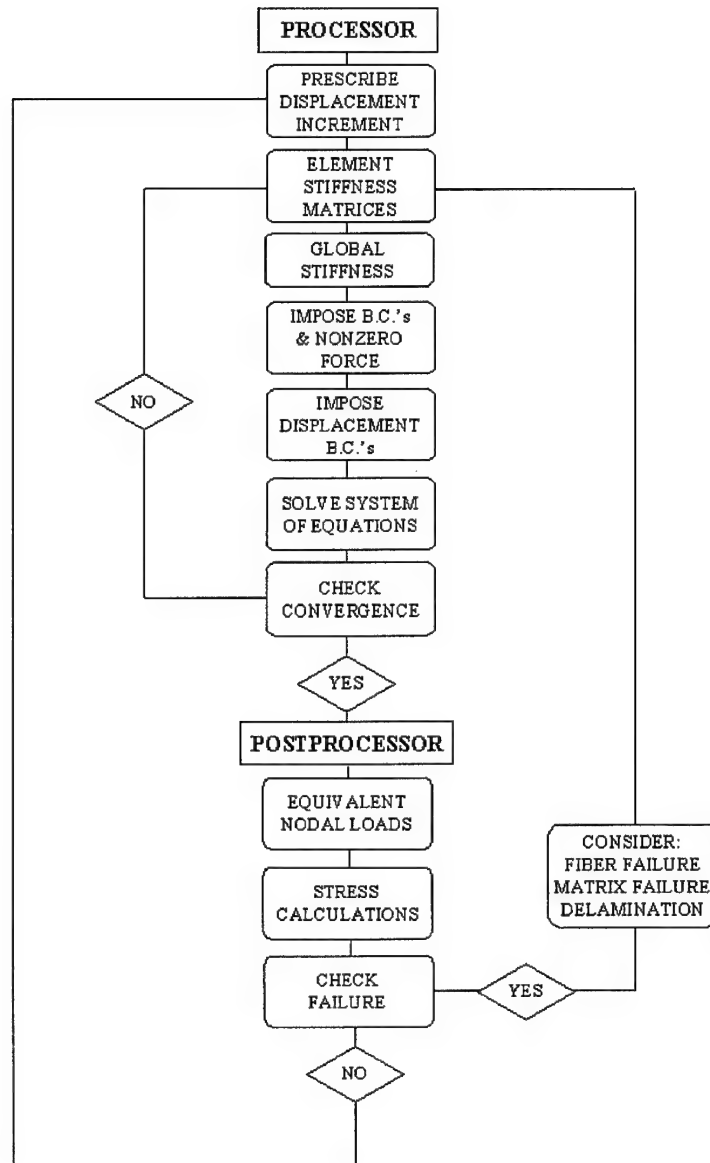
Figure 9. SLR program flowchart considering failure

3.2.3.1 Fiber Failure

Prior to any occurrence of failure, the ply materials were assumed linearly elastic and orthotropic. Therefore, the reduced k^{th} ply stress-strain relations, written in the local or material ply coordinate system is as follows:

$$\begin{bmatrix} \sigma_1 \\ \sigma_2 \\ \sigma_6 \end{bmatrix}^k = \begin{bmatrix} Q_{11} & Q_{12} & 0 \\ Q_{12} & Q_{22} & 0 \\ 0 & 0 & Q_{66} \end{bmatrix}^k \begin{bmatrix} \varepsilon_1 \\ \varepsilon_2 \\ \varepsilon_6 \end{bmatrix}$$

$$\begin{bmatrix} \sigma_4 \\ \sigma_5 \end{bmatrix}^k = \begin{bmatrix} Q_{44} & 0 \\ 0 & Q_{55} \end{bmatrix}^k \begin{bmatrix} \varepsilon_4 \\ \varepsilon_5 \end{bmatrix} \tag{53}$$

Fiber failure, defined by the following relations:

Maximum stress crtierion:

$$\sigma_{11} \geq \sigma_{FN}$$

Lee criterion [9]:

$$\left(\sigma_{12}^2 + \sigma_{13}^2\right)^{\frac{1}{2}} \geq \sigma_{FS}$$

Hashin criterion [9], [14]:

$$\left(\frac{\sigma_{11}}{\sigma_{FN}}\right)^2 + \frac{\left(\sigma_{12}^2 + \sigma_{13}^2\right)}{\sigma_{FS}^2} \geq 1 \tag{54}$$

occurred when the stresses calculated at the element Gaussian points exceeded the failure envelope defined for fiber failure by the maximum stress, Hashin and Lee criteria. Fiber damage tends to soften the material properties [15]. In order to simulate that softening of the lamina, the constitutive coefficients Q_{11}, Q_{12}, Q_{44} and Q_{66} were reduced. It should be noted that the constitutive relations that were reduced, were the constants in the material axis, or the Q_{ij} terms, and not the constitutive relations in the shell axis system, or $\widehat{Q}_{ij}$. Prior to the failure of all four of the outer Gaussian points, the coefficients Q_{11}, Q_{12}, Q_{44} and Q_{66} were reduced incrementally for that particular element. In

58

other words, the respective constitutive relations for that element were reduced by 25% for the failure of each Gaussian point. When total failure for the fibers, or all four of the outer Gaussian points exceeded the fiber failure envelope, the relations were reduced to a residual value. After all of the Gaussian points within an element had failed and the appropriate stiffness reduction had taken place, the resulting constitutive relations were represented as:

$$
\begin{bmatrix} \sigma_1 \\ \sigma_2 \\ \sigma_6 \end{bmatrix}^k = \begin{bmatrix} 0 & 0 & 0 \\ 0 & Q_{22} & 0 \\ 0 & 0 & 0 \end{bmatrix}^k \begin{bmatrix} \varepsilon_1 \\ \varepsilon_2 \\ \varepsilon_6 \end{bmatrix}
$$
$$
\begin{bmatrix} \sigma_4 \\ \sigma_5 \end{bmatrix}^k = \begin{bmatrix} Q_{44} & 0 \\ 0 & 0 \end{bmatrix}^k \begin{bmatrix} \varepsilon_4 \\ \varepsilon_5 \end{bmatrix} \tag{55}
$$

In order to provide some understanding into the rationale behind the stiffness reduction, consider the following fiber failure example. If each of the Gaussian points in a ply, for an element, exceeded the fiber failure envelope, then as was just mentioned, the entire elemental stiffness properties related to the fiber were equated to a nominal value. If fiber breakage was the only failure detected at the Gaussian points, then the ply would continue to provide strength through the stress-strain relations of Eqn. 55, i.e., σ_2, or the in-plane stress perpendicular to the fibers, and the transverse stress σ_4 is not zero for that particular element within the ply considered.

3.2.3.2 Matrix Failure

If the stresses calculated at the Gaussian points exceeded the failure envelope defined by the following relation for matrix failure in tension:

Maximum stress crtierion:

$$\sigma_{22} \geq \sigma_{MNT}, \ (\sigma_{22} > 0)$$

Lee criterion [9]:

59

$$\left(\sigma_{12}^2 + \sigma_{23}^2\right)^{\frac{1}{2}} \geq \sigma_{MS}$$

Hashin criterion [9], [14]:

$$\frac{1}{\sigma_{MNT}^2}\left(\sigma_{22} + \sigma_{33}\right)^2 + \frac{1}{\sigma_{MS}^2}\left(\sigma_{23}^2 - \sigma_{22}\sigma_{33}\right) +$$
$$\frac{1}{\sigma_{FS}^2}\left(\sigma_{12}^2 + \sigma_{13}^2\right) \geq 1,\ \left(\sigma_{22} + \sigma_{33}\right) > 0 \tag{56}$$

or the following relation for matrix failure in compression:

Maximum stress crtierion:

$$\sigma_{22} \geq \sigma_{MNC}$$

Lee criterion [9]:

$$\left(\sigma_{12}^2 + \sigma_{23}^2\right)^{\frac{1}{2}} \geq \sigma_{MS}$$

Hashin criterion [9], [14]:

$$\frac{1}{\sigma_{MNC}^2}\left[\left(\frac{\sigma_{MNC}}{2\sigma_{MS}}\right)^2 - 1\right]\left(\sigma_{22} + \sigma_{33}\right) + \frac{1}{4\sigma_{MS}^2}\left(\sigma_{22} + \sigma_{33}\right)^2 +$$
$$\frac{1}{\sigma_{MS}^2}\left(\sigma_{23}^2 - \sigma_{22}\sigma_{33}\right) + \frac{1}{\sigma_{FS}^2}\left(\sigma_{12}^2 + \sigma_{13}^2\right) \geq 1,\ \left(\sigma_{22} + \sigma_{33}\right) < 0 \tag{57}$$

then matrix failure was assumed to have occurred. Again it should be noted that σ_{33}, or the transverse direct stress was neglected. Matrix failure or cracking also softens the lamina [15]. In order to simulate the softening of the lamina, the constitutive coefficients Q_{22}, Q_{12}, Q_{55} and Q_{66} were equated to zero for each of the Gaussian points in each of the plies where matrix failure had occurred. As with the fiber failure, reducing the coefficients of one Gaussian point reduces the appropriate element constitutive relations by 25% on a ply basis. Once total failure had occurred,

60

or matrix failure had occurred for all Gaussian points, the constitutive coefficients Q_{22}, Q_{12}, Q_{55} and Q_{66} were reduced to a nominal value resulting in the following lamina stress-strain relations:

$$\begin{bmatrix} \sigma_1 \\ \sigma_2 \\ \sigma_6 \end{bmatrix}^k = \begin{bmatrix} Q_{11} & 0 & 0 \\ 0 & 0 & 0 \\ 0 & 0 & 0 \end{bmatrix}^k \begin{bmatrix} \varepsilon_1 \\ \varepsilon_2 \\ \varepsilon_6 \end{bmatrix}$$

$$\begin{bmatrix} \sigma_4 \\ \sigma_5 \end{bmatrix}^k = \begin{bmatrix} 0 & 0 \\ 0 & Q_{55} \end{bmatrix}^k \begin{bmatrix} \varepsilon_4 \\ \varepsilon_5 \end{bmatrix} \tag{58}$$

Again, the ply could continue to provide strength, as σ_1 and σ_5 were not equated to zero. One can see that if total fiber and total matrix failure occurred for all of the Gaussian points within an element on a ply basis, the total stiffness was effectively removed, as Q_{11}, Q_{22}, Q_{12}, Q_{44}, Q_{55} and Q_{66} were reduced to a residual value.

3.2.3.3 Delamination

In the event the stresses calculated at the Gaussian points exceed the failure envelope defined for delamination in the following Eqns.:

Maximum stress criterion

$\sigma_{13} \geq \sigma_{DS}$ or $\sigma_{23} \geq \sigma_{DS}$

Lee criterion [9]:

$\left(\sigma_{12}^2 + \sigma_{23}^2 \right)^{\frac{1}{2}} \geq \sigma_{DS}$

Hashin criterion [9]:

$$\left(\frac{\sigma_{33}}{\sigma_{ZN}} \right)^2 + \frac{\sigma_{12}^2 + \sigma_{13}^2}{\sigma_{DS}^2} \geq 1 \tag{59}$$

61

interply delamination was assumed to have occurred. Again, note that σ_{33} was neglected. Interpreting delamination failures using this method was accomplished in the following manner. If an intraply delamination for the nth ply occurred, then an interply delamination was assumed to have occurred at the interface of the nth ply and the $n^{th}\pm1$ plies. However, the stiffness reduction only took place in the nth ply. In other words, the $n^{th}\pm1$ plies continued to maintain transverse stiffness. For the nth ply, delamination resulted in the reduction of the constitutive relations Q_{44} and Q_{55}. In a manner similar to the fiber and matrix stiffness reductions, the reduction of each Gaussian point equated to a 25% reduction of Q_{44} and Q_{55} for that element within the ply in question. Total reduction resulted in the removal of all transverse elemental strength, again for the element within the ply considered, as the element stiffness was assigned a residual value. The resulting lamina stress-strain constitutive relations for an element whose outer Gaussian points had failed and thereby resulting in the reduction of Q_{44} and Q_{55} are expressed in the following relations:

$$
\begin{bmatrix} \sigma_1 \\ \sigma_2 \\ \sigma_6 \end{bmatrix}^k = \begin{bmatrix} Q_{11} & Q_{12} & 0 \\ Q_{12} & Q_{22} & 0 \\ 0 & 0 & Q_{66} \end{bmatrix}^k \begin{bmatrix} \varepsilon_1 \\ \varepsilon_2 \\ \varepsilon_6 \end{bmatrix}
$$
$$
\begin{bmatrix} \sigma_4 \\ \sigma_5 \end{bmatrix}^k = \begin{bmatrix} 0 & 0 \\ 0 & 0 \end{bmatrix}^k \begin{bmatrix} \varepsilon_4 \\ \varepsilon_5 \end{bmatrix} \tag{60}
$$

3.2.3.4 Core

The sandwich core was treated as an orthotropic lamina, oriented 0^0 from the SLR panel axis system as shown in Fig. 5. The core was divided into five layers, thereby allowing the elasticity relations and tangent stiffness calculations to be accomplished in the same manner as they were for the face sheets. To put it another way, each core layer was treated as a simple lamina. The purpose of the core in any sandwich composite is to provide transverse direct and shear stiffness, while the face sheets provide the panel bending resistance. Since the core is designed to provide transverse

62

and not in-plane strength, the core was treated in a slightly different manner than the facesheets. Several assumptions were required when modeling the core. Since the transverse direct stress was neglected, the resulting core transverse stiffness was completely modeled by the transverse shear strength. Therefore, the primary core failure mode, core shear failure, was modeled by the transverse shear strengths. Second, delamination was obviously not a factor in the core "layers", so the delamination failure was considered as a transverse shear failure, and thus still included in the analysis. The maximum stress, Hashin and Lee failure criterion were evaluated in the same manner for the core as they were evaluated for the facesheets. In other words, the transverse components of each of the respective criteria was evaluated for the core "layers". Once a transverse core failure occurred, or the transverse failure envelopes for either the maximum stress, Hashin or Lee criteria were exceeded, the entire core stiffness at that point was reduced. Since the core "layers" were treated in the same manner as the facesheets, the stiffness reduction took place in the same manner as was conducted in the facesheets. Since the facesheets primarily provide the bending stiffness while the core resists transverse stress, the in-plane strength contribution of the core was assumed negligible as compared to the transverse strength. Therefore, the following stiffness reduction took place. For an elemental transverse core failure at a particular Gaussian point within a given layer, all of the constitutive properties for that point were removed, which differs from the facesheet or general composite lamina stiffness reduction. For example, for fiber failure calculated at all Gaussian points for a particular element within a given ply, the in-plane constitutive coefficients Q_{11}, Q_{12}, Q_{66} and Q_{55} were reduced to a residual value. To reiterate, due to the greater significance of the transverse strength, when a core failure occurred, all of the respective constitutive coefficients, or Q_{11}, Q_{22}, Q_{12}, Q_{66}, Q_{44} and Q_{55} were reduced within that layer.

Chapter 4 - Results and Discussions

The purpose of this research was to gauge the accuracy and applicability of the existing SLR finite element analysis code, with and without the addition of failure criteria, as well as examine the modeling of composite sandwich panels. Prior to the addition of the failure criteria, a comparison was made between the SLR finite element method, a preexisting experimental study, and the commercial finite element program, ABAQUS$^{\circledR}$. The initial intent of the comparison was to gauge the accuracy of the code, and therefore the relative merits placed upon those results and the results of future SLR program modifications. The accuracy of the results led to an understanding of the SLR methodology and its applicability as a structural analysis tool. Once the accuracy and applicability of the code was established, the effect of progressive ply damage was included within the SLR finite element method. With the addition of failure criteria, a comparison was once again made with the experimental results. Finally, an analysis of a sandwich composite shell took place, both with and without failure analysis considered, to examine the various effects of the sandwich core and the core stiffness reduction.

4.1 Composite Panels without Failure Analysis

Due to the simplifying assumptions made in the development of the SLR finite element method, an analysis was needed to determine how the SLR results would compare to actual experimental results. It should be noted that initial comparisons were made for accuracy purposes only. In other words, progressive failure analysis was not considered. As will be discussed shortly, a general case was considered for the purposes of creating an SLR baseline. The results were compared with both the commercial finite element program ABAQUS$^{\circledR}$, as well as experimental data [44]. This general case was also reexamined with progressive failure and compared with experimental data in order to examine how the stiffness reduction compared.

64

The accuracy and applicability of the code was examined through a comparison of published experimental test data [44] with results generated using the existing finite element code. Various composite shell configurations were considered, however an exhaustive comparison effort was not undertaken. In other words, only sample shell configurations meant to represent extreme cases were modeled using the SLR FEM. Two geometric shell variables, thickness and radius, were analyzed with the SLR FEM. Of great importance in any analysis using the SLR FEM, was the effect of panel thickness. The SLR theory enforces zero direct stress through the thickness and neglects the higher order transverse Green's strain-displacement terms, for the purposes of modeling the transverse shear effects. The accuracy of this assumption was reduced as the thickness of the panel increased. Therefore, an analysis of panel thickness was performed. The effect of shell radius versus span was also investigated. The shell radius and span dimensions determine whether or not a cylindrical shell is shallow or deep. The SLR theory assumes small to moderate rotations, and since the rotations a shell can undergo are affected by whether or not a shell is deep or shallow, an investigation was warranted.

4.1.1 Finite Element Formulation for a General Shell

Before discussing the results of the investigations, the process leading up to the final modeling configuration, or the boundary conditions, mesh refinement and discreization choices, needs to be reviewed. The general baseline shell case will be considered here as an example of the process used to formulate the input file for the SLR program. The experimental data, taken from Ref. [44], investigated the quasi-static and dynamic response of various plate and cylindrical composite panels. The experimentation included an investigation of three structural parameters, namely, shell radius, span and thickness. All specimens were constructed of AS4/3501-6 graphite/epoxy in $[\pm 45_n/0_n]_s$ $(n = 1, 2, 3)$ layup configurations. The material properties for AS4/3501-6 graphite/epoxy can

65

be found in Table 1 [24]. The specimens reviewed and compared with the SLR results included composite cylindrical concave and convex shells as well as composite plates under a quasi-static transverse center load. The convex composite shell specimens were tested in a rigid test fixture as shown in Ref. [44], with the axial edges in pinned/no in-plane sliding, or hinged boundary conditions. The axial edges are those edges in the "u" direction, as shown in Fig. 5. The circumferential edges, or the edges in the "v" direction in Fig. 5, remained free. The general case chosen as the baseline specimen was in a "R1T1S1" configuration, where "R" represents the shell radius, "T" represents the shell thickness and "S" represents the shell span. The "1" refers to the choice of geometric multiplier. The specimen layout is represented in Fig. 10, [44]. Simply put, it was the

$E_1 = 142\,GPa$
$E_2 = 9.7\,GPa$
$G_{12} = 6.0\,Gpa$
$G_{13} = 6.0\,Gpa$
$G_{23} = 3.6\,Gpa$
$\nu_{12} = 0.3$
$t_{ply} = 0.134\,mm$
$\rho = 1580\,kg/m^3$

Table 1. AS4/3501-6 ply properties

smallest and thinnest of the specimens considered by Wardle and Lagace [44]. The dimensions for the specimen radius, span and thickness were, 152, 102 and 0.804 mm respectively, with a ply layup for this configuration of $[\pm 45/0]_s$. It is important to note that, unless otherwise stated, the ply angle orientation is defined as shown in Fig. 10.

When modeling any composite panel, there are numerous modeling conditions available to the analyst, each of which can significantly affect the outcome of the analysis. For instance, the obvious finite element discretization approach would be to consider symmetry for the plate or shell panel. That is a reasonable choice if the panel considered was isotropic, orthotropic, or in the case of a composite, a cross ply laminate. Utilizing symmetry, or only considering one quadrant,
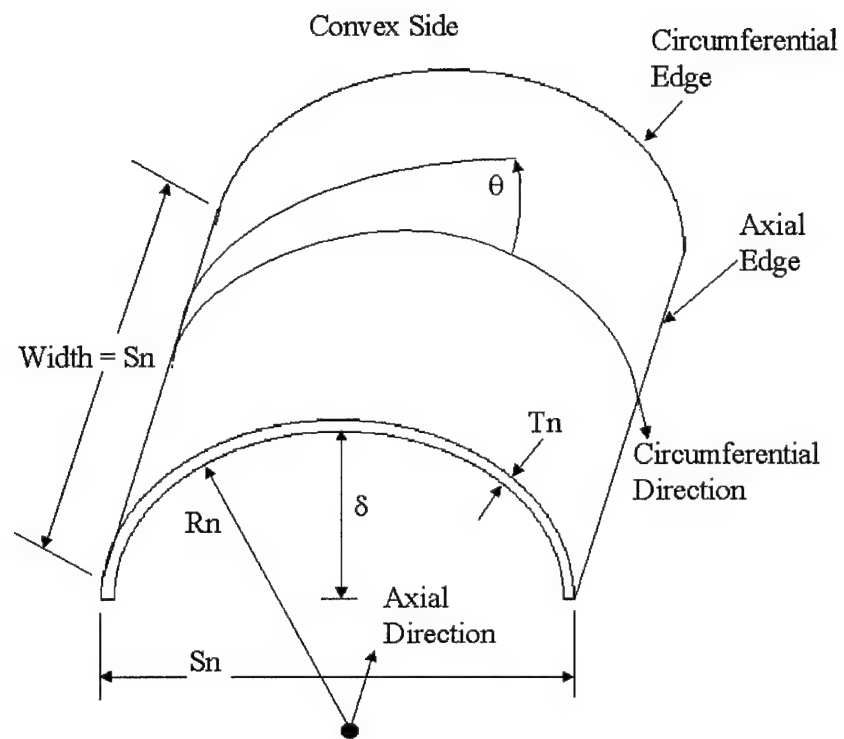
Figure 10. Illustration of a generic test specimen defining the radius, span, thickness and ply angle

allows the user to save computing time and resources, by reducing the number of elements, thus reducing the number of nodal displacement, load, and elemental stress calculations. For angle-ply laminates however, the D_{16} and D_{26}, or the laminate bending stiffness terms negate the biaxial symmetry assumption valid for the previously mentioned cases [27]. However, worst case analysis (±60 degree angle ply laminates) for a flat plate under uniform pressure, revealed a difference in quarter-panel maximum displacements of only 6% [27]. Results using the SLR finite element method indicate that modeling the entire panel will result in a stiffer response as shown in Fig. 11.
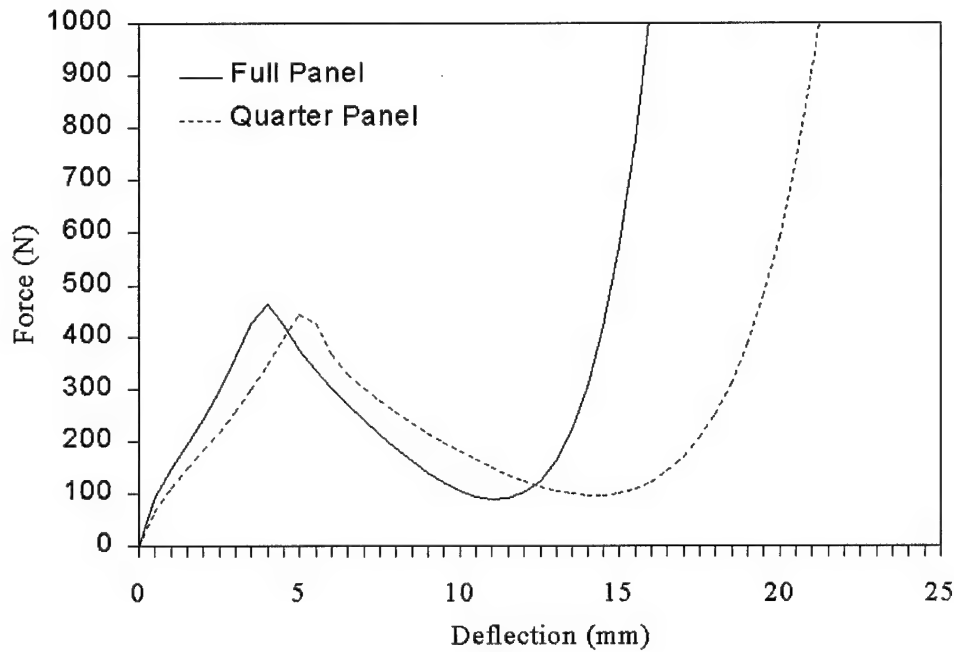
Figure 11. Full versus quarter panel finite element modeling

In other words, the same transverse panel deflection will result in greater calculated loads for a full panel model. The effects of asymmetry due to the angle ply layup can be seen in Fig. 12, which represents a topographical view of the shell's midsurface. The shell in Fig. 12 is experiencing the

68

Diagonal quadrants of
symmetry
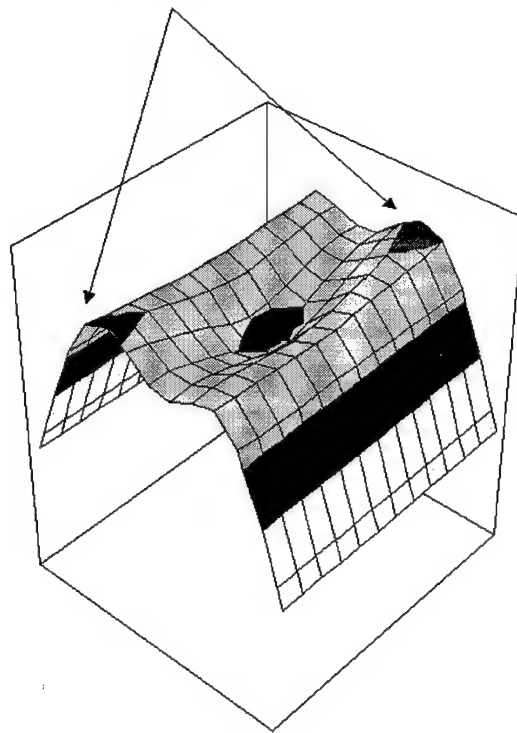
Figure 12. Asymmetrical effects of angle ply composite laminate

instability phenomenon known as snapping, which will be described in greater detail in subsequent sections. Fig. 12 represents a composite laminate without considering progressive failure analysis. A transverse direct point load has been applied in a displacement control analysis, the effect of which can be seen in the "depressed" center of the panel. The various shades of gray represent the elevation above the base or floor of the figure. For example, all of the elements within a specific shade of gray, are within the same elevation range. This coloring scheme was specifically used to examine the shell through its various stages of deformation. As shown in Fig. 12, the darkly shaded areas on the top surface diagonal quadrants represent a higher elevation than the other two diagonal quadrants. In other words, those darkly shaded diagonal quadrants at the top surface of the shell represent true symmetry for this composite, and specifically for the cases considered in this research. Even though the angle ply laminate modeling results can be expected to differ by as much as 6%, the choice was made to continue the analysis modeling the entire shell, as the effects of progressive failure were unknown.

There were many choices available with respect to the shell boundary conditions. There were seven degrees-of-freedom at each corner node: u, v, w, $w_{,1}$, $w_{,2}$, ψ_1 and ψ_2. In addition, there were four "mid-nodes" with the degrees-of-freedom, u and v. The convex composite shell specimens in the experimental analysis were tested in a rigid test fixture, with the axial edges in a pinned, no in-plane sliding condition. The initial choice for the SLR FEM analysis was to allow the axial edge degrees of freedom u, v, w, and ψ_1 to remain fixed. This condition fixed the rotation of a normal to the shell mid-surface in the "u" direction, but allowed for rotation in the "v" direction. At the time, this seemed the most logical approach to modeling the pinned/no in-plane sliding or hinged boundary conditions along the axial edges. Early results tracked the experimental data quite well, until reaching shell instability point. After reaching that critical shell snapping load, the SLR data achieved equilibrium only with a load sign reversal. Since the sign reversal of the force vector

70

was meaningless for this research, a new approach was required. Thus, the final configuration for experimental comparison purposes was settled upon. The boundary conditions ψ_1 and ψ_2 along both axial edges were fixed. The midsurface slopes, $w_{,1}$ and $w_{,2}$ were not fixed, although along the axial edges $w_{,1}$ was implicitly zero. Holding ψ_2 fixed was in essence equating the total midsurface rotation, or $w_{,2}$ to the midsurface shear rotation, or β_2. If both ψ_2 and $w_{,2}$ were fixed along the axial edge, then a condition of zero transverse shear stress would exist at those boundaries. With the final boundary conditions settled upon, results were stiffer, but continued to track the experimental data reasonably well, as will be discussed in subsequent sections. Likewise, after the critical snapping load or shell instability point, a load sign reversal was no longer required to achieve equilibrium. Initial results obtained while generating the final ABAQUS$^{\circledR}$ configuration yielded similar force results if the axial edge nodes were not maintained in a manner similar to the SLR configuration. The final boundary configuration, element numbering and SLR ply orientation angle for a $12x12$ mesh can be seen in Fig. 13.

A finite element convergence study was carried out for the general shell case using the previously mentioned boundary conditions. All cases used displacement controlled incrementation with a user specified displacement convergence criteria of 0.1%. The purpose of the convergence study was to balance the need for accuracy with computing time and memory restrictions. The results of the convergence study were used as a basis for the remainder of the SLR research, including the composite sandwich specimens. The full panel convergence study results are illustrated in Fig. 14. Just as using the pinned/hinged boundary conditions resulted in the load sign reversal, the same scenario resulted when the panel discretization was too coarse. An examination of Fig. 14 reveals a significant difference between the various mesh configurations. The coarsest mesh, the $8x8$ configuration, reached its respective critical snapping load at a transverse deflection of 5 mm, as opposed to 4.5 mm for the $10x10$, $12x12$ and $14x14$ configurations. At the critical snapping point,

71

Transverse Center Point Load
u & v Degrees of Freedom Fixed

Axial Edge
u, v, w, ψ_1,
ψ_2 Fixed

Axial Edge
u, v, w,
ψ_1, ψ_2 Fixed

Elements
1 - 12

Elements
133 - 144

θ
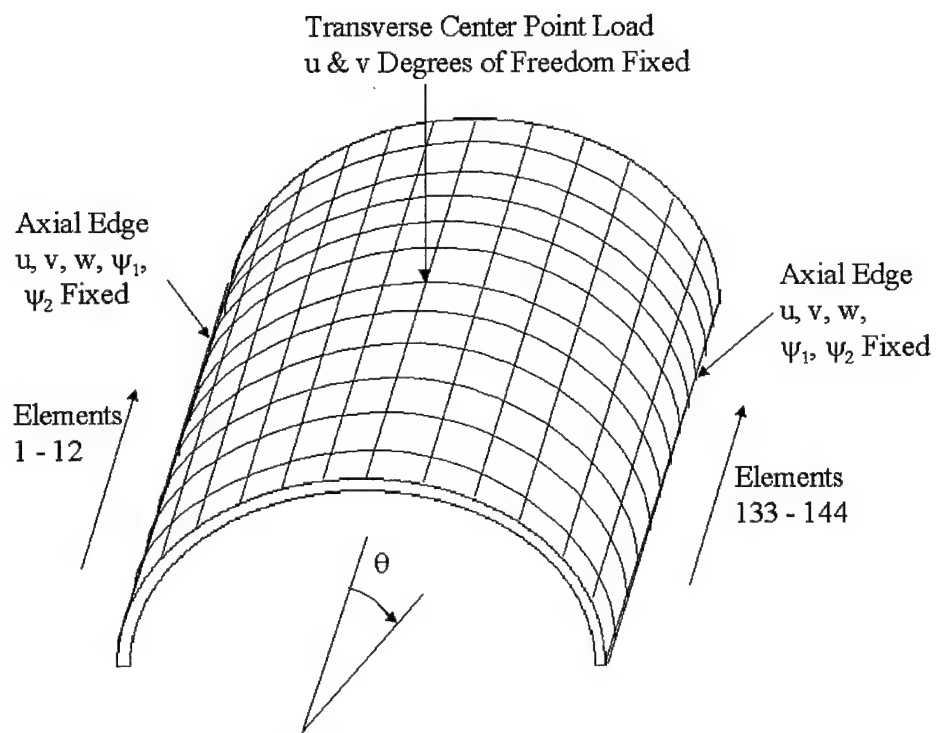
Figure 13. Boundary conditions and finite element modeling for a general shell specimen
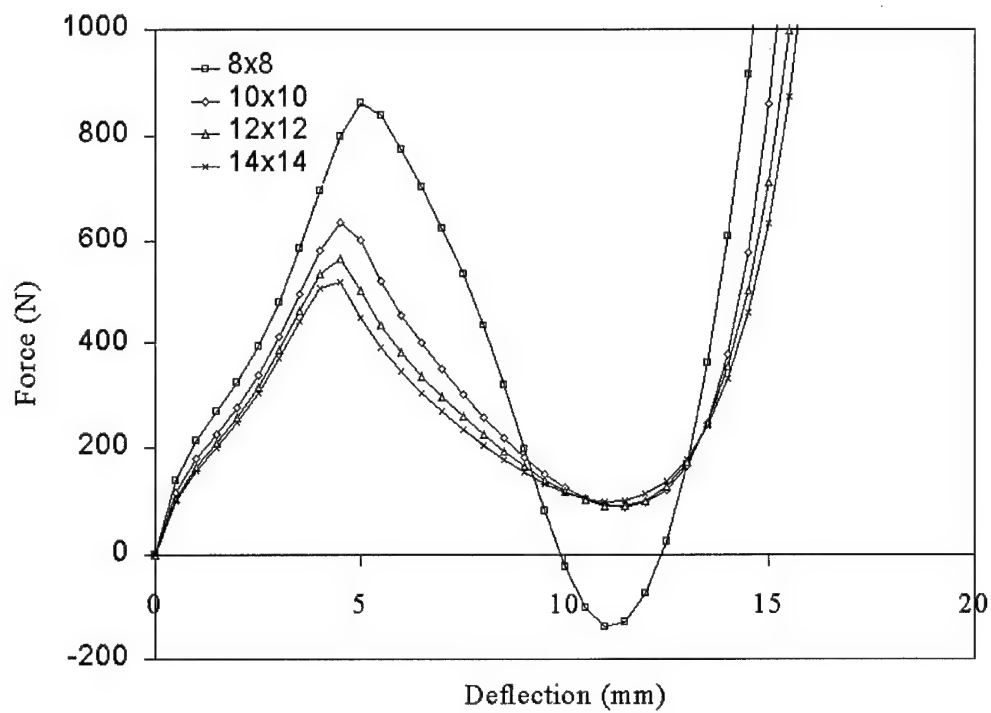
Figure 14. Convergence study for center loaded shell

73

the respective loads for the $8x8$, $10x10$, $12x12$ and $14x14$ configurations were 868 N, 637 N, 565 N and 520 N, representing a difference of 55%, 23% and 9% as compared to the $14x14$ mesh. For the cases considered in this analysis, modeling was accomplished using $12x12$ mesh discretization. Results using the $14x14$ mesh discretization were not appreciably better and extended computing time by days.

4.1.2 Baseline Comparison

The phrase "critical snapping point" or "instability point" has been mentioned several times when discussing the physical response seen in shells without an adequate description of the phenomenon. As a convex shell is deflected in the transverse direction, the response can be separated into three distinct regions as seen in Fig. 15 [44]. Referencing Fig. 15 and Fig. 16, a shell will pro-
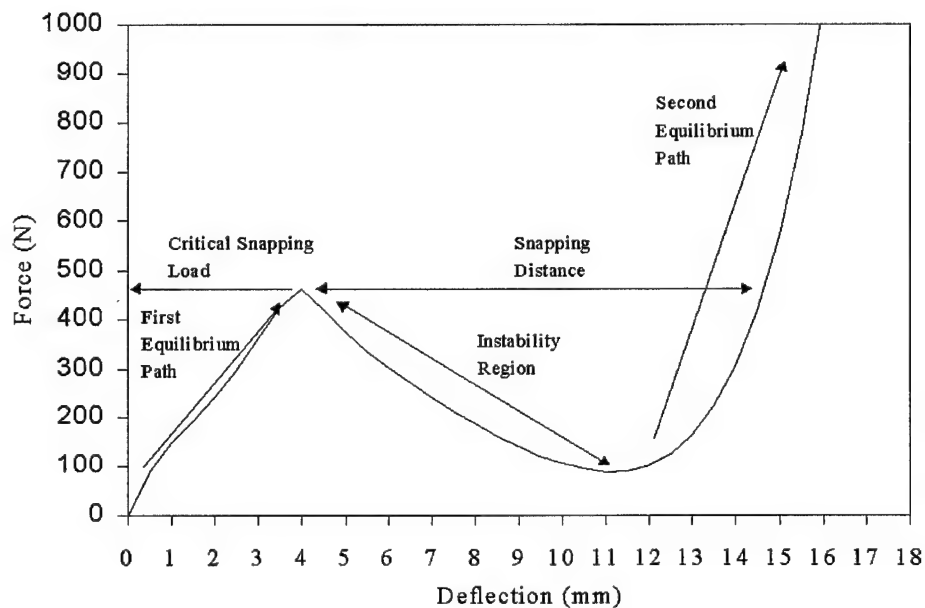
Figure 15. Illustration of the three distinct shell physical response regions

ceed along the first equilibrium path until reaching the critical snapping load or the buckling load

shown in Fig. 16B. In this first region, the shell transverse displacement will increase with an increase in the transverse loading. Compressive membrane stresses in the circumferential direction dominate the shell's response along the first equilibrium path. After reaching the critical snapping load, the shell proceeds into the instability region, resulting in the shell ending up in an inverted or concave position shown in Fig. 16C. As seen in Fig. 15, the transverse displacement between the first and second equilibrium points is quite significant, or roughly 31% of the total deflection for this general case. That transverse displacement represents a significant amount of energy absorption, all of which should be taken into account when examining ply failure in composite panels. In other words, the energy absorbed throughout the instability region, or the energy required to "snap" the shell is energy that otherwise would have gone into ply damage. Thus, the existence of the instability region serves as damage resistance for the convex shell. It has been shown that convex shells can resist damage to a greater extent than a plate of similar geometry by absorbing the energy within the instability region, that otherwise would have resulted in ply damage. Conversely, the plate, having no instability region, absorbs quasi-static or impact energy by continued monotonic loading thus incurring more damage [44]. In a shell, the compressive membrane stresses associated with the first equilibrium path undergo a sign reversal after the critical snapping load, thereby becoming tensile membrane stresses. Upon reaching the second stable equilibrium path, the shell will once again increase in displacement with an increase in load, and will exhibit a physical response similar to that seen in concave shells. It is well established that the critical snapping load associated with different convex shell geometries will result in differences in the damage extent and type, and that the damage exhibited by a composite panel is directly associated with the peak force that the panel is exposed to [15], [44]. As mentioned previously, the panel stresses associated with the first equilibrium path are compressive membrane in nature and are responsible for sublaminate buckling and delamination [44]. Since the type of stress seen in the panel depends

75
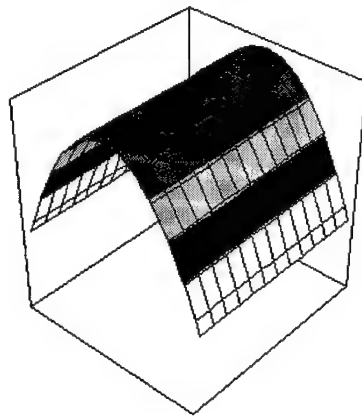
A) Composite panel at the start of the first equilibrium path.
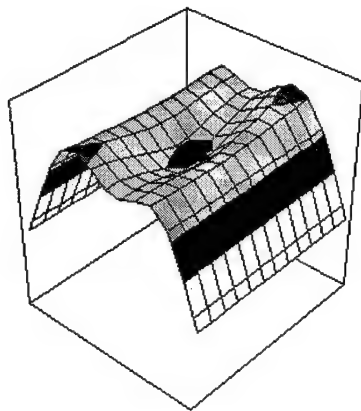
B) Composite panel at the critical snapping point.
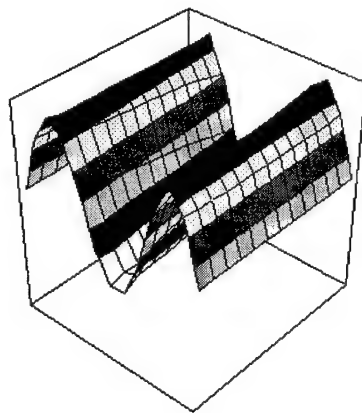
C) Composite panel at the end of the instability region.

Figure 16. Graphical representation of a general shell's response encompassing initial loading, shell buckling and the final equilibrium path

upon the physical response "region", then the type of panel damage also depends upon the physical response "region". This makes any discussion concerning composite panel damage irrelevant without including a discussion of the convex shell's total response. Since the type and extent of panel damage is associated with the physical response region, those structural parameters associated with affecting the critical snapping point need to be examined.

Continuing with the SLR finite element method accuracy check, a comparison was made between the SLR FEM, the Wardle and Lagace experimental data [44] and the ABAQUS$^{\circledR}$ commercial finite element package. This case served as a baseline against which to compare the experimental data before and after incorporating the effects of progressive failure. The motivation behind the ABAQUS$^{\circledR}$ comparison was to test the SLR method against an industry "standard" finite element package. The AS4/3501-6 graphite/epoxy composite panel used in the comparison was the general shell displayed previously, with a radius, span and thickness of 152, 102 and 0.804 mm respectively, and a composite layup of $[\pm 45/0]_s$. Both the SLR and ABAQUS$^{\circledR}$ data compared favorably with the experimental data as displayed in Fig. 17. As mentioned earlier, the ABAQUS$^{\circledR}$ results generated using hinged boundary conditions along the axial edges resulted in the same sign reversal of the transverse force vector after the critical snapping point that was seen with the initial SLR data. With shell elements and similar axial edge boundary conditions as those used in the SLR analysis, results generated using ABAQUS$^{\circledR}$ compared favorably with the SLR results for this particular specimen configuration. The ABAQUS$^{\circledR}$ input deck also included the same $12x12$ mesh and displacement control analysis. The analytical data generated using both SLR and ABAQUS$^{\circledR}$ was stiffer than the experimental data. Several factors were responsible. First, a finite element method assumes consistent material properties, as opposed to the material defects inherent in a test specimen. Those defects result in a reduction of the stiffness or strength of the panel. The same analogy is true for the test fixture as well. While the finite element method

77
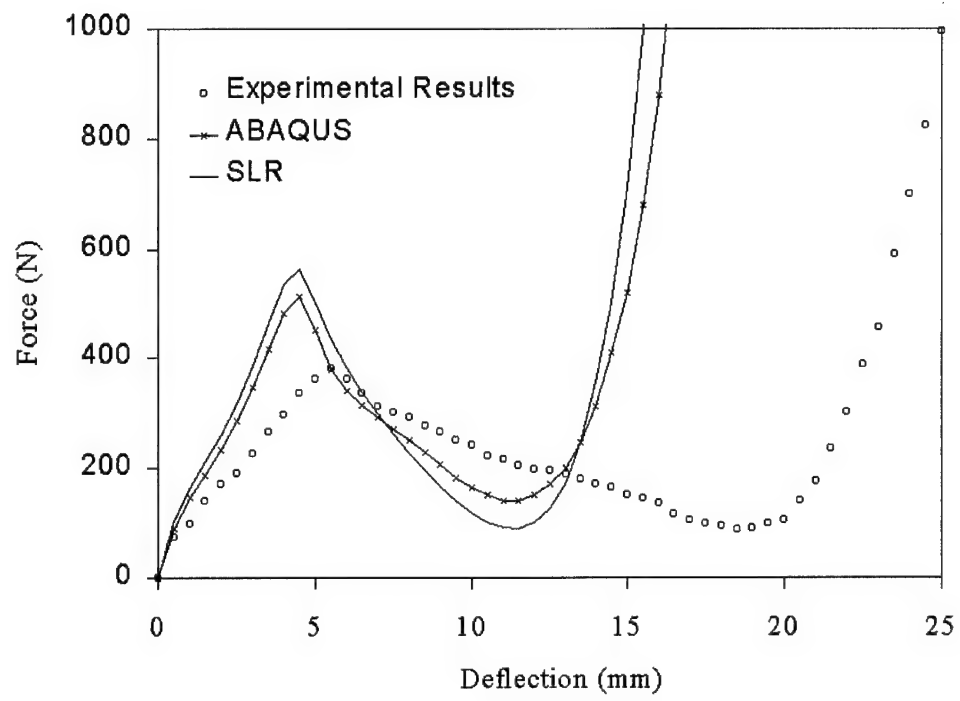
Figure 17. Comparison between SLR, ABAQUS and experimental data

will be exact in its application of the boundary conditions and location of the loading, an experiment will again inherently have a margin of error. The loading will not be applied exactly in the center of the panel, and similarly, the boundary conditions can not possibly be applied with as great a degree of accuracy. Finally, the finite element methods used in this research considered a geometrically perfect cylindrical shell, while an actual cylindrical test specimen will again have tolerances or errors associated with the radius and thickness. Examining the results shows that the SLR data displays the critical snapping point being reached at a center transverse displacement of $4.5mm$ and accompanying transverse center point load of 565 N, versus the ABAQUS$^{\textregistered}$ and experimental critical snapping point displacements and loads of $4.5mm$ and 515 N, and $5.5mm$ and 380 N respectively. At the start of the second stability region, the ABAQUS$^{\textregistered}$ data is the stiffest, resulting in a minimum transverse load of 140 N versus 90 N for the SLR data and 88 N for the experimental data. Both the ABAQUS$^{\textregistered}$ and SLR models reached their respective minimum load points at a transverse deflection of 11.5 mm. Therefore, for this baseline specimen, the SLR and ABAQUS$^{\textregistered}$ analytical data are less conservative in transverse deflection and loading characteristics when compared with experimental data.

4.1.3 Panel Thickness

Thickness has a considerable influence on the overall response of a composite shell. Wardle and Lagace [44] investigated the effects of thickness on a convex shell's physical response, and found that the shell thickness has a significant effect on the bending and membrane contributions to panel stiffness. Increasing the shell thickness resulted in an increase in stiffness for both the first and second equilibrium paths [44]. Three specimen configurations examined in the experiment, were examined using the SLR FEM, all with the same span and radius of 457 mm and 305 mm respectively. The three thicknesses examined were 0.804 mm, 1.608 mm and 2.412 mm re-

spectively. Using displacement controlled increments of 0.5 mm, a 12x12 mesh discretization, a displacement convergence criteria of 0.1%, and using the previously mentioned simple boundary conditions, yielded the results shown in Fig. 18. The experimental data in Fig. 18 was taken from Ref. [44]. As shown in Fig. 18, as the thickness increased, the difference in stiffness between
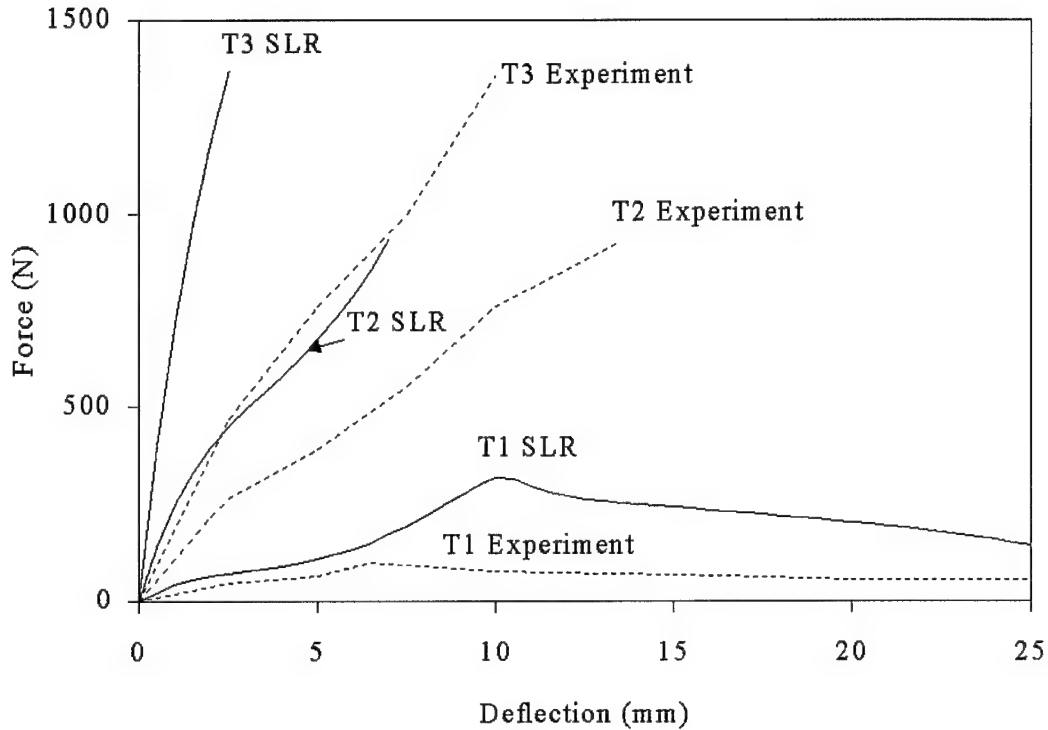
Figure 18. Physical response of convex shells with varying thicknesses

the experiment and SLR data also increased. However, the physical response trends for the SLR data were consistent with the experimental data, even with the stiffness discrepancies. In other words, the snap characteristics or general loading responses generally correspond with the experiment. For the SLR "$T1$" specimen, the critical snapping load was 318 N with a corresponding deflection of 10 mm. The experimental data reached a peak load of 100 N and a corresponding

deflection of 6.5 mm. For both the SLR and experimental "$T2$" and "$T3$" specimens, there were no critical snapping phenomenon. However, for the "$T2$" specimen, there was an inflection in the load-deflection curve at approximately 250 N and 2.5 mm. The SLR data shows a corresponding change in slope at a load of 450 N and a deflection of 2.5 mm. There was no critical snapping load or significant change in slope experienced with the "$T3$" specimen.

Of the structural parameters considered in the experiment, thickness has the greatest effect on the bending and membrane panel stiffness [44]. With that in mind, increasing the shell thickness impacts the critical snapping point in two ways. First, an increase in thickness will increase the load at which the critical snapping point occurs. With too great a thickness, the panel will not reach a critical snapping point, as seen in the "$T2$" and "$T3$" specimens. Thus, a thick panel will approach the response seen in plates. It should be noted that the shell response only approaches that seen in plates. The slope of the load-deflection curve is still decreasing with increasing deflection, unlike a plate load-deflection response curve having an increasing slope with increasing deflection. Also, the shell, even when thick, will still experience membrane compression stiffness whereas a plate will load monotonically, experiencing tensile stresses. Finally, an increase in thickness will result in the critical snapping load being reached at a reduced transverse deflection.

4.1.4 Panel Radius

Ultimately, a study will be made of the response characteristics of sandwich composite shells. Since the study will include an analysis of the impact of failure criteria and the corresponding stiffness reduction, an understanding of the impact that the geometric radius has on a panel is necessary. For the purposes of this research, a shell is considered deep if the ratio "δ/S" is greater than 25%, where "δ" and "S" are defined in Fig. 10. Shallow cylindrical shells tend to approach the physical response seen in flat plates. Deep shells undergo large rotations and tend

to exhibit extreme changes in the load-displacement response due to the buckling phenomenon known as snapping. The effects of rotation were therefore examined by varying the radius of the specimen and comparing the results with Wardle and Lagace [44]. The specimens considered by Wardle and Lagace had a constant span and thickness of 203 mm and 0.804 mm respectively, with varying radii of 152 mm, 305 mm and 457 mm. Using the previously defined definition for the "deepness" of a shell, the δ/S ratio was 20%, 8.5% and 5.7% respectively. According to the definition, only the first shell would be considered "deep". Using displacement controlled increments of $0.5mm$, a $12x12$ mesh discretization, a displacement convergence criteria of 0.1%, and the boundary conditions shown in Fig. 13, the results of the analysis are expressed in Fig. 19.
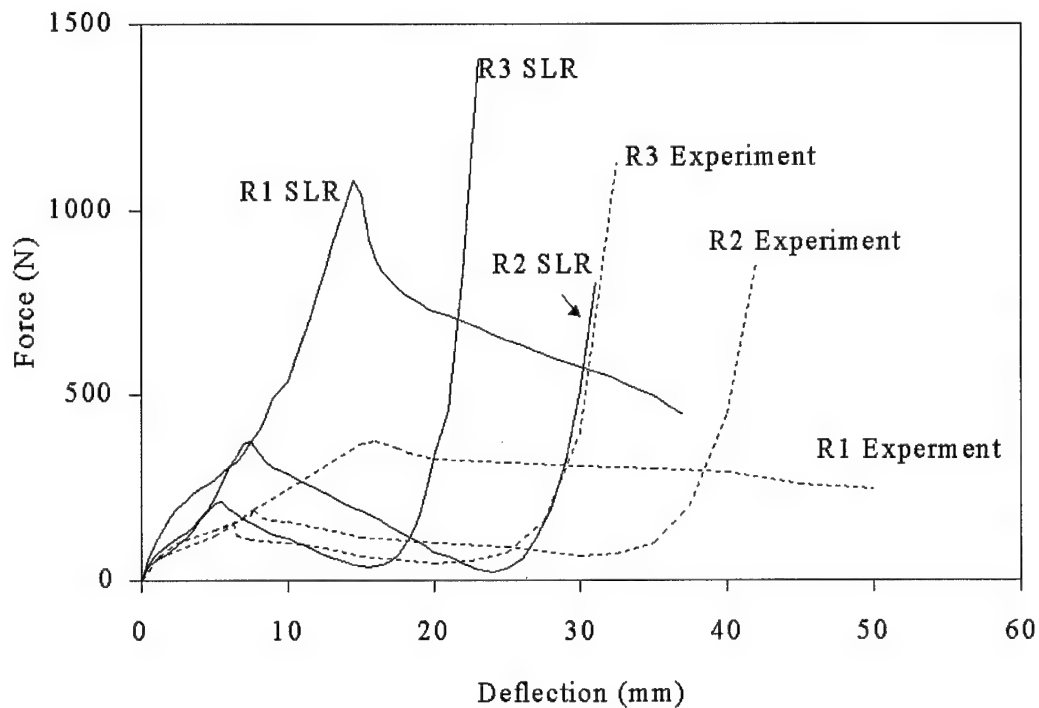
Figure 19. Physical response of convex shells with varying radii

Once again, the SLR results were stiffer than the experimental results, while the critical snap phenomenon was modeled reasonably well by the SLR FEM. Increasing the panel radius while holding all other parameters constant produced some interesting results. For the SLR and especially the experimental data, the slope of the load-deflection curves was generally consistent until the respective critical snapping load was reached. The same phenomenon holds true after the critical snapping load as well. As the shell radius was increased, the critical snapping load and the transverse deflection within the instability region decreased for both the SLR and the experimental data. For the "$R3$" specimen, the SLR analysis produced a critical snapping load and corresponding transverse deflection of 214 N and 5.5 mm respectively. The experimental data shows the critical snapping load and transverse deflection to be approximately 150 N and 6 mm respectively. For the "$R2$" specimen, the SLR analysis produced a critical snapping load and corresponding transverse deflection of 373 N and 7.5 mm respectively. The experimental data shows the critical snapping load and transverse deflection to be approximately 190 N and 8 mm respectively. For the "$R1$" specimen, the SLR analysis produced a critical snapping load and corresponding transverse deflection of 1077 N and 14.5 mm respectively. The experimental data shows the critical snapping load and transverse deflection to be approximately 380 N and 15 mm respectively. It is therefore obvious that as the shell radius decreases, or the shell becomes deeper, the SLR FEM results in data that is stiffer than the corresponding experimental results.

4.1.5 Results of the Comparison

There were three comparisons made with the experiment conducted by Wardle and Lagace [44]. First, a general thin shell specimen was compared, followed by comparisons on the effect of panel thickness and radius respectively. The increase in panel thickness tended to exaggerate the stiffness discrepancies between the SLR and experimental results. The discrepancies can be

attributed to material defects, load application, test methods and imperfect specimen geometry. As an example, the SLR theory is very sensitive to thickness. With the likelihood of thickness variation in the experimental specimens, significant differences in stiffness will result. The results of the SLR comparison show that the difference in panel stiffness was a minimum when comparing the "$T1$", or the thinnest of the specimens, however, the panel stiffness tended to diverge significantly as the shell thickness or number of plies was increased. There were several possibilities for the stiffer response of the SLR finite element modeling in addition to material defects and test methods. Remember that the SLR theory is based upon a two dimensional assumption, i.e., a "thin" structure in a state of relative plane stress. That "thinness" allowed the developers of the SLR theory to approximate the transverse shear effects with respect to the panel midsurface. For the cases where in-plane effects dominate, this is a valid assumption, as seen in the "$T1$" comparison. As the thickness of the panel increases, the problem develops into a three dimensional one. This three dimensional problem is manifested in several ways. First, the transverse direct stress in the vicinity of the applied load becomes important. Second, as the shell thickness increases, the parabolic transverse shear strain assumption loses accuracy. From the development of the kinematics, the transverse shear strain was solved for by forcing the value of the shear to be zero at the upper and lower surfaces. The result was parabolic shear distribution through the panel thickness. In the SLR FEM, transverse shear strains were assumed and forced to be continuous through the thickness, while transverse shear stresses were discontinuous. In reality, the transverse shear stress is continuous. For thin shells, the SLR assumptions are reasonable. However, as the thickness increases and the problem becomes three dimensional, the parabolic transverse shear assumption loses accuracy.

Changing the radius while holding the thickness, span and material properties constant allowed for an investigation into the effect that the "δ/S" ratio had on the shell. As the panel radius was

increased, the SLR and experimental differences in the shell force-deflection response increased as well, although the SLR FEM shell instability characteristics were consistent with the experimental data. As discussed previously, the SLR theory included transverse shear effects. Because the transverse shear was not considered as crucial as the in-plane effects in an analysis of thin panels, only the linear terms of the respective Green's strain-displacement relations were used. Therefore, for generally large rotations and displacements, like those experienced in the snapping phenomenon of shells, the through-the-thickness transverse stresses and displacements were not accurately represented. However, through the use of the higher order kinematics and nonlinear in-plane Green's strain relations, the displacement and rotation of the panel midsurface was represented reasonably well [27]. Thus, the shell snapping phenomenon was generally well predicted as seen in the "radius" comparison. However, recall that in the SLR kinematic formulation, small to moderate rotations were assumed. The "$R1$", "$R2$" and "$R3$" SLR specimens experienced maximum rotations in the circumferential direction, in the vicinity of the applied load at the critical snapping point of approximately 21^0, 12^0 and 8^0 respectively. As the rotation of the shell midsurface increased, the small to moderate rotation assumption began to lose accuracy. In other words, the rotations were too large for the SLR theory to predict accurate displacements, thus the greatest discrepancy was noted for the "$R1$" or the deepest of the three shells considered.

Finally, a thin shell specimen was chosen as the baseline for future comparisons including composite and sandwich composite failure criteria. The shell chosen was a relatively shallow shell, with a "δ/S" ratio of 8.6%. The SLR data was compared with both the experimental data as well as the results generated from the ABAQUS® finite element program. The baseline SLR data compared favorably with both the ABAQUS® and experimental data, exhibiting reasonably close similarity with respect to the critical snapping and post buckling characteristics. The SLR force-deflection response was slightly stiffer with the critical snapping point occurring at a lower value

85

of transverse deflection, when compared with the experimental data. The SLR response was also stiffer than the ABAQUS$^{\circledR}$ data, however the transverse deflection at the critical snapping point was the same as the corresponding ABAQUS$^{\circledR}$ deflection.

4.2 Composite Panel with Failure Analysis

The Hashin, Lee and maximum stress failure criterion were added to the SLR FEM in order to provide a more realistic representation of the total physical response of the shell. An analysis was made of the baseline configuration using each of the various failure criterion. For each of the failure analyses, the first ply failure, as well as the first of each form of failure for each ply was determined. For example, the Hashin failure criteria predicts three forms of failure, fiber breakage, matrix cracking and delamination. Therefore, for any case involving the Hashin criteria, the location of the first of each of those failures was determined. The location refers to the specific element as well as the ply that failure occurred in. For all specimens, the type and extent of failure for significant points on the load-deflection curve were recorded. For the composite shell analysis, significant points include the "snapping" phenomenon and the corresponding snapping distance point, described in previous sections. The failures leading up to this phenomenon as well as failures at the corresponding snapping distance point, shown in Fig. 15, were analyzed.

The experimental analyses considered in this comparison was the previously discussed analysis carried out by Wardle and Lagace [44]. The specimen referred to as the general baseline specimen was again used as a standard against which the modified SLR FEM was compared. One specimen from the experiment was chosen as a baseline, and the SLR FEM with the failure criteria capability incorporated was used to analyze the shell response. The AS4/3501-6 graphite/epoxy material strengths used in the analysis are listed in Table 2, where "F", "M" and "D" refer to ma-

trix, fiber and delamination, "N" and "S" refer to normal and shear, and "T" and "C" to tension or compression [13].

$\sigma_{FN} = 1.5\,GPa$
$\sigma_{FS} = 0.22\,GPa$
$\sigma_{MNT} = 43.8\,MPa$
$\sigma_{MNC} = 43.8\,MPa$
$\sigma_{MS} = 43.8\,MPa$
$\sigma_{DN} = 0.05\,GPa$
$\sigma_{DS} = 0.086\,GPa$

Table 2. AS4/3501-6 material strengths

Before entering into a discussion of the analysis and results, there are several points that need to be explained with respect to the experimental data. First, none of the experimental specimens reached final ply failure within the deflections recorded. Second, the type of failure analysis detail available with the SLR FEM greatly exceeds the information available from the experimental data. While there was limited information available from the experiment, only general trends can be made concerning the analyses. Each of the chosen failure criteria allowed the user to determine the type and location of failure. Because of the format of the SLR finite element method, the location of failure includes the ply or layer, element and Gaussian point. Obviously, the detail of this type of damage evaluation exceeds that available in most experimental analyses. As a result, only general comparisons can be made between the analytic and experimental results. Those comparisons include specimen stiffness reduction, peak loads or general load-deflection characteristics, and general failure characteristics.

4.2.1 Composite Comparison using Hashin Failure Criteria

The Hashin failure criteria is ideally suited for use in the SLR finite element method, as it combines in-plane direct stresses with in-plane and transverse shear stress effects. Important in the development of the SLR theory was the ability to include transverse shear effects. However, the SLR theory also makes simplifying assumptions concerning those transverse effects. Namely,

87

the linear transverse shear strain approximation, parabolic through-the-thickness transverse shear, and the insignificance placed upon the direct transverse effects. Since the Hashin criteria considers the effects of both in-plane and transverse shear stress, the simplifying assumptions concerning the SLR transverse effects should be balanced with the complete modeling of the in-plane effects. Also important for any failure criteria used in a composite progressive failure analysis is the determination of the mode of failure. The Hashin criteria allows the user to predict and identify a failure mode, thus allowing for accurate stiffness reduction. For the purposes of this portion of the research, the baseline configuration, previously compared to the ABAQUS$^{\circledR}$ and experimental data, was used. The specimen had six plies in a $[\pm 45/0]_s$ configuration, with a radius, span and thickness of 152, 102 and 0.804 mm respectively. A $12x12$ mesh configuration was used along with 0.5 mm displacement increments and a user specified displacement convergence criteria of 0.1%. Unless otherwise noted, references to displacement or transverse deflection refer to the center point of the shell, where the transverse point load was applied.

The total response of the baseline specimen analyzed with Hashin failure criteria can be seen in Fig. 20. The shell stiffness at the critical snapping load was reduced by approximately 6%, or to within 100 N of the experimental data through the reduction method explained earlier. The transverse deflection at which the critical snapping load occurred, remained constant. Given the entire physical response of the shell, the next step in the data analysis was to determine first failures. In order to accomplish this, the displacement increments were reduced to 0.005 mm. This provided the necessary detail required to accurately determine first ply failures. The term "accurately" is used with respect to the finite element code and not as a reference to any comparison with the experimental data. As previously mentioned, the experimental data did not provide that level of detail. The displacement increments were initially kept small to determine the first instance of a particular failure. Using relatively large increments resulted in numerous types of failures
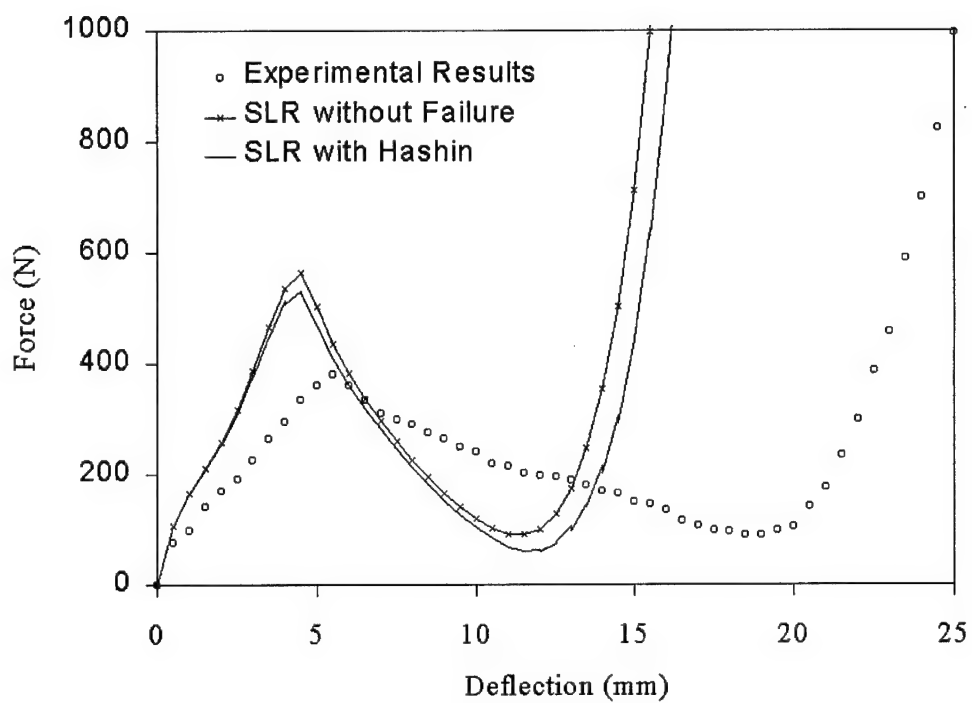
Figure 20. Physical response of the baseline convex shell with Hashin failure criteria

in multiple layers occurring all at once. Therefore, using the small, 0.005 mm displacement increments, the first of each mode of failure was determined. Results of these failures can be seen in Fig. 21, where "M" refers to matrix, "F" refers to fiber, and "D" refers to delamination. The ply orientation precedes the previously mentioned failure mode descriptor. If no distinction is made between the $\pm45°$ layers in the nomenclature, then a representative of each orientation failed at that respective increment. It should be noted that all of the first ply failure modes occurred along the axial edge encompassing elements 133 through 144, where the element numbering is displayed in Fig. 13. First failure was defined as the first failure detected for a particular ply. The first ply failure detected using the Hashin failure criteria was matrix cracking in the $\pm45°$ layers. This failure occurred at a transverse deflection of 0.10 mm and a corresponding load of 27 N. The first failure in the $0°$ layers was fiber breakage occurring at a transverse load and deflection of 40 N and 0.15 mm. The next failures to occur were matrix cracking in the $0°$ layers and fiber failure in the $\pm45°$ layers, at a corresponding load and deflection of 0.25 mm and 61 N. The next detected failure was delamination in the ply interfaces encompassing the $0°$ layers at a load and deflection of 257 N and 1.5 mm. Delamination occurred next in the ply interfaces encompassing the $-45°$ layers at a load and deflection of 311 N and 2.5 mm. Finally, delamination occurred in the ply interfaces encompassing the outermost layers, or the $+45°$ layers, at a load and deflection of 514 N and 4 mm respectively.

At the critical snapping load, the general shell had experienced failure, as evidenced in the stiffness reduction in Fig. 20. In order to present the failure results in as understandable a format as possible, a "scan" of the failures for each ply is presented. Each layer was separated into individual elements and the failed elements were identified as a "darkened" element. Therefore, the results of the Hashin failure case at the critical snapping load are displayed in the following three figures, or Figs. 22 through 24.
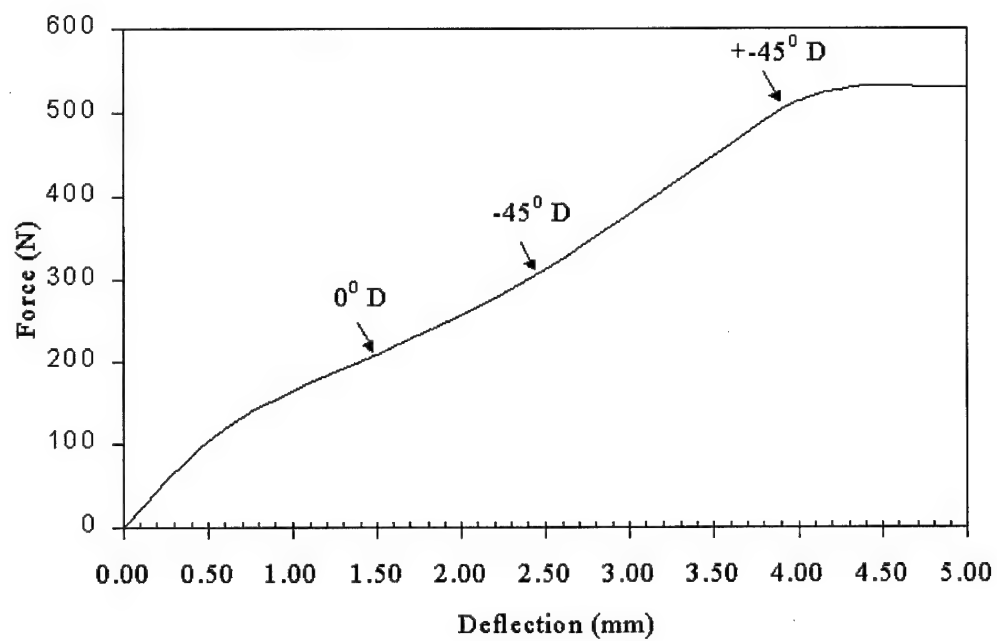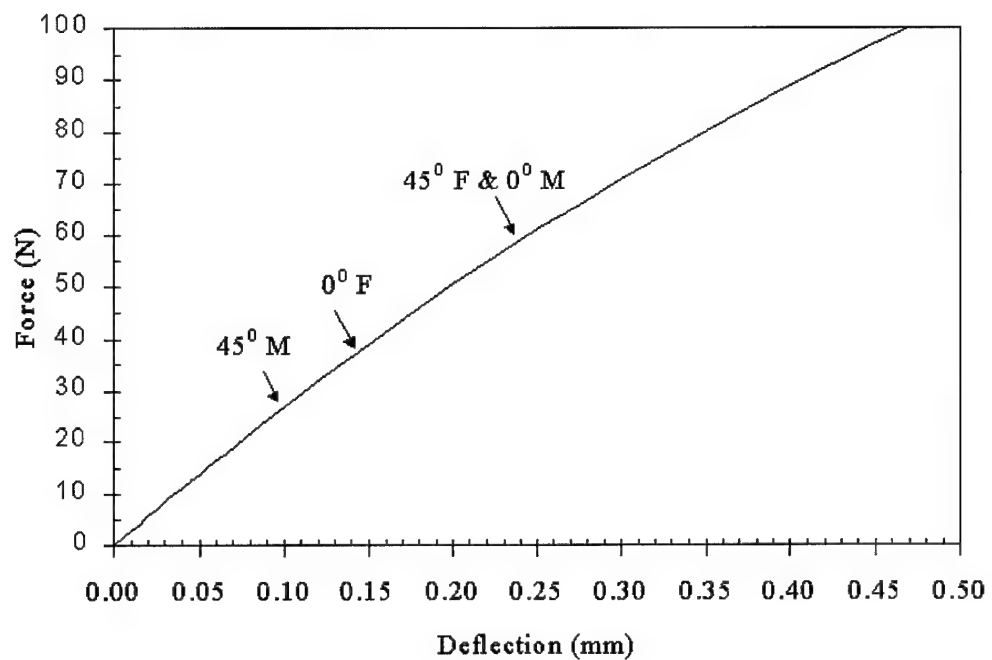
Figure 21. First failures identified using Hashin failure criteria

91

Fiber Failure

Layer 1, 45⁰   Layer 2, -45⁰   Layer 3, 0⁰

Layer 4, 0⁰   Layer 5, -45⁰   Layer 6, 45⁰

$+\theta$

☐   Failures at the "Snapping Distance" Point

▓   Failures at the "Snapping Point"
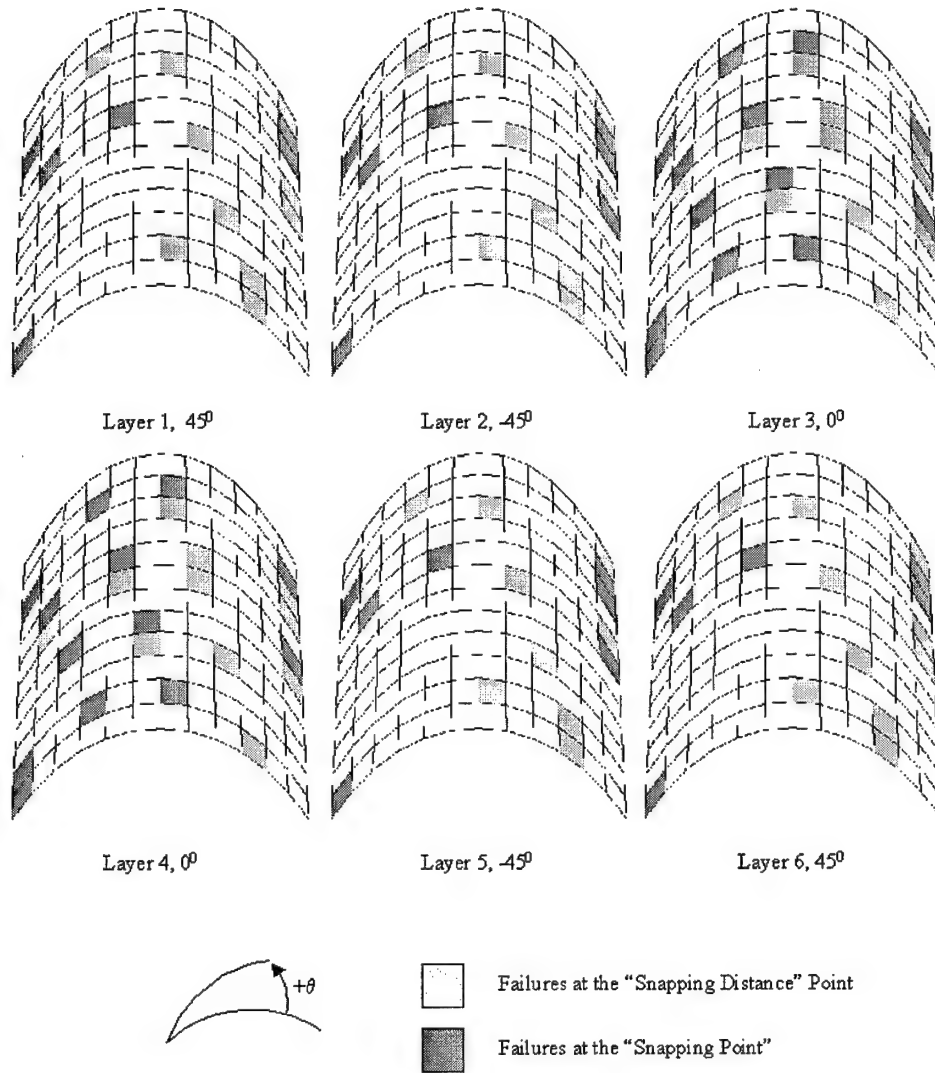
Figure 22. Baseline convex shell illustrating fiber failure using Hashin failure criteria

92

Matrix Failure

Layer 1, 45⁰   Layer 2, -45⁰   Layer 3, 0⁰

Layer 4, 0⁰   Layer 5, -45⁰   Layer 6, 45⁰

$+\theta$

Failures at the "Snapping Distance" Point

Failures at the "Snapping Point"
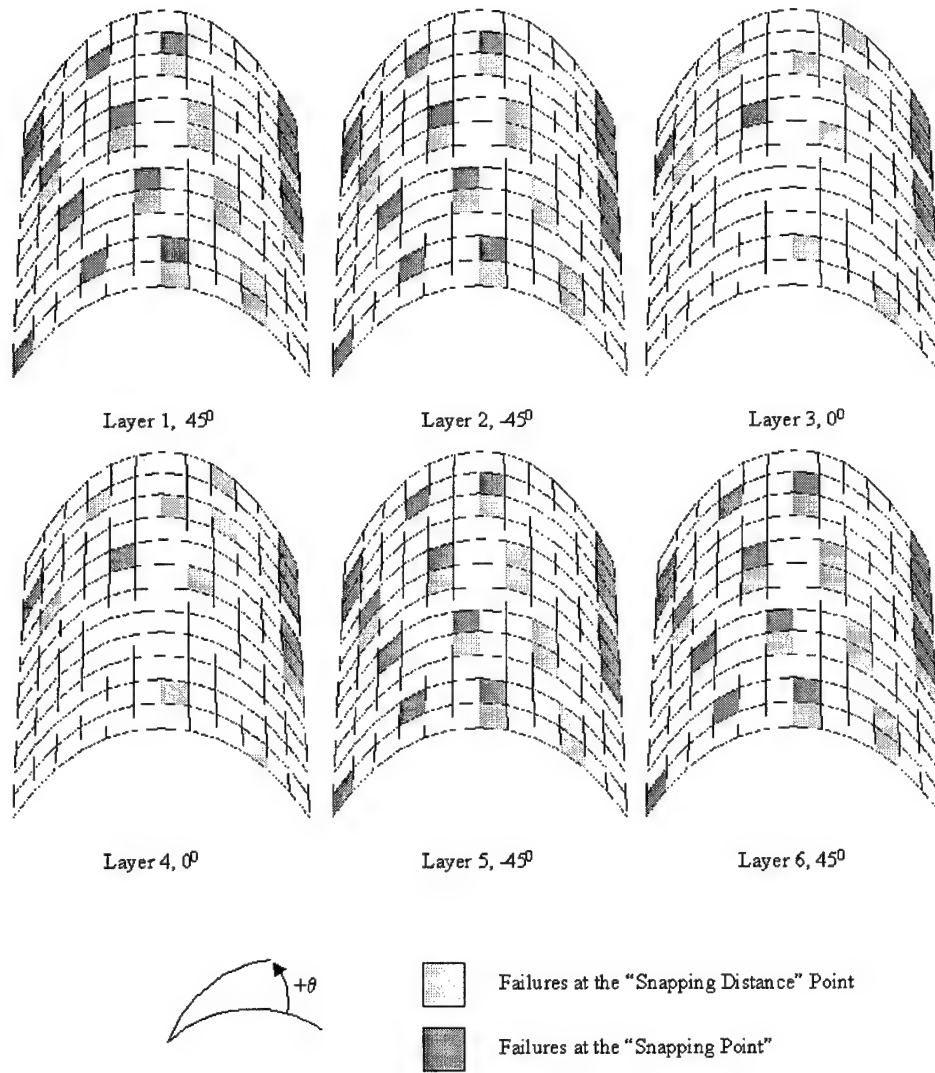
Figure 23. Baseline convex shell illustrating matrix failure using Hashin failure criteria

93

Delamination Failure

Layer 1, 45⁰   Layer 2, -45⁰   Layer 3, 0⁰

Layer 4, 0⁰   Layer 5, -45⁰   Layer 6, 45⁰

$+\theta$

Failures at the "Snapping Distance" Point

Failures at the "Snapping Point"
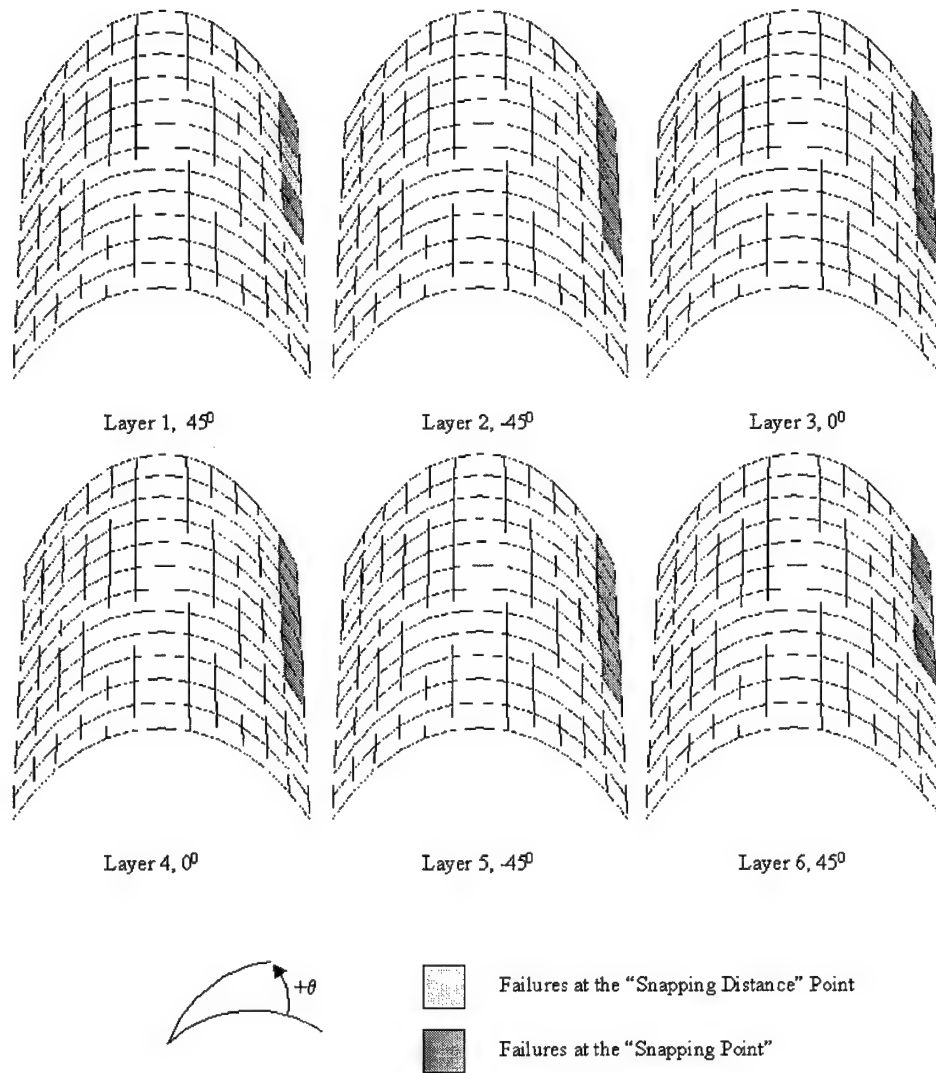
Figure 24. Baseline convex shell illustrating delamination using Hashin failure criteria

94

As mentioned earlier, two locations along the shell load-displacement curve were analyzed for failure, the critical snapping point and the corresponding load on the second equilibrium path, or the snapping distance point. The reasoning for the choice of evaluation points was the effect of the critical snapping load and its relation to damage resistance. The corresponding snapping point allowed the author to study the effect that achieving the critical snapping load on the second equilibrium path had on ply damage. The elements exhibiting failure at the critical snapping point are displayed as the dark gray areas on the shell, and the elements exhibiting failure at the "snapping distance point" are displayed as the light gray areas on the shell. The shell layers, failure type and location are easily identified in Figs. 22 through 24. While the previously mentioned figures illustrate the various failures in terms of layers and elements, there was no attempt made to distinguish between the individual Gaussian points of each element. One indicator of the success of the convergence study was that for all elements, the Gaussian points all indicated the same failure with the exception of a single element. Therefore, all "shaded" elements, or those elements representing failure, did accurately represent all four failed Gaussian points.

At the critical snapping point, the Hashin failure criteria detected all three forms of failure for all plies. Note that delamination was limited to the far end of the axial edge for all layers, as indicated in Fig. 24. That fiber failure in the $0°$ plies occurred to a much greater degree than the $\pm45°$ plies was expected, given the difference in ply orientation. In other words, the fibers in the $0°$ plies were oriented as shown in Fig. 22. This orientation exposes the fibers to larger stresses experienced during the shell snapping phenomenon, than those seen by the fibers of the $\pm45°$ plies. In other words, σ_{11} in the $\pm45°$ plies, or the stress in the material fiber direction, is a function of θ, σ_{xy} and σ_x, or the ply orientation angle with respect to the SLR axis system, in-plane shear stress and direct axial stress in the SLR axis system respectively. On the other hand, for the $0°$ plies, σ_{11} is a function only of σ_y, or the stress in the "v" direction in the SLR axis system, as shown in

95

Fig. 5. This assertion is further validated by noting that the 0° plies experienced fiber failure at an earlier point in Fig. 21 than did the ±45° plies. Therefore, as expected, there was greater fiber failure for the 0° plies. Conversely, given the orientation of the ±45° plies, greater matrix cracking was experienced in those layers, as evidenced in Fig. 23.

At the snapping distance point, or the point on the second equilibrium path where the transverse load is equal to the transverse load at the critical snapping point, the pattern of matrix and fiber failure continued along the ±45° directions. There was a noticeable increase in the number of elements experiencing both fiber and matrix failure for all layers. However, there was little increase in delamination at the snapping distance point. An investigation into the volume percent of failure yields some interesting results. Specifically, at the critical snapping point, 4.2%, 4.9% and 9.0% of the 45°, −45° and 0° layers experienced fiber failure, while at the snapping distance point, the percent of shell volume experiencing fiber failure increased to 11%, 11% and 17% respectively. Similarly, at the critical snapping point, 11%, 12% and 4.9% of the 45°, −45° and 0° layers experienced matrix failure, while at the snapping distance point, the percent of shell volume experiencing matrix failure increased to 20%, 20% and 11% respectively. Finally, at the critical snapping point, 1.4%, 4.9% and 4.9% of the interfaces between the 45°, −45° and 0° layers experienced delamination, while at the snapping distance point, the percent of shell volume experiencing delamination only increased to 4.2% at the interfaces encompassing the 45° plies. Therefore, at the snapping distance point, fiber and matrix failures predicted by the Hashin criteria essentially doubled.

4.2.2   Composite Comparison using Lee Failure Criteria

The Lee failure criteria, like the Hashin criteria, is also an interactive criteria. That implies that the loads, displacements and resulting stresses interact to define the failure environment. However, unlike the Hashin failure criteria, the Lee criteria relies solely on the shear effects to define the

failure environment. Once again, the 12x12 mesh discretization was used, along with 0.5 mm displacement increments and a 0.1% displacement convergence. Unless otherwise noted, references to displacement or transverse deflection refer to the center point of the shell, where the transverse point load was applied.

The total response of the baseline specimen analyzed with Lee failure criteria can be seen in Fig. 25. The shell stiffness at the critical snapping load was reduced by 15 N, or to within 170 N of the experimental data through the stiffness reduction method explained earlier. The deflection at which the critical snapping load occurred, remained constant. Next, the displacement increments
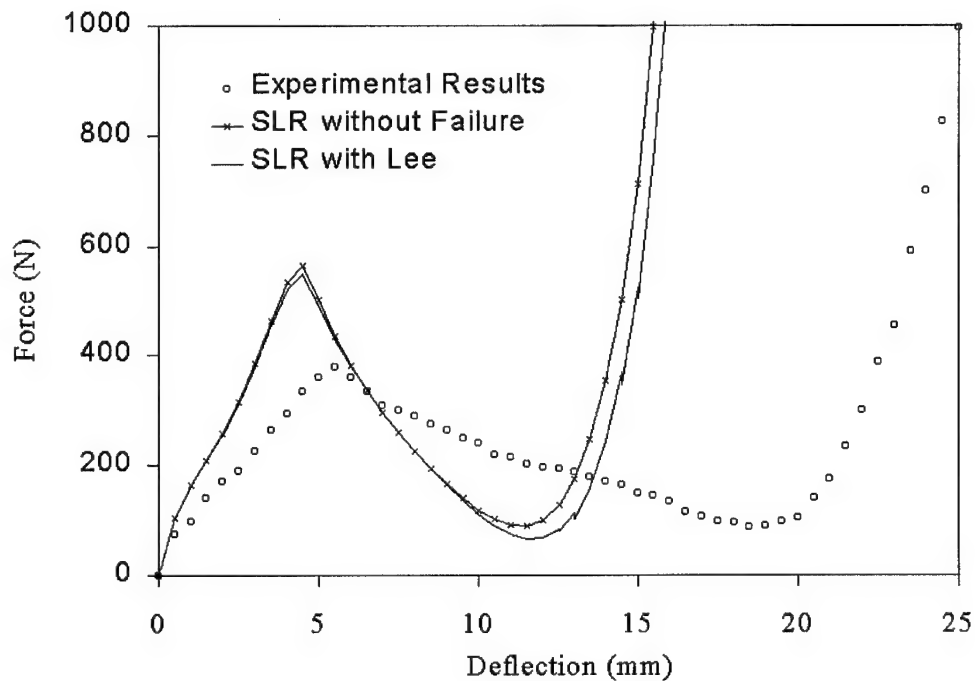
Figure 25. Physical response of the baseline convex shell with Lee failure criteria

were reduced to 0.005mm, while holding all other variables constant in order to determine first

failures. This provided the necessary detail required to accurately determine the first ply failure. Using the small, $0.005mm$ displacement increments, the first of each mode of failure was determined. Results of these failures can be seen in Fig. 26, where "M" refers to matrix, "F" refers to fiber, and "D" refers to delamination. All of the first failures detected using the Lee criteria were detected along the same axial edge as they were detected using the Hashin criteria. The first ply failure detected using the Lee criteria was matrix cracking in the $\pm 45°$ plies at a transverse load and deflection of 27 N and 0.10 mm. Fiber breakage in the $\pm 45°$ plies occurred next at a load and deflection of 98 N and 0.5 mm. Next, matrix cracking in the $0°$ plies occurred at a load and deflection of 150 N and 0.85 mm. Fiber failure occurred in the $0°$ plies at a load and deflection of 457 N and 3.5 mm. Delamination was again noted to occur from the inner layer interfaces outward, as a result of the parabolic transverse shear stress distribution. The load and displacement of the first detected delamination failures for the ply interfaces encompassing the $0°$, $-45°$, and $45°$ plies was 209 N and 1.5 mm, 380 N and 2.5 mm, and 523 N and 4.0 mm respectively.

At the critical snapping point, the shell again experienced all three forms of failure. The results of the Lee failure analysis are displayed in Figs. 27 through 29. The critical snapping point and the corresponding load on the second equilibrium path, or the snapping distance point were again analyzed for failure. The same coloring scheme used in the Hashin analysis was used for the Lee analysis. Elements exhibiting failure at the critical snapping point are displayed as the dark gray areas on the shell, and the elements exhibiting failure at the corresponding snapping distance point are represented as light gray elements. The shell layers, failure type and location are easily identified in Figs. 27 through 29. Again, there was no attempt made to distinguish between the individual Gaussian points of each element. All "shaded" elements, or those elements representing failure, did accurately represent all four failed points. Note that the shell again experienced matrix failure in the $\pm 45°$ directions. Also, as in the Hashin failure analysis, delamination was only

98
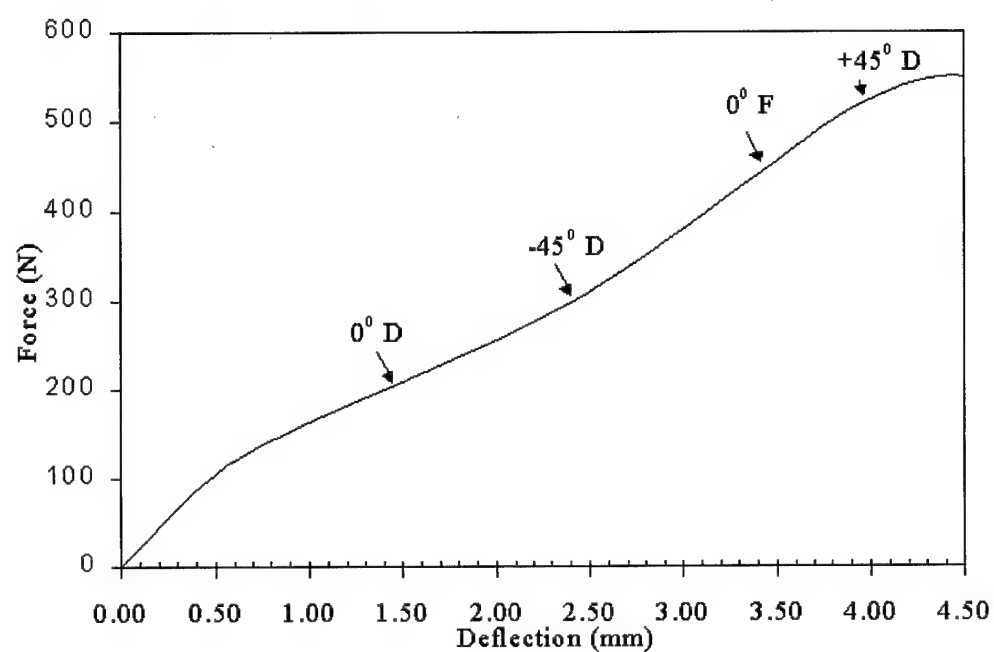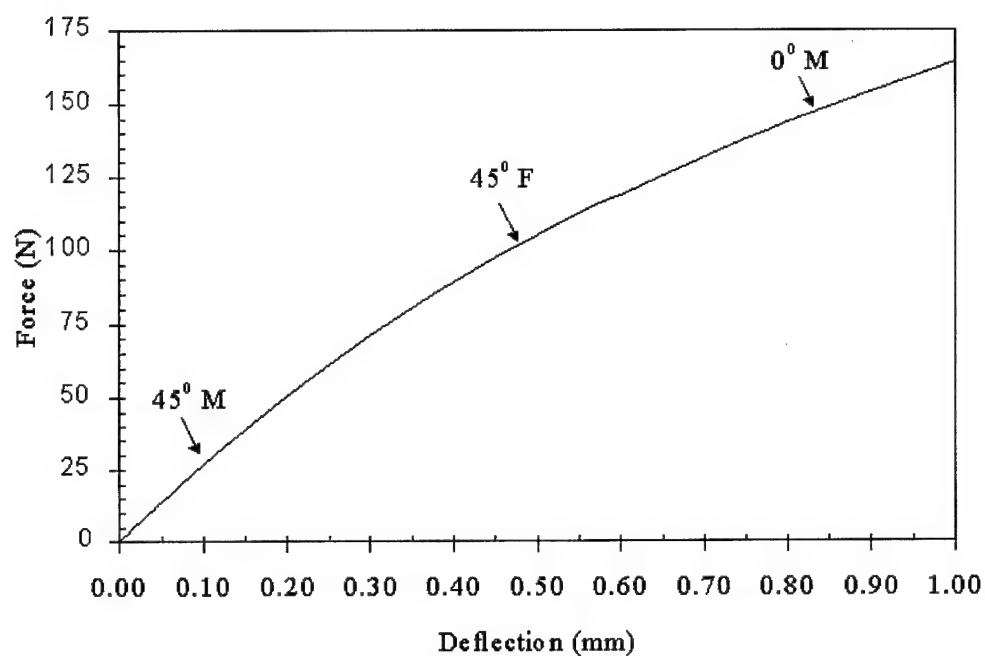
Figure 26. First failures identified using Lee failure criteria

Figure 27. Baseline convex shell illustrating fiber failure using Lee failure criteria

Matrix Failure

Layer 1, 45⁰   Layer 2, -45⁰   Layer 3, 0⁰

Layer 4, 0⁰   Layer 5, -45⁰   Layer 6, 45⁰

$+\theta$

☐ Failures at the "Snapping Distance" Point

■ Failures at the "Snapping Point"

Figure 28. Baseline convex shell illustrating matrix failure using Lee failure criteria

101

Delamination Failure

Layer 1, 45⁰   Layer 2, -45⁰   Layer 3, 0⁰

Layer 4, 0⁰   Layer 5, -45⁰   Layer 6, 45⁰

Failures at the "Snapping Distance" Point

Failures at the "Snapping Point"
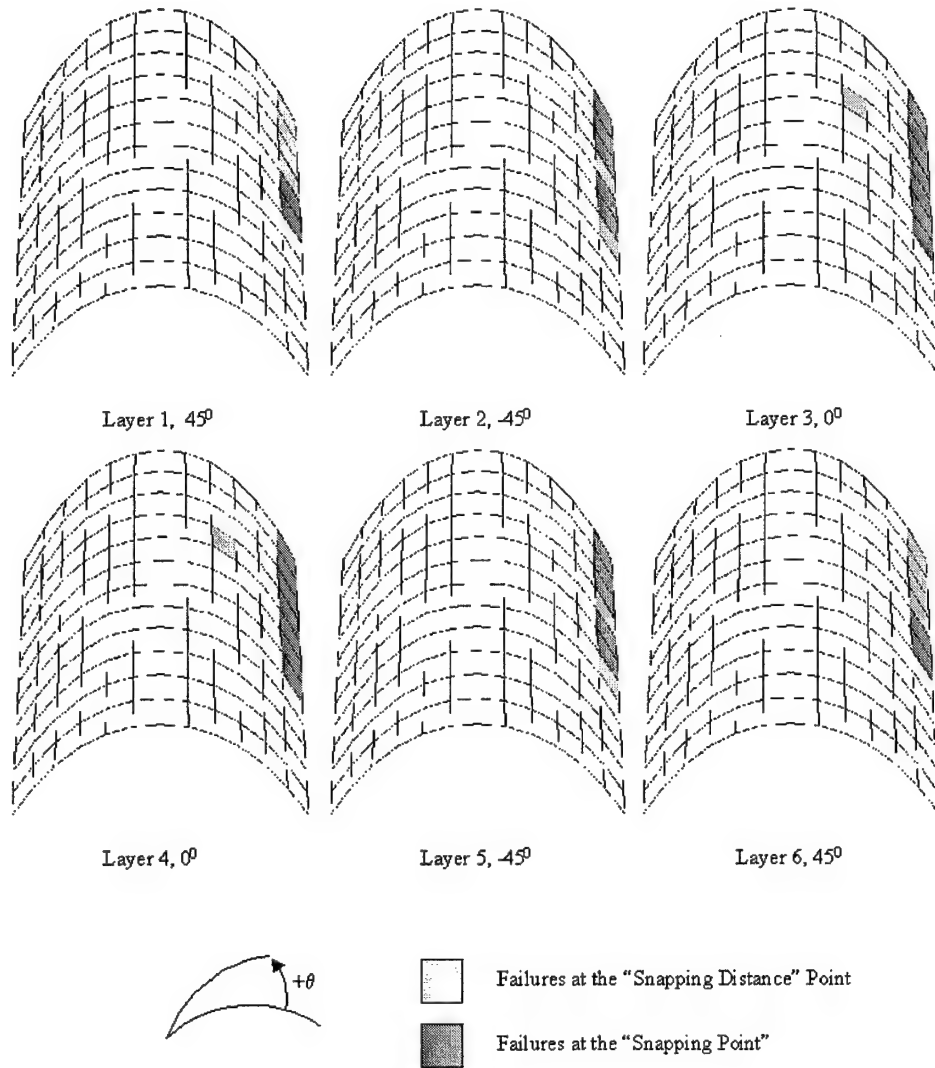
Figure 29. Baseline convex shell illustrating delamination using Lee failure criteria

102

predicted between plies along the axial edge as shown in Fig. 29. Unlike the Hashin analysis, there was not a noticeable increase in the number of elements experiencing fiber, matrix and delamination failure for all layers. Again, examining the percent volume of failure, approximately 2.7%, 2.1% and 1.4% of the 45°, −45° and 0° plies experienced fiber failure at the critical snapping point, while at the snapping distance point, the percent of shell volume experiencing fiber failure increased to 4.2%, 4.2% and 2.7% respectively. Similarly, at the critical snapping point, 10%, 10% and 2.1% of the 45°, −45° and 0° layers experienced matrix failure, while at the snapping distance point, the percent of shell volume experiencing matrix failure increased to 15%, 15% and 5.5% respectively. Finally, at the critical snapping point, 2.7%, 3.5% and 3.9% of the ply interfaces encompassing the 45°, −45° and 0° layers experienced delamination, while at the snapping distance point, the percent of shell volume experiencing delamination increased marginally at the respective ply interfaces to 4.2%, 4.8% and 5.5%. Therefore, the Lee criteria predicted twice as much fiber failure at the snapping distance point, although the total percent volume of fiber failure was minimal. Predicted matrix failures increased by 150% in the ±45° plies, while doubling in the 0° layers. Finally, delamination increased by approximately 150%, 140% and approximately 800% in the interfaces encompassing the 45°, −45° and 0° layers, although the location of delamination continued to remain along the same axial edge shown in Fig. 29.

4.2.3 Composite Comparison using Maximum Stress Failure Criteria

The maximum stress failure criteria is an independent failure criteria, which implies that there is no accounting for stress interaction when determining the state of failure. For example, fiber failure has occurred when the stress along the fiber exceeds the allowable material strength in the fiber direction. This is different from the Hashin and the Lee criterion, which both considered the effects of shear stress. The same $12x12$ mesh discretization used in the Hashin and Lee anal-

103

ysis was again used for the maximum stress analysis, along with the same 0.5 mm displacement increments and 0.1% displacement convergence criteria. Unless otherwise noted, references to displacement or transverse deflection refer to the center point of the shell, where the transverse point load was applied. Referencing Eqns. 54, 56 and 57, the identification of matrix and fiber failure was straightforward.

The total response of the baseline specimen analyzed with the maximum stress failure criteria can be seen in Fig. 30. The load at the critical snapping point was reduced by approximately 30 N, or to within 100 N of the experimental critical snapping load. The deflection at which the critical snapping load occurred for the SLR shell remained constant. The next step in the data analysis was
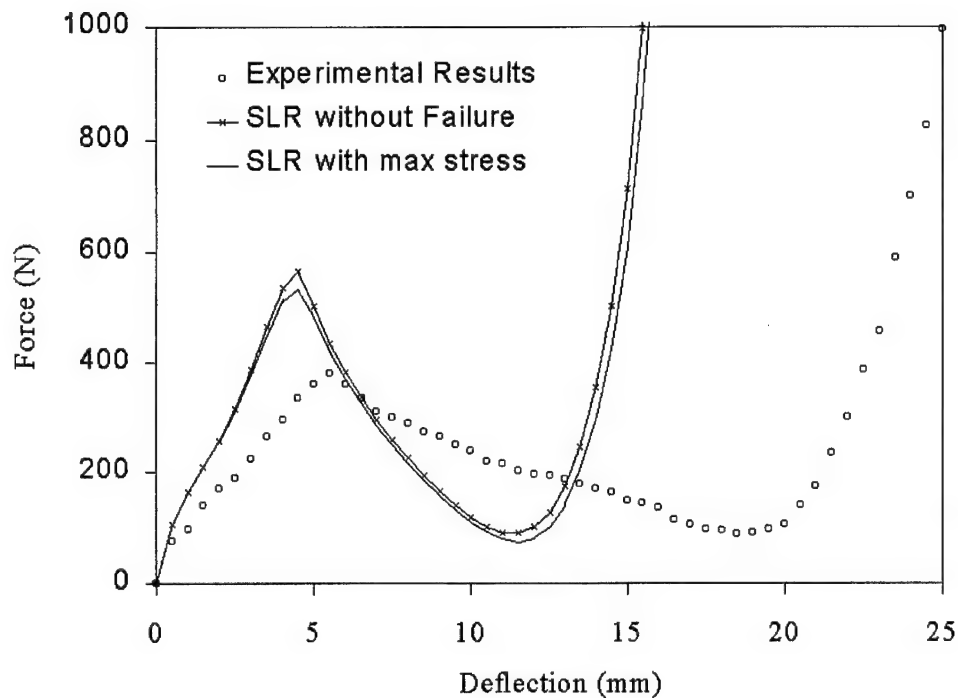
Figure 30. Physical response of the baseline convex shell with maximum stress failure criteria

to determine the first failures predicted by the maximum stress theory. Again, the displacement increments were reduced to 0.005 mm, while holding all other variables constant. This provided the necessary detail required to accurately determine the first failures. Using the small, 0.005 mm displacement increments, the first of each mode of failure was determined. Results of these failures can be seen in Fig. 31, where "M" refers to matrix, "F" to fiber, and "D" refers to delamination. If no distinction is made between the $\pm 45°$ layers in the nomenclature, then a representative of each orientation failed at that point.   As in the Hashin and Lee failure cases, all of the first failures for the maximum stress failure criteria occurred along the axial edge, in elements 139 through 144, where the element numbering is displayed in Fig. 13. The first ply failure was matrix cracking in the $\pm 45°$ layers at a transverse load and deflection of 27 N and 0.1 mm. The next failure to occur was fiber failure in the $0°$ plies, at a transverse load and deflection of 40 N and 0.15 mm. Next, matrix failure in the $0°$ plies and fiber failure in the $\pm 45°$ layers occurred at a load and deflection of 61 N and 0.25 mm respectively. As in the Hashin and Lee cases, delamination predicted by the maximum stress theory occurred first in the ply interfaces encompassing the inner $0°$ plies and then proceeded to occur in the ply interfaces encompassing the $-45°$ layers and finally the ply interfaces encompassing the $+45°$ layers. Therefore, delamination first occurred at the interfaces surrounding the $0°$ layers at a load and deflection of 210 N and 1.5 mm. Delamination next occurred in the interfaces surrounding the $-45°$ plies at a load and deflection of 380 N and 3.0 mm. Finally, delamination occurred in the interfaces encompassing the $+45°$ plies at a load and deflection of 480 N and 5.0 mm.

The graphical representation of failure at the critical snapping point and the corresponding snapping distance point, or Figs. 32 through 34, illustrate the three forms of failure considered, fiber, matrix and delamination. The critical snapping point and the corresponding load on the second equilibrium path, or the snapping distance were analyzed for failure using the maximum
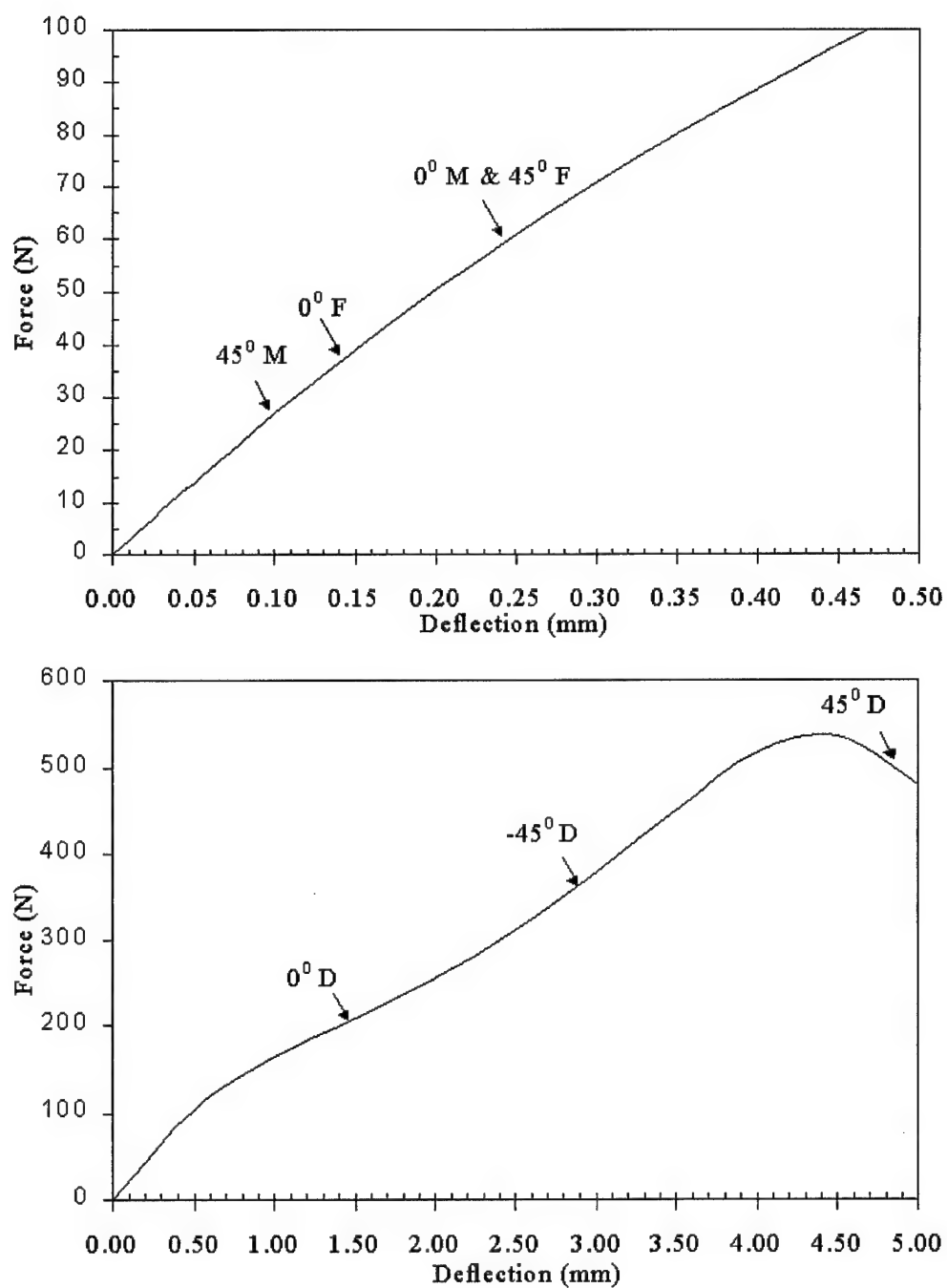
Figure 31. First failures identified using the maximum stress failure criteria

Fiber Failure

| Layer 1, 45^0 | Layer 2, -45^0 | Layer 3, 0^0 |

| Layer 4, 0^0 | Layer 5, -45^0 | Layer 6, 45^0 |

$+\theta$

Failures at the "Snapping Distance" Point
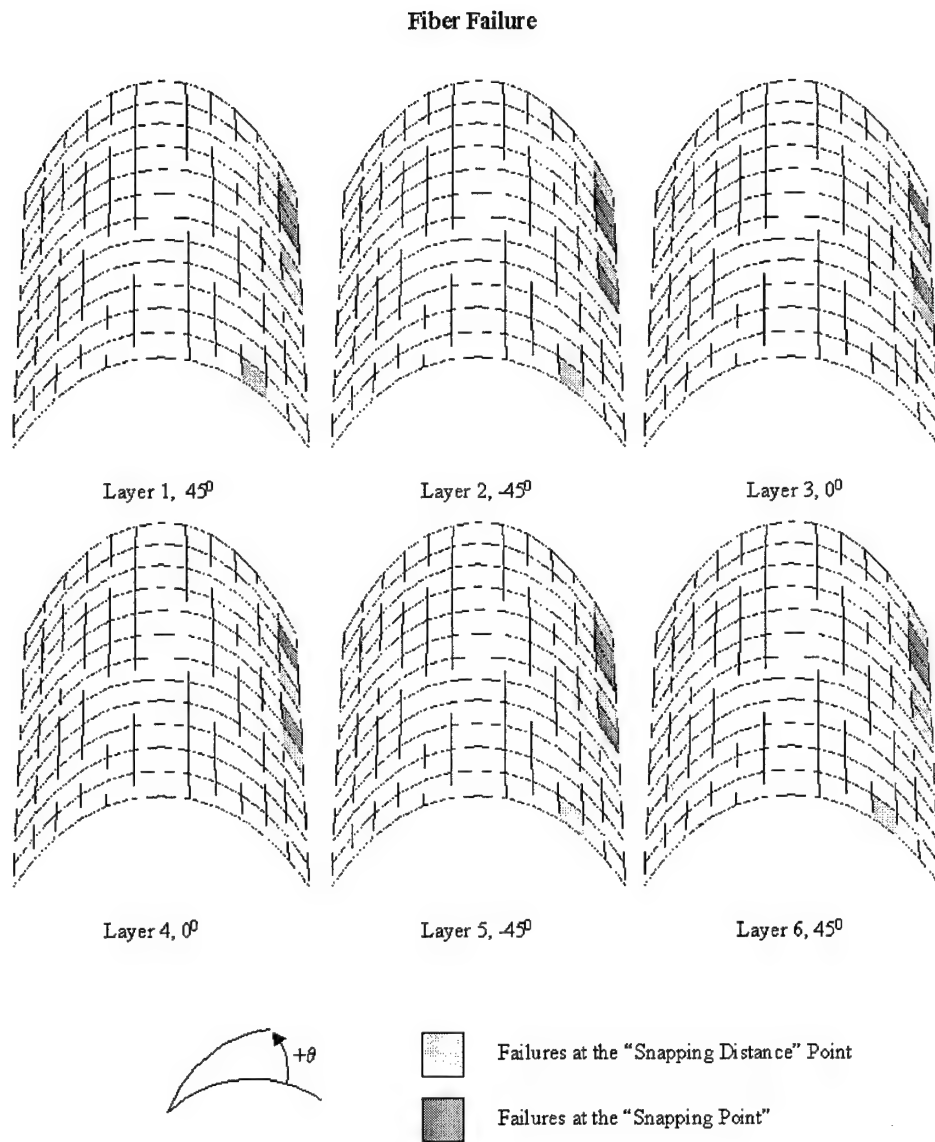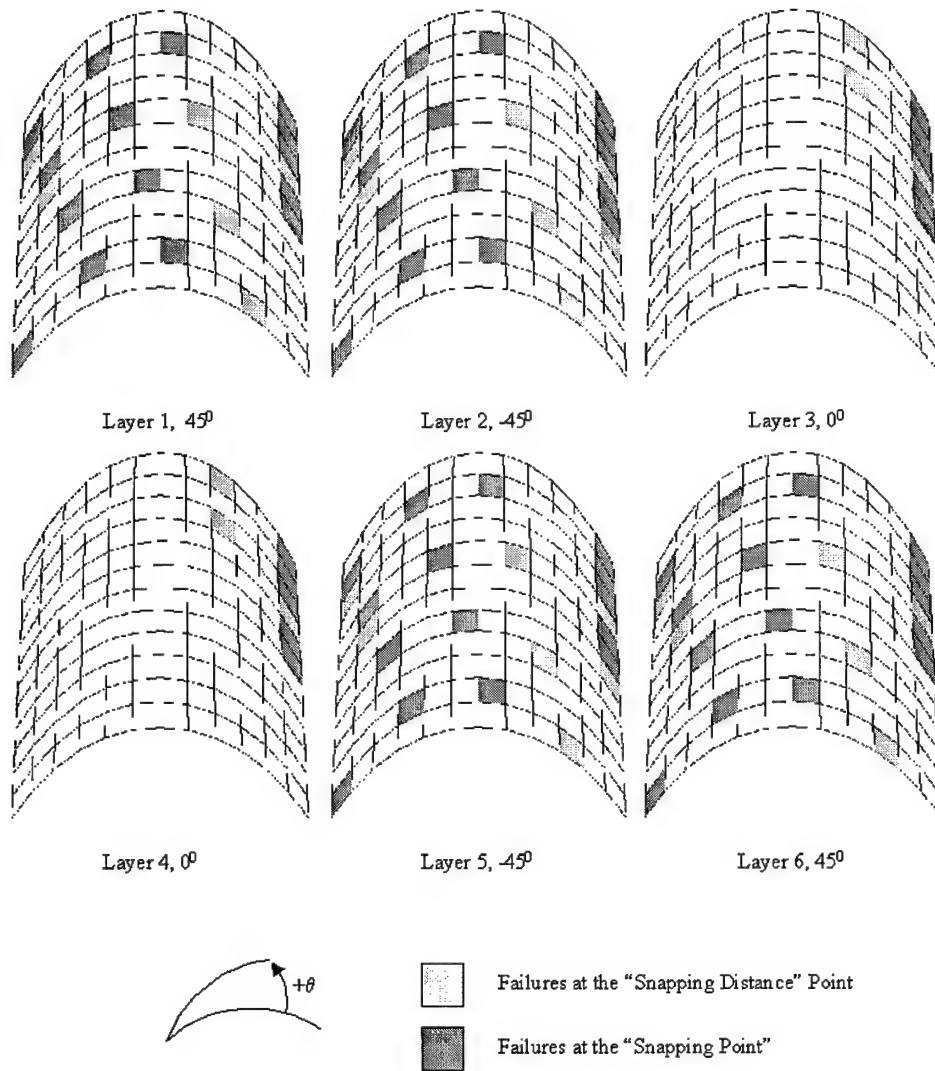
Failures at the "Snapping Point"
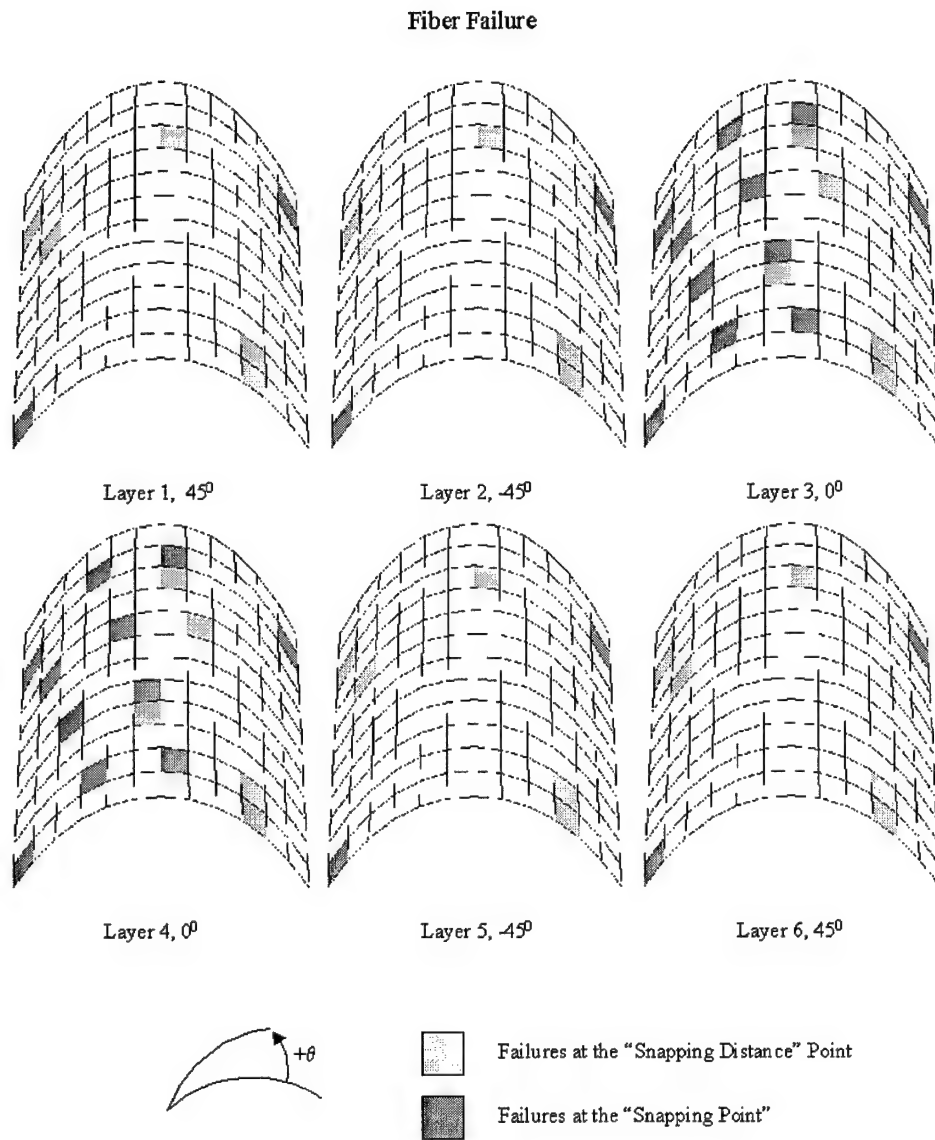
Figure 32. Baseline convex shell illustrating fiber failure using maximum stress failure criteria
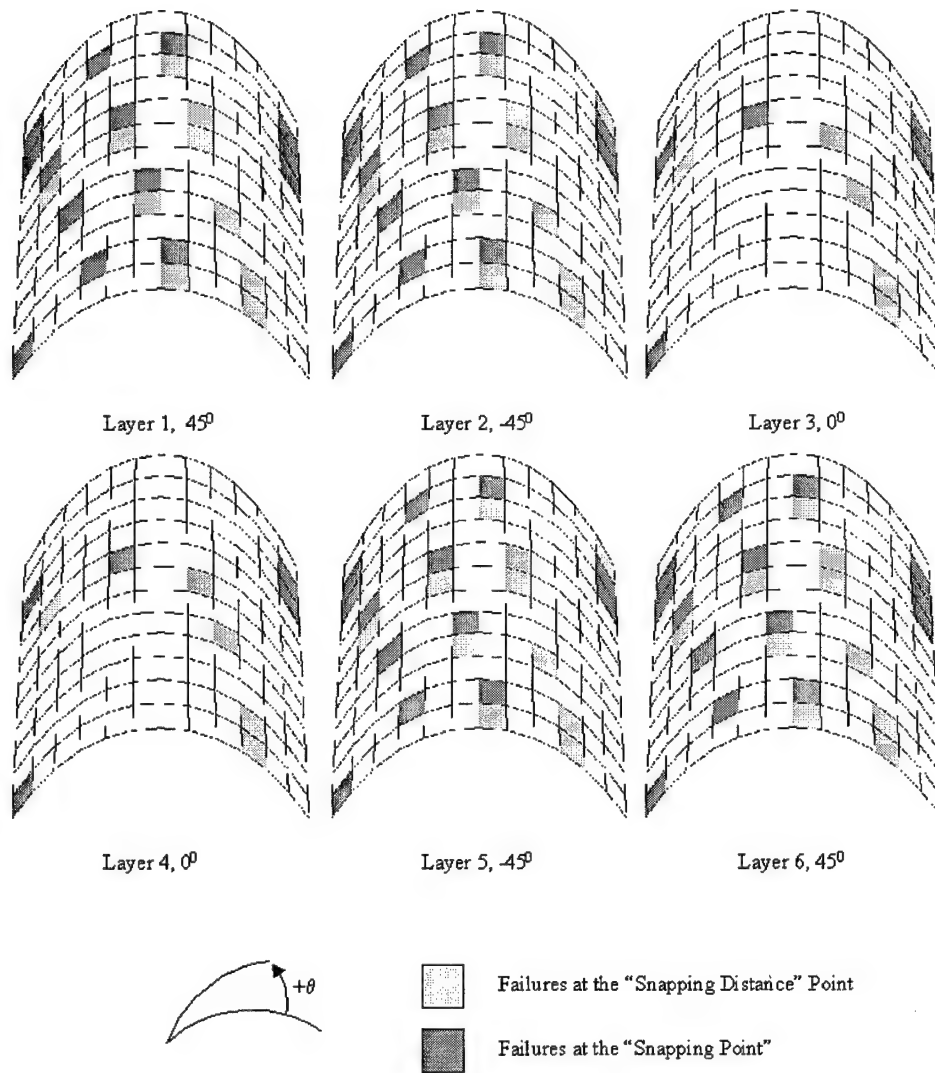
Matrix Failure

Figure 33. Baseline convex shell illustrating matrix failure using maximum stress failure criteria

108

Delamination

Layer 1, 45°   Layer 2, -45°   Layer 3, 0°

Layer 4, 0°   Layer 5, -45°   Layer 6, 45°

+θ

Failures at the "Snapping Distance" Point

Failures at the "Snapping Point"
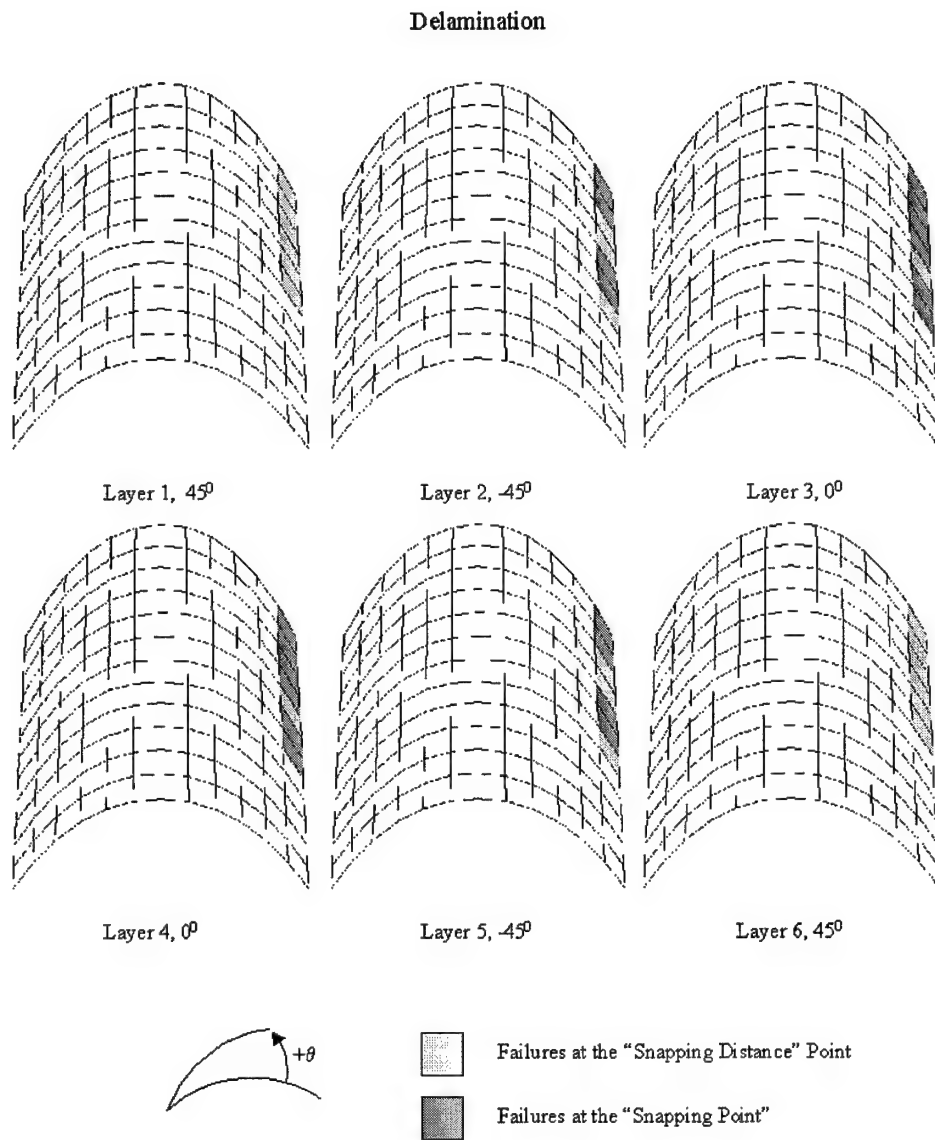
Figure 34. Baseline convex shell illustrating delamination using maximum stress failure criteria

stress failure criteria. The same coloring scheme used in the Hashin and Lee analyses was also used for the maximum stress analysis. Elements exhibiting failure at the critical snapping point are displayed as the dark gray areas on the shell, and elements exhibiting failure at the corresponding snapping distance point are represented as the light gray elements. The shell layers, failure type and location are easily identified in Figs. 32 through 34. Just as in the Hashin and Lee criteria, there was no attempt made to distinguish between the individual gaussian points of each element. Note the similar ±45° failure patterns for the fiber and matrix failure modes, especially in the ±45° plies illustrating matrix failure and in the 0° layers illustrating fiber failure. Delamination was also determined to exist in the same interfaces, as was calculated with Hashin and Lee failure criterion.

Examining the percent volume of the shell experiencing failure again yields some interesting results. Specifically, at the critical snapping point, 1.4%, 1.4% and 7.6% of the 45°, −45° and 0° layers experienced fiber failure, while at the snapping distance point, the percent of shell volume experiencing fiber failure increased to 4.8%, 4.8% and 11% respectively. Similarly, at the critical snapping point, 9.7%, 9.0% and 3.5% of the 45°, −45° and 0° layers experienced matrix failure, while at the snapping distance point, the percent of shell volume experiencing matrix failure increased to 17%, 17% and 6.9% respectively. Finally, at the critical snapping point, 1.4%, 4.8% and 4.8% of the interfaces between the 45°, −45° and 0° layers experienced delamination, while at the snapping distance point, the percent of shell volume experiencing delamination only increased to 4.2% at the interfaces encompassing the 45° plies. At the snapping distance point, matrix failures predicted by the maximum stress criteria essentially doubled. Fiber failures more than doubled in the ±45° plies and increased by approximately 150% in the 0° plies. Delamination increased only marginally.

110

4.2.4 Results of the Comparison

Typically, the success or relevance of this type of failure comparison would be quantified using several comparison metrics. In addition to force-deflection curves, a damage comparison would also be beneficial, allowing insight into the strengths and weaknesses of the various assumptions made, as well as the various failure criterion used. Unfortunately, the level of detail required for the damage comparison was not available, and the success of the comparison was therefore based on the force-deflection curves, or the effect that the stiffness reduction had on the SLR FEM and on limited damage characteristics noted in the experimental analysis. Comparisons were also made with respect to the three failure criterion used. In other words, the type, location and extent of failures detected will be discussed as well as the extensive failure along the axial edge noted for all criterion.

Based upon the metrics just mentioned, all of the progressive failure analysis provided reasonably good results as compared to the experimental data. That conclusion is based upon several factors. First, note the failure patterns obtained for matrix cracking detected using all of the criteria. At the critical snapping point, the dominant matrix cracks are noted to extend in the $\pm 45°$ directions. This pattern was noted by Wardle and Lagace in their experimental analysis [44]. Results for impact specimens in the experimental analysis also indicated the same $\pm 45°$ delamination patterns, which were not seen in the SLR analytical failure analysis. Again, it should be stressed that the interply delamination calculated using all of the criterion was based upon the stress field at the center of each ply. Second, there were no significant drops in transverse load, i.e., the load-deflection curve for the reduced SLR data did not have sudden extreme load drops indicative of sudden failures. As this type of failure would have been revealed in the experimental quasi-static analysis, again the SLR results proved comparable. Finally, as in the experimental analysis, the SLR results did not achieve final ply failure, which would indicate too conservative an analysis.

111

A comparison between the failure criterion also reveals some interesting results. Note the first failures predicted in Figs. 21, 26 and 31. There are several conclusions that can be made with respect to those first failures. First, all of the respective criterion predicted matrix cracking in the $\pm45°$ plies as the first ply failure. Second, the Hashin and maximum stress criterion predicted the same first failures for all three failure modes considered. In fact, matrix cracking and fiber breakage for all plies were detected at the same transverse loads and displacements. The delamination results were similar as well. The similarities between the Hashin and maximum stress criterion should not come as a surprise, given the thinness of the shell essentially resulting in a plane stress condition and the Hashin criteria's reliance on both direct and shear stresses to define the failure environment. Although the first failure modes were similar between the Hashin and maximum stress criteria, a close examination of Figs. 22-24 and 32-34 reveal significant differences in the extent and frequency of further progressive failure modes. The Lee criteria also predicted the same delamination as the Hashin and maximum stress criterion as well as the same first ply failure. However, fiber breakage in both of the $0°$ plies was not detected until just prior to the shell critical snapping point. Again, the predicted delamination similarities and nature of occurrence for all three cases were expected. First, note that the Hashin criteria reduced to the Lee criteria since the transverse direct stress σ_{33} was neglected in the SLR theory as shown in Eqn. 59, repeated hear for convenience.

Lee criterion [9]:

$$\left(\sigma_{12}^2 + \sigma_{23}^2\right)^{\frac{1}{2}} \geq \sigma_{DS}$$

Hashin criterion [9]:

$$\left(\frac{\sigma_{33}}{\sigma_{ZN}}\right)^2 + \frac{\sigma_{12}^2 + \sigma_{13}^2}{\sigma_{DS}^2} \geq 1 \tag{61}$$

112

Second, the maximum stress delamination failure envelope was also defined by the transverse stresses. Finally, the parabolic transverse shear stress generated as a result of the SLR FEM formulation, resulted in the maximum transverse shear stress occurring at the shell midsurface and tapering off to zero at the upper and lower surfaces of the shell. Therefore, the first and greatest occurrence of the delamination should and did occur in the interfaces encompassing the inner plies.

Examining the force-deflection curves for all three cases reveals little difference in the outcome of the progressive failure analysis as shown in Figs. 20, 25 and 30. However, a closer examination of Figs. 22-24, 27-29, and 32-34 reveal the differences in individual failures detected using the various criteria. The Hashin failure criteria yielded the most conservative results, followed by the maximum stress and then the Lee criteria. The phrase "most conservative" implies the maximum amount of failures predicted and therefore the greatest reduction in the shell stiffness. As noted previously, the experimental results indicated the same matrix cracking patterns noted for all three cases [44]. However, the similarities between all three criterion ended there. Again, note the agreement between the Hashin and maximum stress predicted matrix and fiber failures. Both cases predicted the greatest occurrence of matrix cracking in the $\pm 45°$ layers and conversely the greatest amount of fiber breakage in the $0°$ layers. On the other hand, the Lee criteria predicted minimal fiber breakage for all layers, both at the critical snapping point and at the corresponding snapping distance point. Again, the differences can be attributed to the maximum stress and Hashin reliance on direct, in-plane stress and the Lee reliance solely on shear stress, indicating the dominance of the in-plane stress field.

Finally, a discussion is warranted regarding the propensity for failure along the axial edge encompassing elements 133 through 144. As mentioned several times, all of the first failures occurred in this general region. The reason for the occurrence can be traced back to the discussion on the asymmetry of angle-ply laminates. Consider the topographical views of the shell midsurface

113

at the critical snapping point, both with and without the effects of progressive failure analysis, shown in Fig. 35. As in Fig. 12, the various shaded regions represent differences in elevation above the base of each respective diagram. The use of this format aids in the representation of asymmetry brought about by the progressive failure analysis. Using the Hashin results as an example, note the loss of diagonal symmetry at the critical snapping point. Especially note elements 139 through 144 pointed out in part (b) of Fig. 35. Those are the elements where the first failures were detected and also the elements where delamination was predicted. The loss of symmetry, seen in the darkly shaded area above elements 139 through 144, resulted in an increase in the moment seen at that axial edge and therefore greater stress, thus the greater occurrence of failure, i.e., a greater tendency to exceed the respective failure envelopes. Remember, as shown in Fig. 13, the axial edges boundary conditions were all fixed with the exception of $w_{,1}$ and $w_{,2}$, although $w_{,1}$ was implicitly zero, as the boundary conditions u, v and w were also fixed along the same axial boundaries. This condition allowed for the occurrence of transverse shear at the axial edges. The possibility of asymmetrical deformation modes was expressed by Wardle and Lagace [44]. In fact, future areas of study recommended by Wardle and Lagace included investigations into the effects of boundary conditions and possible asymmetrical deformation modes as a result of ply failures [44]. All of the failure criterion used in this analysis resulted in asymmetrical deformation modes as a result of the asymmetrical predicted failures as shown in Fig. 35.

4.3 Composite Sandwich Panel Analysis

Understanding the physical response, including failure, of a sandwich composite panel is critical, given their increased use in the aerospace industry. The Hashin, Lee and maximum stress failure criterion were added to the SLR finite element method in order to provide a more realistic representation of the total physical response of a sandwich shell. An analysis was made on

114

Note the asymmetrical deformation modes

Elements 144-139

(a)

(b)
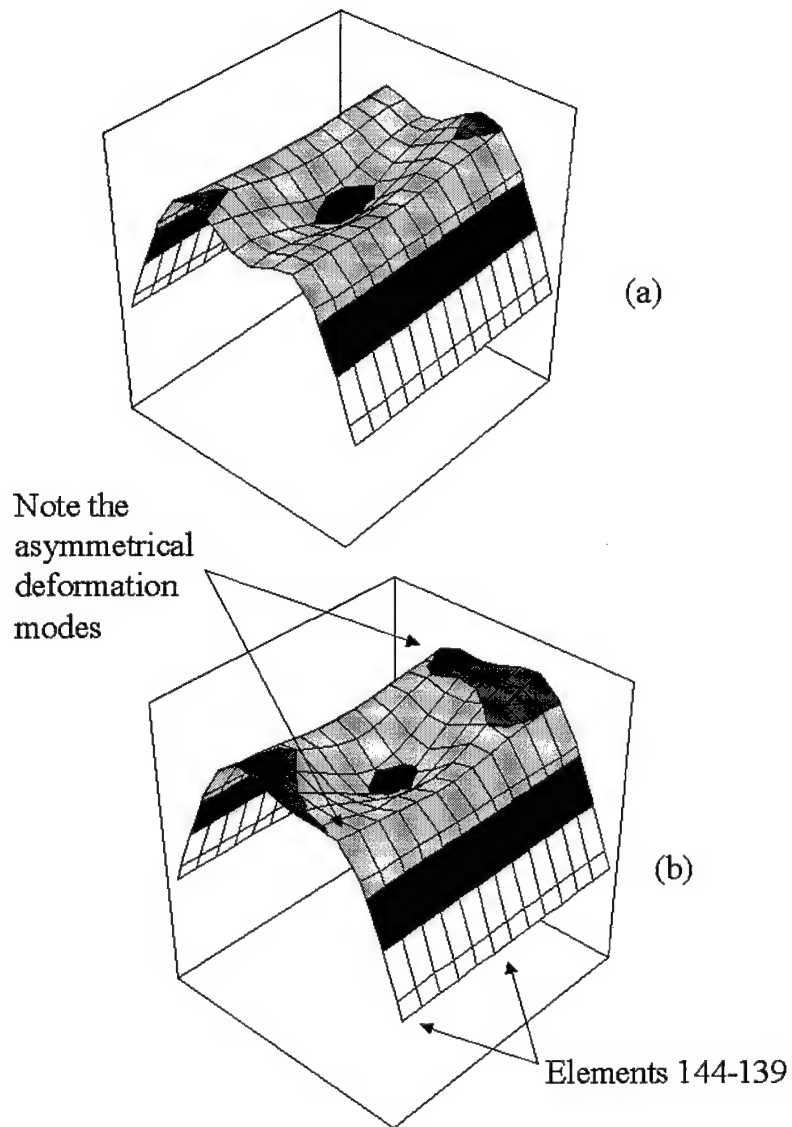
Figure 35. Baseline convex shell at the critial snapping point (a) without failure analysis and (b) with Hashin failure analysis

115

the baseline sandwich configuration using each of the various failure criterion. The primary purpose of this comparison was to investigate the assumptions made in modeling the sandwich core. The maximum stress, Hashin and Lee failure criterion were evaluated in the same manner for the core, as they were evaluated for the facesheets. Although failure of the sandwich core was considered using the same criterion used for the composite facesheets, only transverse core failures were accounted for. In other words, the conditions of fiber failure and matrix cracking had no real significance with respect to the sandwich core. Furthermore, in-plane core material strengths were unavailable for an in-plane core failure analysis. Therefore, for any transverse failure calculated using the respective criterion, all of the material constitutive relations were incrementally reduced to a nominal value per the discussion in Chapter 3. In modeling the failure of the core, several assumptions were required. Since the transverse direct stress was neglected in the SLR theory, the resulting core transverse stiffness was completely modeled by the transverse shear strength. Therefore, the primary core failure mode, core shear crushing, was modeled by the transverse shear strengths. In order to reiterate, although a facesheet failure analysis was carried out along with the core analysis, the primary purpose of this comparison was to quantify the sandwich core modeling and failure. For each of the failure analyses, first core failures were determined, as well as significant points along the load-deflection curves. Significant points were defined as any sudden "load-drop" as seen in Figs. 1 and 2.

The general baseline specimen used in the composite shell analysis, was again used for the sandwich analysis, with the addition of a sandwich core material. In other words, the material (AS4/3501-6 graphite-epoxy face sheets), geometry of the shell (radius, span and ply thickness of 152, 102 and 0.134 mm respectively) and facesheet orientation, $[\pm 45°, 0°]$ were constant. A 1.27 cm (0.5 in) sandwich core was added to the baseline composite specimen resulting in a total panel thickness of 13.5 mm, or approximately 0.54 in. The baseline sandwich specimen was first

modeled without failure to provide a means of gauging the failure analysis. The sandwich material

modeled in this analysis was a HRH10-1/8-4.0 honeycomb core material with material properties

listed in Table 3,where "X" , "Y" and "Z" are the strengths in longitudinal, lateral and transverse

$E_1 = 80.4 \, MPa$
$E_2 = 80.4 \, MPa$
$E_3 = 1.005 \, GPa$
$G_{23} = 75.8 \, GPa$
$G_{13} = 120.6 \, MPa$
$G_{12} = 32.2 \, MPa$
$\nu_{23} = 0.02$
$\nu_{13} = 0.02$
$\nu_{12} = 0.25$
$X_t = N/A$
$X_c = N/A$
$Y_t = N/A$
$Y_c = N/A$
$Z_c = 3.83 \, MPa$
$S_{23} = 142.3 \, MPa$
$S_{13} = 177.9 \, MPa$
$S_{12} = N/A$

Table 3. HRH10-1/8-4.0 core material strengths

lamina directions and S_{ij} are the shear strengths [15].

Modeling the composite sandwich panel for the SLR finite element analysis was accomplished

in the manner described in Chapter 3. To reiterate, the sandwich core was treated as an orthotropic

lamina, oriented at $0°$ from the SLR panel axis system, where the orientation is displayed in Fig.

13. The core was separated into five layers, thereby allowing the elasticity relations and tangent

stiffness calculations to be calculated in the same manner as the face sheets. To put it another

way, each core layer was treated as a simple ply. Given the angle-ply orientation of the sandwich

shell facesheets, the full panel was again modeled for the analysis, with the same $12x12$ shell

discretization. Boundary conditions for the sandwich composite were also the same as those chosen

for the composite analysis and are shown in Fig. 13.

4.3.1 Composite Sandwich Failure Comparison

Using the $12x12$ mesh to model the sandwich shell, the boundary conditions of Fig. 13, a displacement convergence criteria of 0.1%, displacement increments of $0.25\ mm$, and the respective failure criterion, resulted in the load deflection curves shown in Fig. 36.   The most notable
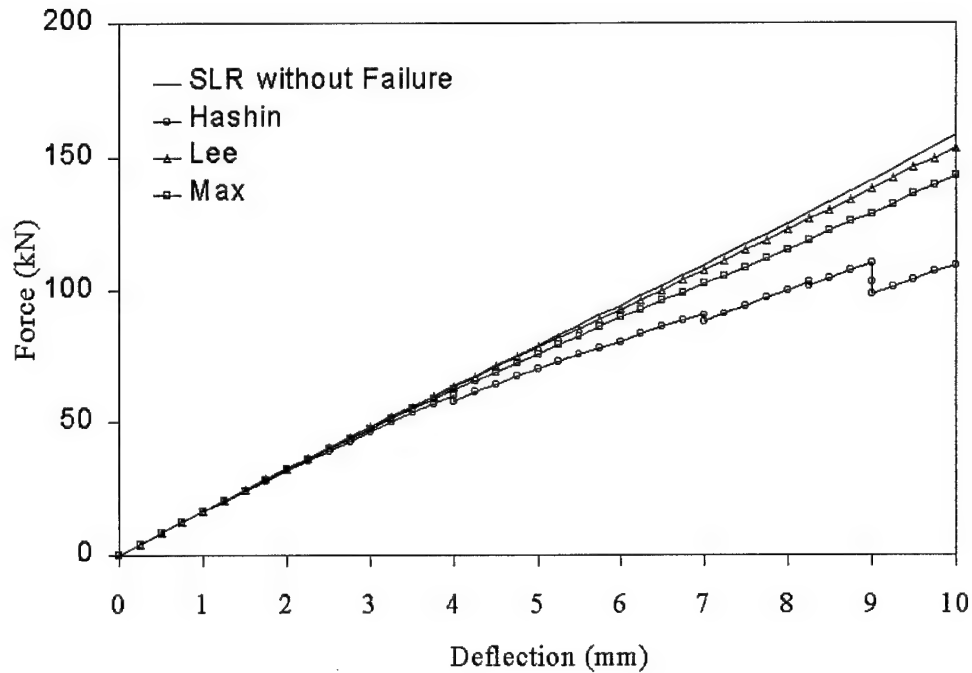
Figure 36. Illustration of core failure modeling in a sandwich shell using Hashin, Lee and maximum stress failure criteria

difference between the load-deflection curves with and without the sandwich core, is the dramatic increase in shell stiffness as a result of the core addition. Note that all of the criterion resulted in a reduction in stiffness to varying degrees. Again, it should be pointed out that the transverse Lee and the Hashin criterion used for the sandwich core reduced to the same expression, as σ_{33} was

118

neglected in the SLR FEM, as shown in Eqn. 59 and repeated here for convenience.

Lee criterion [9]:

$$\left(\sigma_{12}^2 + \sigma_{23}^2\right)^{\frac{1}{2}} \geq \sigma_{DS}$$

Hashin criterion [9]:

$$\left(\frac{\sigma_{33}}{\sigma_{ZN}}\right)^2 + \frac{\sigma_{12}^2 + \sigma_{13}^2}{\sigma_{DS}^2} \geq 1 \tag{62}$$

Therefore the differences in the progressive stiffness reduction due to the two criterion were a result of the manner in which the face sheet damage was evaluated. Furthermore, the maximum stress criteria for the core is also based solely on transverse shear and as a result all three criterion should predict similar core failure patterns. The first core failure predicted using the Hashin criteria was at a load and deflection of 12576 N and 0.75 mm. Not surprisingly, the Lee criteria predicted the initial core failure at the same transverse load and deflection. The maximum stress criteria predicted first core failure at a transverse load and deflection of 8445 N and 0.5 mm.

When examining the response generated using the Hashin failure criteria, the significant load drop occurring at a transverse load and deflection of 110 kN and 9 mm, shown in Fig. 36, bears consideration. Specifically, what caused the drop in load and why, when utilizing the same transverse core failure inequality, was there not a similar load drop seen in the Lee and maximum stress failure cases. In other words, what was the impetus behind the load drop and why did it not occur when using the other criterion. An examination of the state of failure at the point in question sheds light on the issue. Looking at Figs. 37 through 45, illustrates the similarities and differences between the failures predicted by the three criterion. Notice the similar state of core failure predicted in all three cases. Again, using the volume percent of failure as a comparison metric, all of the criterion predicted approximately 35% of the inner most core layer or layer 6 of the shell, 32% of layers 5 and 7, and 23% of layers 4 and 8 experienced core failure. However, the state of facesheet

119

Core Failure

Layer 4   Layer 5   Layer 6

Layer 7   Layer 8

$+\theta$

Failures after "Load Drop"

Failures prior to "Load Drop"
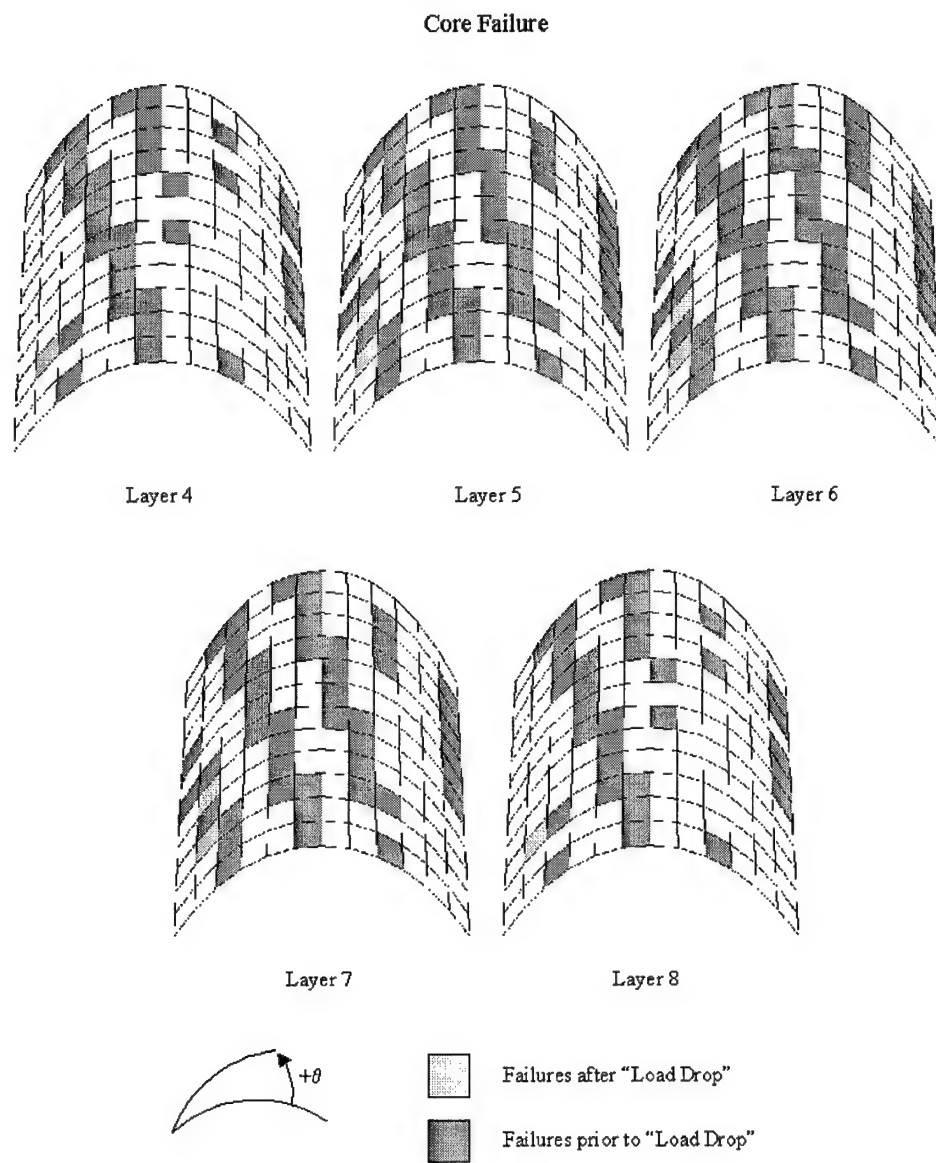
Figure 37. Baseline convex sandwich shell illustrating Hashin transverse core failure

Fiber Failure

Layer 1   Layer 2   Layer 3

Layer 9   Layer 10   Layer 11

$+\theta$

Failures after "Load Drop"

Failures prior to "Load Drop"
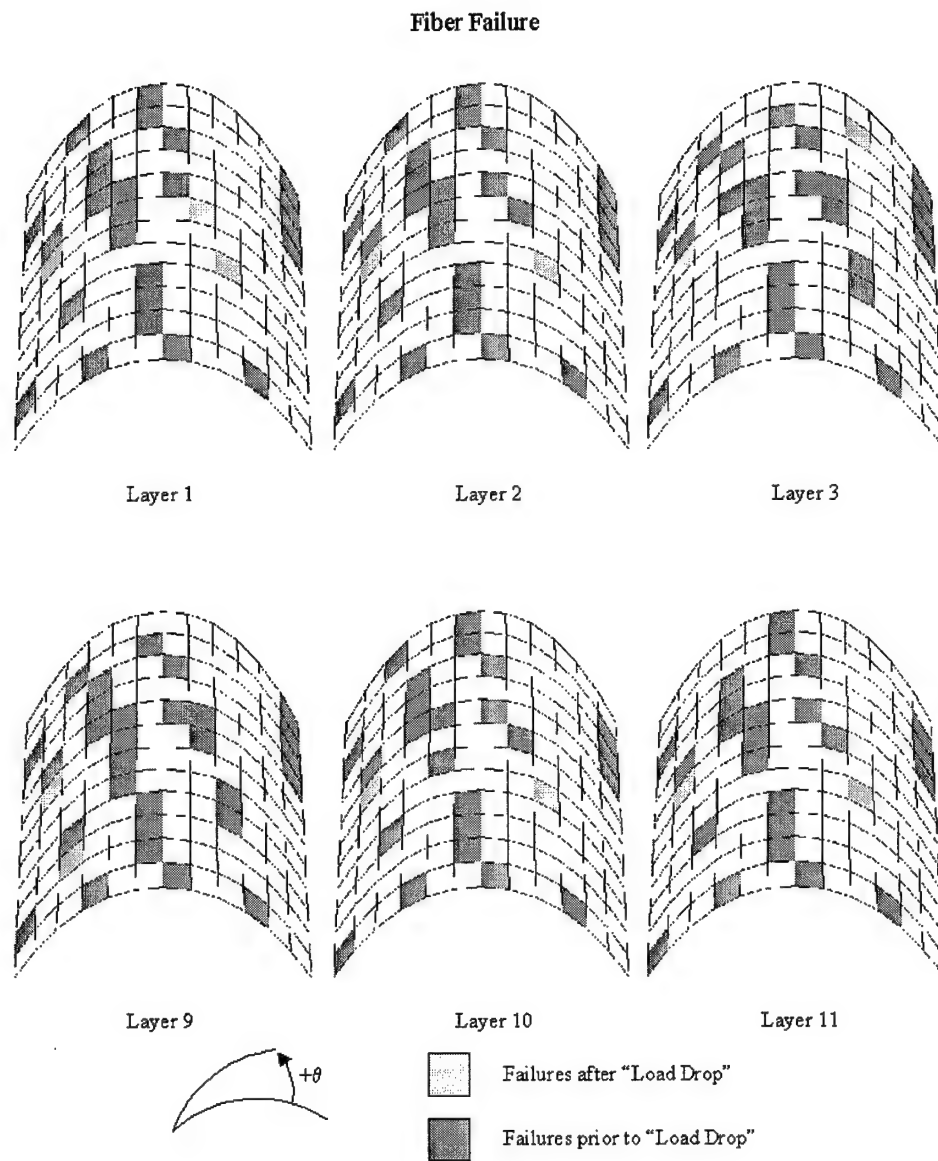
Figure 38. Baseline convex sandwich shell illustrating Hashin fiber facesheet failure
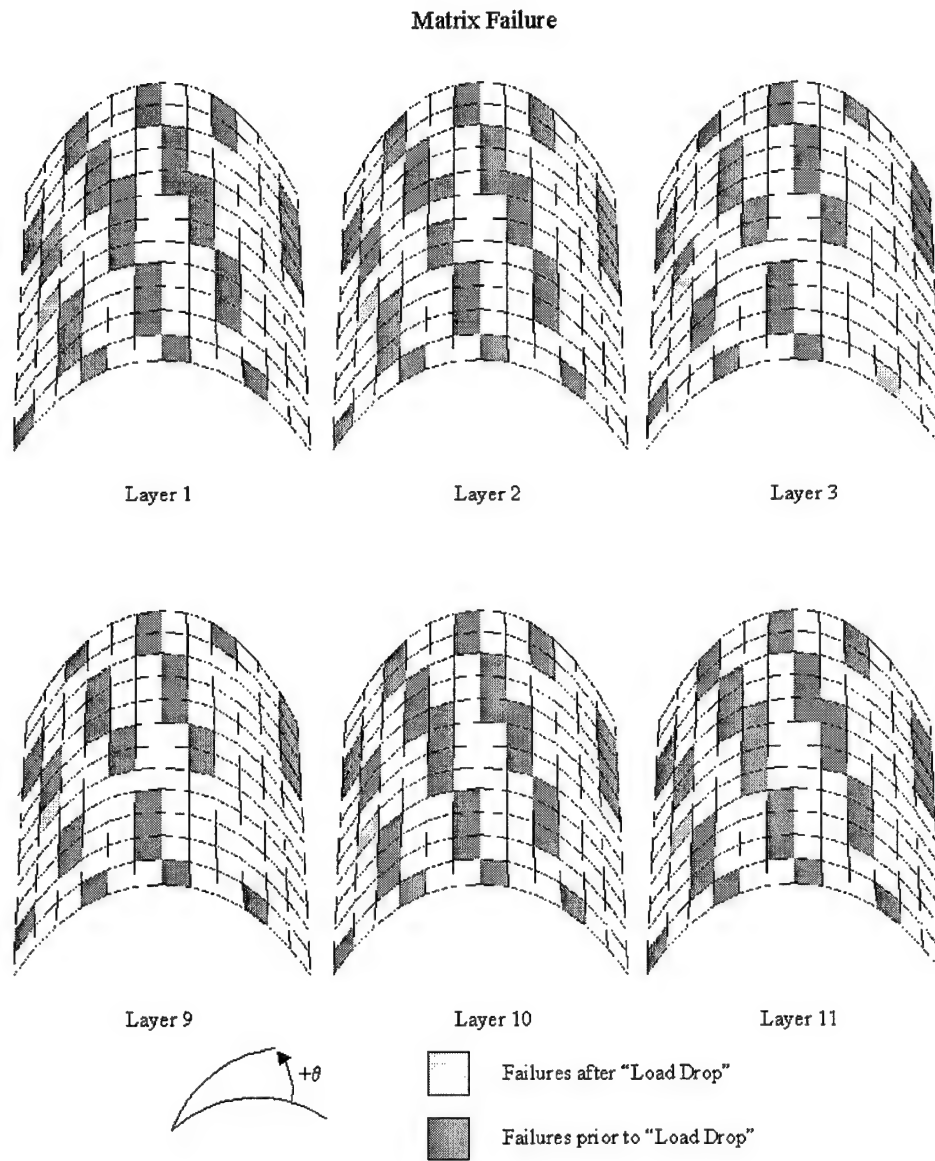
Matrix Failure

Figure 39. Baseline convex sandwich shell illustrating Hashin matrix facesheet failure

122

Core Failure

Layer 4   Layer 5   Layer 6

Layer 7   Layer 8
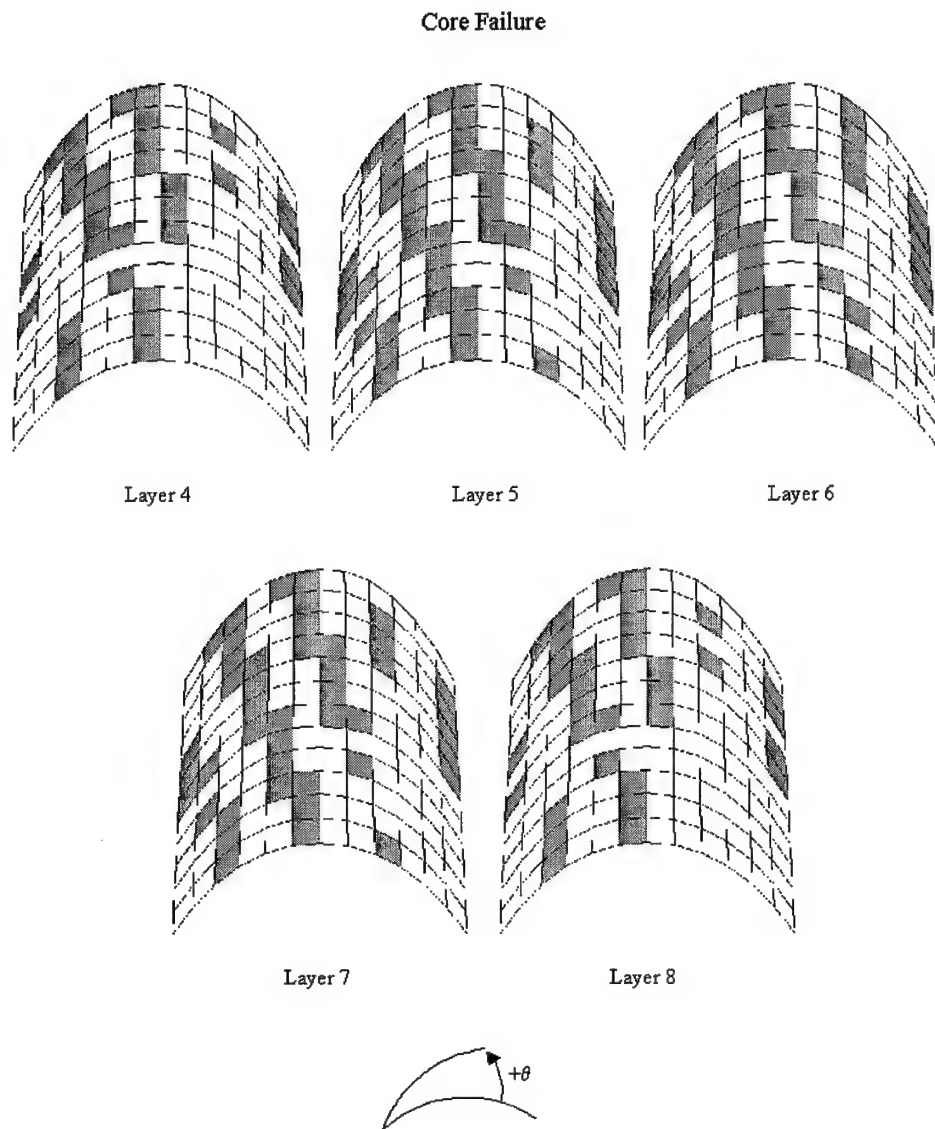
Figure 40. Baseline convex sandwich shell illustrating Lee transverse core failure
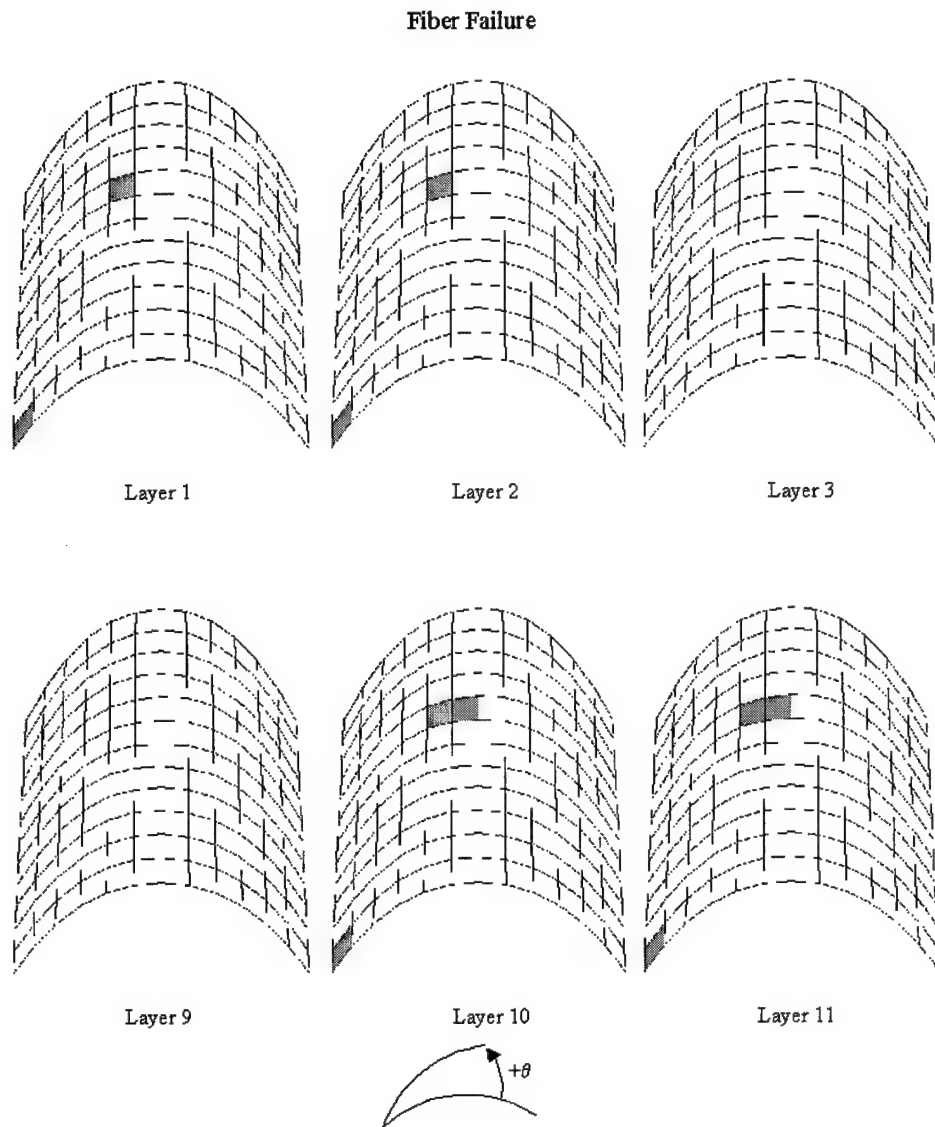
Fiber Failure

Figure 41. Baseline convex sandwich shell illustrating Lee fiber facesheet failure

Matrix Failure

Layer 1   Layer 2   Layer 3

Layer 9   Layer 10   Layer 11
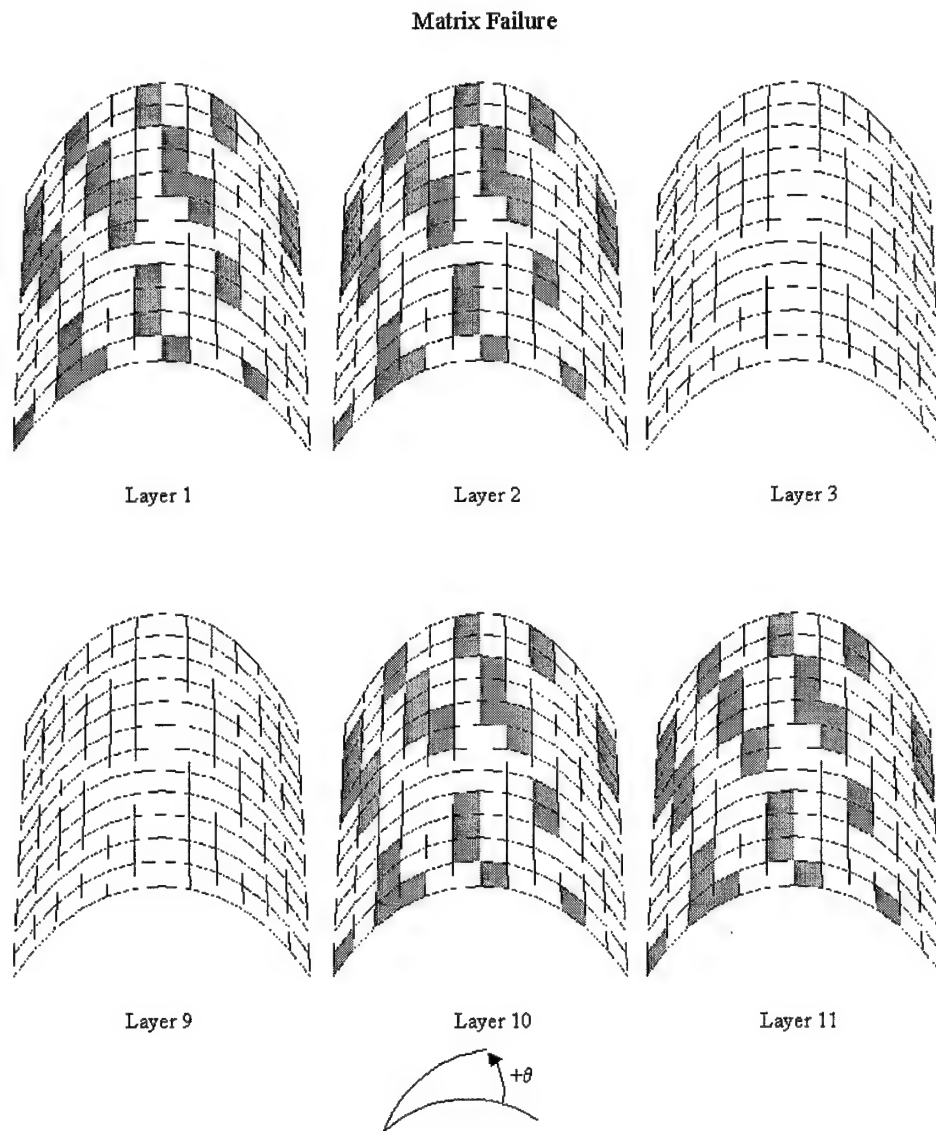
Figure 42. Baseline convex sandwich shell illustrating Lee matrix facesheet failure

125
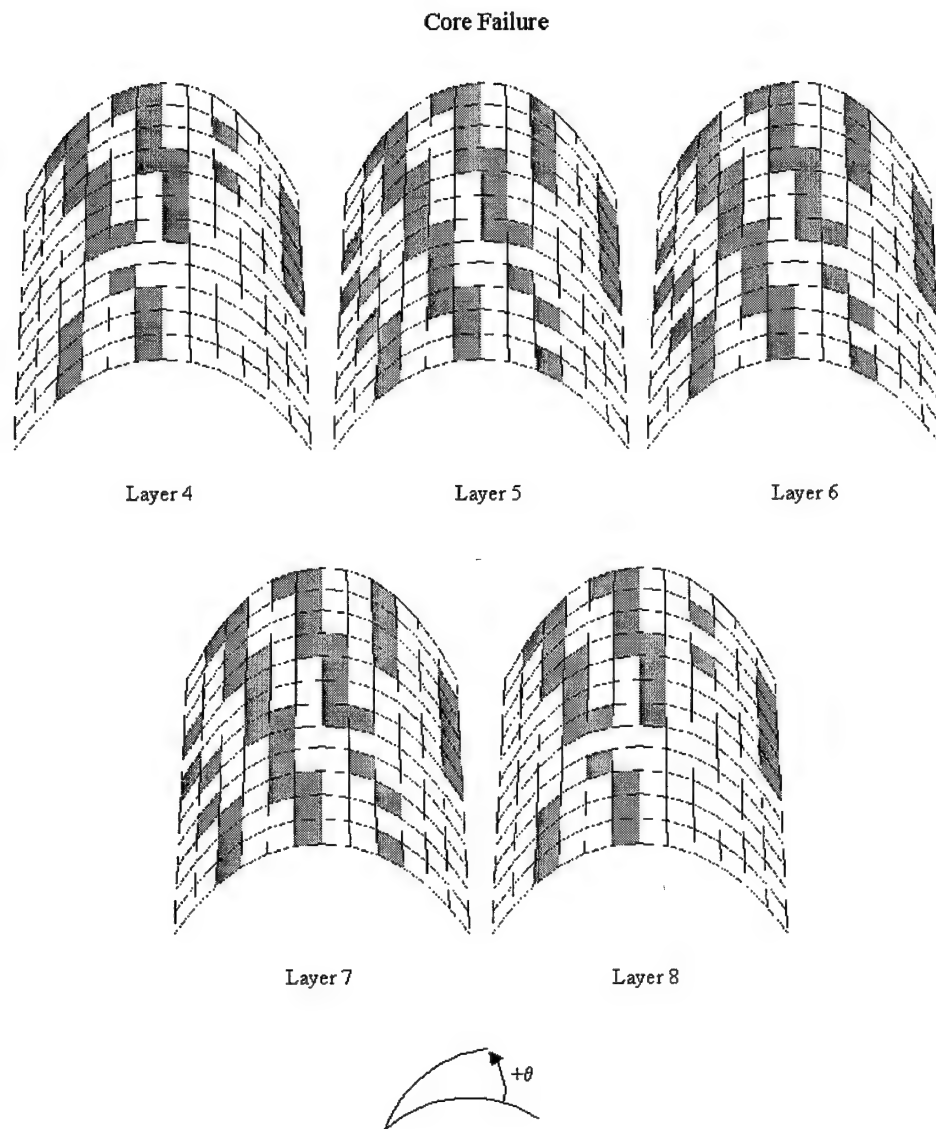
Core Failure

Figure 43. Baseline convex sandwich shell illustrating maximum stress transverse core failure
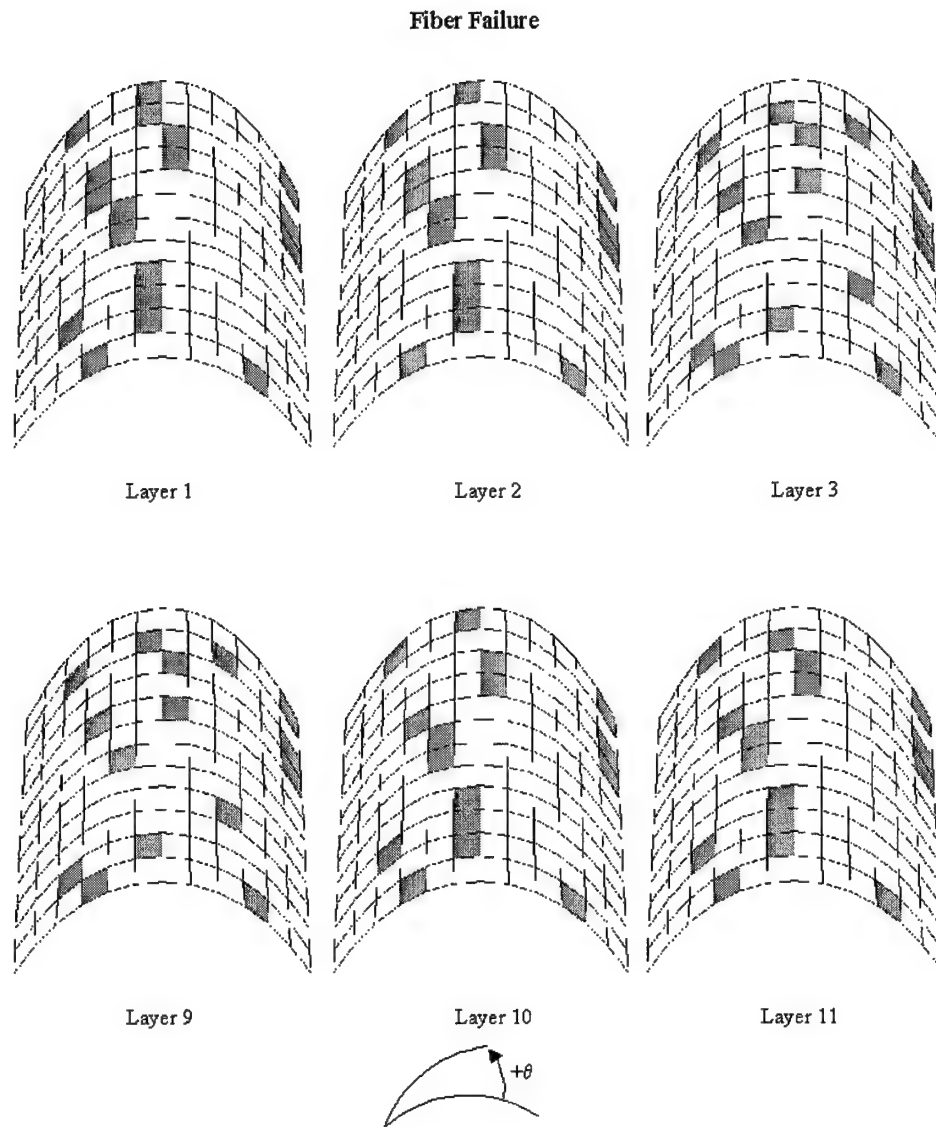
Fiber Failure

Figure 44. Baseline convex sandwich shell illustrating maximum stress fiber facesheet failure

127
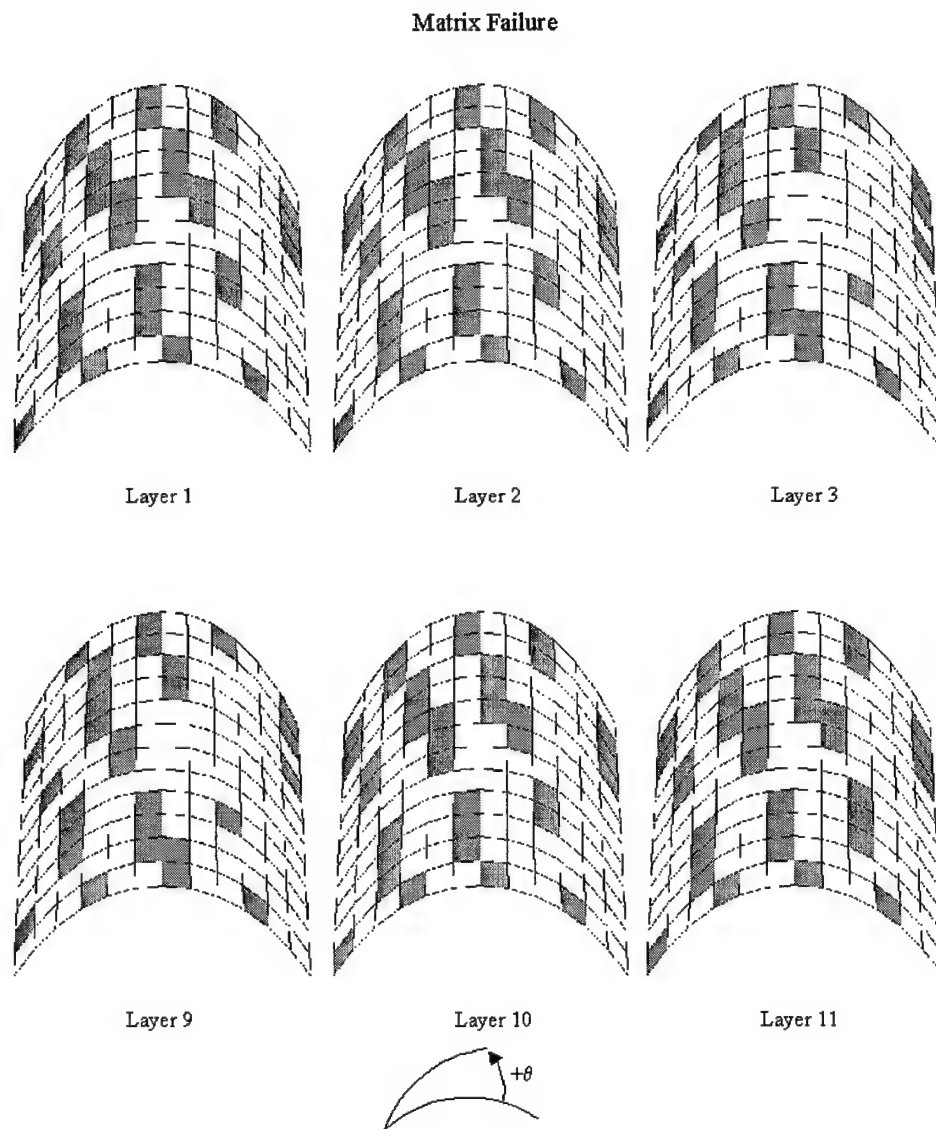
Matrix Failure

Figure 45. Baseline convex sandwich shell illustrating maximum stress matrix facesheet failure

128

failure was quite different. With respect to the predicted facesheet fiber failures, the Hashin criteria predicted a percent volume of fiber failure for the ±45° and 0° plies of 20% for each layer. The Lee criteria predicted a percent volume of fiber failure for the ±45° plies of 1.4% for each layer, while no fiber failures were predicted in the 0° plies. The maximum stress criteria predicted a percent volume of fiber failure for the ±45° and 0° plies of 13%, 11% and 10% respectively. Considering matrix failure, the Hashin criteria predicted a percent volume of failure in the ±45° plies of 28%, while only predicting a percent volume of failure of 22% in the 0° plies. The Lee criteria predicted a percent volume of matrix failure for the ±45° plies of 27% for each layer, while no matrix failures were predicted in the 0° plies. Finally, the maximum stress criteria predicted a percent volume of matrix failure in the ±45° plies of 28%, while only predicting 20% in the 0° plies. Therefore, the reason for the dramatic load drop seen in the Hashin failure case was due to the significant facesheet "softening" as a result of the predicted fiber and matrix facesheet damage. The resulting facesheet softening allowed the sudden loss of transverse stiffness or core damage to be recorded as the load drop in question. Specifically, the sudden load drop in the Hashin analysis was a result of the sudden failure of three elements, throughout the core thickness, shown in Fig. 37. Remember that the core is 12.7 *cm* thick, so although only three elements failed, they failed through the entire sandwich thickness, resulting in a significant loss of transverse strength.

The progression of failure in the sandwich shell occurred in the following manner. For all three criterion, matrix cracking in the facesheets was the first detected failure. These failures were followed by transverse shear failures in the core layers. Core failures were initially detected in the inner most core layers and progressed outwards, a result of the SLR parabolic transverse shear stress assumption. As the core failed in shear and the appropriate constitutive relations reduced, the sandwich facesheets, previously carrying little shear but the majority of the bending moment, were required to compensate for the sudden loss of transverse strength. Therefore, the facesheets

were acting as individual panels, carrying both moment and shear. With the sudden increase in transverse shear stress, facesheet fiber failures began to occur. Notice that fiber damage was negligible when considering the Lee criteria and noticeably less in the maximum stress criteria as compared to the Hashin analysis. Remember that the Hashin criteria is a combination of direct and shear stress components, the Lee criteria is defined solely by shear, and the maximum stress criteria is defined solely by direct stress. That fiber failure occurred to the greatest extent in the Hashin case, followed by the maximum stress case and occurred at a minimum in the Lee case, explains the significance of the in-plane as well as transverse shear stresses with respect to fiber failure. In other words, the Hashin criteria, a combination of direct and shear stress components, predicted the greatest occurrence of fiber failure, followed by the maximum stress case and finally the Lee failure case. Note that for all three cases, the patterns of failure were consistent and continued in the $\pm 45°$ failure patterns seen in the baseline composite shell specimen.

4.3.2 Results of Comparison

Several conclusions can be drawn from the sandwich shell failure analysis. First, as noted previously, all three failure criterion predicted similar failure frequency as well as failure patterns, with the exception of facesheet fiber failure. Damage trends were consistent with the composite shell analysis, with the Hashin criteria predicting the greatest amount of matrix cracking and fiber breakage, followed by the maximum stress and Lee criterion. Note that there was little fiber breakage predicted by the Lee criteria, resulting in minimal stiffness reduction as shown in Fig. 36. Since facesheet softening was the dominant factor with respect to the sudden load drop scenario, it was also anticipated that the order of criteria conservatism would remain consistent with the order noted in the composite shell analysis. In other words, the most conservative, or the criteria predicting the greatest amount of failure, was the Hashin criteria, followed by the maximum stress

130

and finally the Lee criteria. Therefore, the Hashin criteria was the most likely to exhibit the load drop characteristics.

Even with the extensive core failures noted in Fig. 37 through 45, the sandwich panel continued to maintain significant strength. In fact, composite facesheet damage or the lack of damage was the dominating driver in the sandwich load-deflection results, i.e., the sudden load drop exhibited in the Hashin case. Similar results were noted in the analytic effort of reference [15]. In other words, while the initial point of core failure was modeled reasonably well in the aforementioned referenced analysis, the loss of stiffness as a result of the core damage was offset by the lack of significant stiffness reduction in the sandwich facesheets as lamina failures occurred. For the purposes of this research, this was likely due to the kinematic and resulting displacement-strain relations of the SLR theory. Specifically, the in-plane stresses dominated the response, with the transverse strains and stresses having less of an effect in the general response characteristics.

Finally, the transverse loading in the SLR FEM was applied at the shell center node or intersecting lines of symmetry, in effect a point load. As a result, there was no in-plane distribution of the applied loading. Likewise, there was no modeling of the shell-load applicator interface. Therefore, the transverse point load application combined with the SLR FEM transverse shear versus in-plane stress assumptions are thought to be the reasons behind the lack of distinguishing core failure patterns in the vicinity of the applied loading for all three failure cases considered.

Chapter 5 - Conclusions

As the use of composite and sandwich composite material increases in the aerospace community, understanding their physical response to loading is critical. The inclusion of failure analysis into a finite element method is an important step in gaining insight into the behavior of damaged composite and sandwich composite shells. Namely, how do composite and sandwich composites react to first ply failures and the resulting progressive failures under continued use or loading. This research has generated some interesting conclusions as well as opened the door to new areas of study.

There were several goals with respect to this analysis. First was the need to quantify the SLR analytical results. In other words, how did the SLR theory predict the behavior of composite shells with respect to actual experimental results and compared to an industry standard finite element package. A comparison was made between the SLR FEM and both a recently conducted experimental investigation, as well as the finite element program ABAQUS$^{®}$. Some general results are as follows. First, the SLR theory reasonably predicted the snapping phenomenon seen in some shell structures, for the baseline case evaluated with ABAQUS$^{®}$ and the results generated from the aforementioned experiment. Further investigation into the snapping phenomenon showed the SLR theory more accurately predicted "snapping" in both thin and shallow shells. Second, as the shell thickness was increased and the problem became three dimensional, the SLR results tended to diverge from the experimental data. Finally, as the shell became deeper and the magnitude of rotations increased, the SLR theory again overpredicted the general stiffness of the shell structure. In the development of the SLR theory, simplifying assumptions were made both with respect to the thickness of the shell and the rotations exhibited by the shell, thus the discrepancies for both parameters was exaggerated. However, consideration should also be made with respect to material

132

defects, experimental load application and boundary condition discrepancies and geometric variances in the experimental specimens.

Next, a thin and relatively shallow baseline specimen was chosen for the first of two failure investigations. Three failure criterion, Hashin, Lee and the maximum stress theories, were incorporated into the SLR FEM and the resulting load deflection responses compared to the undamaged baseline response. All three criterion predicted failures resulting in stiffness reduction, with the Hashin predicting the greatest occurrence of failure, followed by the maximum stress and Lee criterion. The Hashin and maximum stress criterion predicted similar first ply failures, while further failure progression resulted in significant differences in fiber and matrix failures between all three theories. The delamination predicted were very similar between all three criterion. Results of the failure analysis compared reasonably well with the experimental analysis. First, none of the failure cases considered resulted in final ply failure. Next, the matrix cracking predicted by all of the criteria occurred in the $\pm 45°$ directions, as observed in the experimental analysis [44]. Fiber breakage predicted by the SLR theory was also seen to occur in the same patterns, however no mention was made of fiber failure patterns in the experimental analysis. An interesting result of the failure investigation were the asymmetrical failure modes resulting from the predicted failures. The possibility of this asymmetry was raised by Wardle and Lagace [44].

Finally, the same baseline specimen used in the composite shell failure comparison was again analyzed, however, this time a sandwich core was added to the shell. The purpose of the comparison was to analyze the core modeling and failure assumptions made with respect to the changes incorporated into the SLR theory. The same failure criterion were used to model failure, and again the Hashin was the most conservative, followed by the Lee and maximum stress theories. Similar core damage was predicted by all three theories, while facesheet damage was significantly different amongst the various criterion. The Hashin criteria was the only failure theory to result in a sudden

133

load drop, resulting from the sudden loss in transverse stiffness due to core failure. The Hashin criteria also exhibited the greatest amount of facesheet damage, particularly fiber failure, therefore, facesheet damage or the softening of the sandwich facesheets due to failure, was seen as the dominating variable in the sandwich shell analysis.

APPENDIX A - Elasticity Relations

A.1 Green's Strain Relations in Cylindrical Shell Coordinates

The following relations are written in general curvilinear coordinates, followed by a description of the cylindrical shell shape factors used to derive the strain relations in general cylindrical shell coordinates. The displacement vector, $\overline{u}(1,2,3)$ is defined as, $\overline{u} = u_1\widehat{i} + u_2\widehat{j} + u_3\widehat{k}$ [36].

$$
\gamma_{11} = h_1\frac{\partial u_1}{\partial y_1} + \frac{h_1 u_2}{h_2}\frac{\partial h_1}{\partial y_2} + \frac{h_1 u_3}{h_3}\frac{\partial h_1}{\partial y_3}
$$
$$
+ \frac{1}{2}\left(\frac{\partial u_1}{\partial y_1} + \frac{u_2}{h_2}\frac{\partial h_1}{\partial y_2} + \frac{u_3}{h_3}\frac{\partial h_1}{\partial y_3}\right)^2
$$
$$
+ \frac{1}{2}\left(\frac{\partial u_2}{\partial y_1} - \frac{u_1}{h_2}\frac{\partial h_1}{\partial y_2}\right)^2 + \frac{1}{2}\left(\frac{\partial u_3}{\partial y_1} - \frac{u_1}{h_3}\frac{\partial h_1}{\partial y_3}\right)^2
$$

$$
\gamma_{22} = h_2\frac{\partial u_2}{\partial y_2} + \frac{h_2 u_3}{h_3}\frac{\partial h_2}{\partial y_3} + \frac{h_2 u_1}{h_1}\frac{\partial h_2}{\partial y_1}
$$
$$
+ \frac{1}{2}\left(\frac{\partial u_2}{\partial y_2} + \frac{u_3}{h_3}\frac{\partial h_2}{\partial y_3} + \frac{u_1}{h_1}\frac{\partial h_2}{\partial y_1}\right)^2
$$
$$
+ \frac{1}{2}\left(\frac{\partial u_3}{\partial y_2} - \frac{u_2}{h_3}\frac{\partial h_2}{\partial y_3}\right)^2 + \frac{1}{2}\left(\frac{\partial u_1}{\partial y_2} - \frac{u_2}{h_1}\frac{\partial h_2}{\partial y_1}\right)^2
$$

$$
\gamma_{33} = h_3\frac{\partial u_3}{\partial y_3} + \frac{h_3 u_1}{h_1}\frac{\partial h_3}{\partial y_1} + \frac{h_3 u_2}{h_2}\frac{\partial h_3}{\partial y_2}
$$
$$
+ \frac{1}{2}\left(\frac{\partial u_3}{\partial y_3} + \frac{u_1}{h_1}\frac{\partial h_3}{\partial y_1} + \frac{u_2}{h_2}\frac{\partial h_3}{\partial y_2}\right)^2
$$
$$
+ \frac{1}{2}\left(\frac{\partial u_1}{\partial y_3} - \frac{u_3}{h_1}\frac{\partial h_3}{\partial y_1}\right)^2 + \frac{1}{2}\left(\frac{\partial u_2}{\partial y_3} - \frac{u_3}{h_2}\frac{\partial h_3}{\partial y_2}\right)^2
$$

$$
\gamma_{12} = \frac{1}{2}\left(h_1\frac{\partial u_1}{\partial y_2} + h_2\frac{\partial u_2}{\partial y_1} - u_2\frac{\partial h_2}{\partial y_1} - u_1\frac{\partial h_1}{\partial y_2}\right)
$$
$$
+ \frac{1}{2}\left(\frac{\partial u_1}{\partial y_2} - \frac{u_2}{h_1}\frac{\partial h_2}{\partial y_1}\right)\left(\frac{\partial u_1}{\partial y_1} + \frac{u_2}{h_2}\frac{\partial h_1}{\partial y_2} + \frac{u_3}{h_3}\frac{\partial h_1}{\partial y_3}\right)
$$
$$
+ \frac{1}{2}\left(\frac{\partial u_2}{\partial y_1} - \frac{u_1}{h_2}\frac{\partial h_1}{\partial y_2}\right)\left(\frac{\partial u_2}{\partial y_2} + \frac{u_3}{h_3}\frac{\partial h_2}{\partial y_3} + \frac{u_1}{h_1}\frac{\partial h_2}{\partial y_1}\right)
$$
$$
+ \frac{1}{2}\left(\frac{\partial u_3}{\partial y_1} - \frac{u_1}{h_3}\frac{\partial h_1}{\partial y_3}\right)\left(\frac{\partial u_3}{\partial y_2} - \frac{u_2}{h_3}\frac{\partial h_2}{\partial y_3}\right)
$$

$$
\gamma_{12} = \frac{1}{2}\left(h_3\frac{\partial u_3}{\partial y_1} + h_1\frac{\partial u_1}{\partial y_3} - u_1\frac{\partial h_1}{\partial y_3} - u_3\frac{\partial h_3}{\partial y_1}\right)
$$

$$+\frac{1}{2}\left(\frac{\partial u_1}{\partial y_3}-\frac{u_3}{h_1}\frac{\partial h_3}{\partial y_1}\right)\left(\frac{\partial u_1}{\partial y_1}+\frac{u_3}{h_3}\frac{\partial h_1}{\partial y_3}+\frac{u_2}{h_2}\frac{\partial h_1}{\partial y_2}\right)$$

$$+\frac{1}{2}\left(\frac{\partial u_3}{\partial y_1}-\frac{u_1}{h_3}\frac{\partial h_1}{\partial y_3}\right)\left(\frac{\partial u_3}{\partial y_3}+\frac{u_1}{h_1}\frac{\partial h_3}{\partial y_1}+\frac{u_2}{h_2}\frac{\partial h_3}{\partial y_2}\right)$$

$$+\frac{1}{2}\left(\frac{\partial u_2}{\partial y_1}-\frac{u_1}{h_2}\frac{\partial h_1}{\partial y_2}\right)\left(\frac{\partial u_2}{\partial y_3}-\frac{u_3}{h_2}\frac{\partial h_3}{\partial y_2}\right)$$

$$\gamma_{23}\quad=\quad\frac{1}{2}\left(h_3\frac{\partial u_3}{\partial y_2}+h_2\frac{\partial u_2}{\partial y_3}-u_2\frac{\partial h_2}{\partial y_3}-u_3\frac{\partial h_3}{\partial y_2}\right)$$

$$+\frac{1}{2}\left(\frac{\partial u_2}{\partial y_3}-\frac{u_3}{h_2}\frac{\partial h_3}{\partial y_2}\right)\left(\frac{\partial u_2}{\partial y_2}+\frac{u_3}{h_3}\frac{\partial h_2}{\partial y_3}+\frac{u_1}{h_1}\frac{\partial h_2}{\partial y_1}\right)$$

$$+\frac{1}{2}\left(\frac{\partial u_3}{\partial y_2}-\frac{u2}{h_3}\frac{\partial h_2}{\partial y_3}\right)\left(\frac{\partial u_3}{\partial y_3}+\frac{u_2}{h_2}\frac{\partial h_3}{\partial y_2}+\frac{u_1}{h_1}\frac{\partial h_3}{\partial y_1}\right)$$

$$+\frac{1}{2}\left(\frac{\partial u_1}{\partial y_2}-\frac{u_2}{h_1}\frac{\partial h_2}{\partial y_1}\right)\left(\frac{\partial u_1}{\partial y_3}-\frac{u_3}{h_1}\frac{\partial h_3}{\partial y_1}\right)$$

The physical strain ε_{ij} $(i=j=1,2,3)$ is related to the Green's strains by the following

relation:

$$\varepsilon_{ij}=\frac{\gamma_{ij}}{h_i h_j}\text{ (No Sum)}$$

where the h terms are the scale factors and are defined in detail in Refs. [27], [36].

A.2 Strain-Displacement Relations for Cylindrical Shells

$c = 1/R,\ k = -4/3h^2$ [27]

$$\varepsilon_1 = \varepsilon_1^0 + \zeta^p \kappa_{1p'}$$

$$\varepsilon_1^0 = u_{,1} + \frac{1}{2}(u_{,1}^2 + v_{,1}^2 + w_{,1}^2)$$

$$\kappa_{11} = \psi_{1,1} - v_{,1}^2 c + \psi_{1,1} u_{,1} + \psi_{2,1} v_{,1}$$

$$\kappa_{12} = v_{,1}^2 c^2/2 - \psi_{2,1} v_{,1} c + \frac{1}{2}(\psi_{1,1}^2 + \psi_{2,1}^2)$$

$$\kappa_{13} = k(w_{,11} + \psi_{1,1}) + u_{,1} k(w_{,11} + \psi_{1,1}) + v_{,1} k(w_{,21} + \psi_{2,1})$$

$$\kappa_{14} = -v_{,1} kc(w_{,21} + \psi_{2,1}) + \psi_{1,1} k(w_{,11} + \psi_{1,1}) + \psi_{2,1} k(w_{,21} + \psi_{2,1})$$

$$\kappa_{15} = 0$$

$$\kappa_{16} = (k^2/2)(w_{,11}^2 + 2w_{,11}\psi_{1,1} + \psi_{1,1}^2 + w_{,21}^2 + 2w_{21}\psi_{2,1} + \psi_{2,1}^2)$$

$$\kappa_{17} = 0$$

$$\varepsilon_2 = \varepsilon_2^0 + \zeta^p \kappa_{2p'}$$

$$\varepsilon_2^0 = v_{,2} - wc + \frac{1}{2}(v_{,2}^2 + w_{,2}^2 + u_{,2}^2 + v^2 c^2 + w^2 c^2) + vw_{,2}c - v_{,2}wc$$

$$\kappa_{21} = \psi_{2,2} - wc^2 + u_{,2}^2 c + w_{,2}^2 c + w^2 c^3 - c^2(v_{,2}w - vw_{,2})$$
$$+ v\psi_2 c^2 + v_{,2}\psi_{2,2} + u_{,2}\psi_{1,2} - c(\psi_{2,2}w - \psi_2 w_{,2})$$

$$\kappa_{22} = \psi_{2,2}c + \frac{1}{2}(\psi_{2,2}^2 + \psi_{1,2}^2 + \psi_2^2 c^2) + 2\psi_{1,2}u_{,2}c$$
$$+ v\psi_2 c^3 - 2c^2(\psi_{2,2}w - \psi_2 w_{,2}) + \psi_{2,2}v_{,2}c$$

$$\kappa_{23} = k(w_{,22} + \psi_{2,2}) + c(\psi_{2,2}^2 + \psi_{1,2}^2) + ku_{,2}(w_{,12} + \psi_{1,2})$$
$$+ \psi_2^2 c^3 + kv_{,2}(w_{,22} + \psi_{2,2}) + vkc^2(w_{,2} + \psi_2)$$
$$- wkc(w_{,22} + \psi_{2,2}) + w_{,2}kc(w_{,2} + \psi_2)$$

137

$$\kappa_{24} = kc(w_{,22} + \psi_{2,2}) + 2u_{,2}kc(w_{,12} + \psi_{1,2})$$

$$+vkc^3(w_{,2} + \psi_2) + 2kc^2(-ww_{,22} - w\psi_{2,2} + w_{,2}^2 + w_{,2}\psi_2)$$

$$+k\psi_{2,2}(w_{,22} + \psi_{2,2}) + \psi_{1,2}k(w_{,12} + \psi_{1,2})$$

$$+\psi_2 kc^2(w_{,2} + \psi_2) + v_{,2}kc(w_{,22} + \psi_{2,2})$$

$$\kappa_{25} = 2kc[\psi_{2,2}(w_{,22} + \psi_{2,2}) + \psi_{1,2}(w_{,12} + \psi_{1,2}) + \psi_2 c^2(w_{,2} + \psi_2)]$$

$$\kappa_{26} = (k^2/2)(w_{,22}^2 + 2w_{,22}\psi_{2,2} + \psi_{2,2}^2 + w_{,12}^2 + 2w_{,12}\psi_{1,2}$$

$$+\psi_{1,2}^2 + c^2(w_{,2}^2 + 2w_{,2}\psi_2 + \psi_2^2))$$

$$\kappa_{27} = k^2c[(w_{,22} + \psi_{2,2})^2 + (w_{,12} + \psi_{1,2})^2 + c^2(w_{,2} + \psi_2)^2]$$

$$\varepsilon_6 = \varepsilon_6^0 + \zeta^p \kappa_{6p'}$$

$$\varepsilon_6^0 = u_{,2} + v_{,1} + u_{,1}u_{,2} + v_{,1}v_{,2} + w_{,1}w_{,2} + c(vw_{,1} - v_{,1}w)$$

$$\kappa_{61} = c(u_{,2} - v_{,1}) + \psi_{1,2} + \psi_{2,1} + u_{,1}\psi_{1,2} + \psi_{1,1}u_{,2}$$

$$+c(u_{,1}u_{,2} - v_{,1}v_{,2} + w_{,1}w_{,2} - w\psi_{2,1} + w_{,1}\psi_2) + v_{,1}\psi_{2,2}$$

$$+v_{,2}\psi_{2,1}$$

$$\kappa_{62} = c(\psi_{1,2} + u_{,1}\psi_{1,2} + u_{,2}\psi_{1,1} - cw\psi_{2,1} + cw_{,1}\psi_2)$$

$$+\psi_{1,1}\psi_{1,2} + \psi_{2,1}\psi_{2,2}$$

$$\kappa_{63} = 2kw_{,12} + k\psi_{1,2} + k\psi_{2,1} + ku_{,2}(w_{,11} + \psi_{1,1})$$

$$+ku_{,1}(w_{,12} + \psi_{1,2}) + kv_{,1}(w_{,22} + \psi_{2,2})$$

$$+kcw_{,1}(w_{,2} + \psi_2) - kcw(w_{,12} + \psi_{2,1})$$

$$+c(\psi_{1,1}\psi_{1,2} + \psi_{2,1}\psi_{2,2}) + kv_{,2}(w_{,12} + \psi_{2,1})$$

$$\kappa_{64} = kc(w_{,12} + \psi_{1,2}) + kcu_{,2}(w_{,11} + \psi_{1,1})$$

$$+k\psi_{2,1}(w_{,22} + \psi_{2,2}) - kc^2(ww_{,12} + w\psi_{2,1} - w_{,1}w_{,2}$$

$$-w_{,1}\psi_2) + k(\psi_{1,1}w_{,12} + 2\psi_{1,1}\psi_{1,2} + \psi_{1,2}w_{,11})$$

$$+k\psi_{2,2}(w_{,12} + \psi_{2,1}) + kcu_{,1}(w_{,12} + \psi_{1,2})$$

$$\kappa_{65} = kc(\psi_{1,1}w_{,12} + \psi_{1,2}w_{,11} + \psi_{2,1}w_{,22} + \psi_{2,2}w_{,12}$$

$$+2\psi_{1,1}\psi_{1,2} + 2\psi_{2,1}\psi_{2,2})$$

$$\kappa_{66} = k^2[(w_{,11} + \psi_{1,1})(w_{,12} + \psi_{1,2}) + (w_{,12} + \psi_{2,1})(w_{,22} + \psi_{2,2})]$$

$$\kappa_{67} = k^2c[(w_{,11} + \psi_{1,1})(w_{,12} + \psi_{1,2})$$

$$+(w_{,12} + \psi_{2,1})(w_{,22} + \psi_{2,2})]$$

$$\varepsilon_4 = (w_{,2} + \psi_2) + \zeta^2 3k(w_{,2} + \psi_2)$$

$$\varepsilon_5 = (w_{,1} + \psi_1) + \zeta^2 3k(w_{,1} + \psi_1)$$

APPENDIX B - MATHEMATICA Input File

Included in this appendix is the MATHEMATICA input file for incorporating the B_{ij}, E_{ij}, G_{ij} and I_{ij} arrays into the $\widehat{K}$ stiffness matrix. Given the shear size of the output files, only the input file for this case is included. The format for both the $\widehat{N}_1$ and $\widehat{N}_2$ stiffness matrices is the same. Note that only the first line of the output, i.e., "Write["K.f"..." was included, as the remainder of the output is repetitious, i.e., the same commands continue for all terms in the $18x18$ kmat matrix. Therefore, for the $\widehat{K}$ stiffness matrix:

```
% For K Matrix
otrl1={{0,1,0,0,0,0,0,0,0,0,0,0,0,0,0,0,0,0}}
otrl2={{0,0,0,0,0,1,-P1,0,0,0,0,0,0,0,0,0,0,0}}
otrl6={{0,0,1,0,1,0,0,0,0,0,0,0,0,0,0,0,0,0}}
ttrl1={{0,0,0,0,0,0,0,0,0,0,0,0,0,1,0,0,0,0}}
ttrl2={{0,0,0,0,0,0,0,-P1^2,0,0,0,0,0,0,0,0,0,1}}
ttrl6={{0,0,P1,0,-P1,0,0,0,0,0,0,0,0,1,0,1,0}}
twtrl2={{0,0,0,0,0,0,0,0,0,0,0,0,0,0,0,0,0,P1}}
twtrl6={{0,0,0,0,0,0,0,0,0,0,0,0,0,0,P1,0,0,0}}
thtrl1={{0,0,0,0,0,0,0,0,0,0,K1,0,0,0,0,0,0,K1}}
thtrl2={{0,0,0,0,0,0,0,0,0,0,0,K1,0,0,0,0,0,K1}}
thtrl6={{0,0,0,0,0,0,0,0,0,0,0,2*K1,0,0,K1,0,K1,0}}
fotrl2={{0,0,0,0,0,0,0,0,0,0,0,K1*P1,0,0,0,0,0,K1*P1}}
fotrl6={{0,0,0,0,0,0,0,0,0,0,0,0,K1*P1,0,0,K1*P1,0,0,0}}
otrs4={{0,0,0,0,0,0,0,0,0,1,0,0,0,0,0,0,1,0,0}}
otrs5={{0,0,0,0,0,0,0,0,1,0,0,0,0,1,0,0,0,0,0}}
twtrs4={{0,0,0,0,0,0,0,0,0,3*K1,0,0,0,0,0,0,3*K1,0,0}}
twtrs5={{0,0,0,0,0,0,0,0,3*K1,0,0,0,0,3*K1,0,0,0,0,0}}
ol1=Transpose[otrl1]
ol2=Transpose[otrl2]
ol6=Transpose[otrl6]
tl1=Transpose[ttrl1]
tl2=Transpose[ttrl2]
tl6=Transpose[ttrl6]
twl2=Transpose[twtrl2]
twl6=Transpose[twtrl6]
thl1=Transpose[thtrl1]
thl2=Transpose[thtrl2]
thl6=Transpose[thtrl6]
fol2=Transpose[fotrl2]
fol6=Transpose[fotrl6]
os4=Transpose[otrs4]
os5=Transpose[otrs5]
tws4=Transpose[twtrs4]
tws5=Transpose[twtrs5]
k11=b11*(ol1.ttrl1+tl1.otrl1)+e11*(ol1.thtrl1+thl1.otrl1);
k12=b12*(ol1.ttrl2+tl1.otrl2)+e12*(ol1.thtrl2+thl1.otrl2)+
e12*(tl1.twtrl2)+g12*(tl1.fotrl2)+g12*(thl1.twtrl2)+
i12*(thl1.fotrl2);
```

140

```
k16=b16*(ol1.ttrl6+tl1.otrl6)+e16*(ol1.thtrl6+thl1.otrl6)+
e16*(tl1.twtrl6)+g16*(tl1.fotrl6)+g16*(thl1.twtrl6)+
i16*(thl1.fotrl6);
k21=b21*(ol2.ttrl1+tl2.otrl1)+e21*(ol2.thtrl1+thl2.otrl1)+
e21*(twl2.ttrl1)+g21*(fol2.ttrl1)+g21*(twl2.thtrl1)+
i21*(fol2.thtrl1);
k22=b22*(ol2.ttrl2+tl2.otrl2)+e22*(ol2.thtrl2+thl2.otrl2)+
e22*(tl2.twtrl2+twl2.ttrl2)+g22*(tl2.fotrl2+fol2.ttrl2)+
g22*(twl2.thtrl2+thl2.twtrl2)+i22*(thl2.fotrl2+fol2.thtrl2);
k26=b26*(ol2.ttrl6+tl2.otrl6)+e26*(ol2.thtrl6+thl2.otrl6)+
e26*(tl2.twtrl6+twl2.ttrl6)+g26*(tl2.fotrl6+fol2.ttrl6)+
g26*(twl2.thtrl6+thl2.twtrl6)+i26*(thl2.fotrl6+fol2.thtrl6);
k61=b61*(ol6.ttrl1+tl6.otrl1)+e61*(ol6.thtrl1+thl6.otrl1)+
e61*(twl6.ttrl1)+g61*(fol6.ttrl1)+g61*(twl6.thtrl1)+
i61*(fol6.thtrl1);
k62=b62*(ol6.ttrl2+tl6.otrl2)+e62*(ol6.thtrl2+thl6.otrl2)+
e62*(tl6.twtrl2+twl6.ttrl2)+g62*(tl6.fotrl2+fol6.ttrl2)+
g62*(twl6.thtrl2+thl6.twtrl2)+i62*(thl6.fotrl2+fol6.thtrl2);
k66=b66*(ol6.ttrl6+tl6.otrl6)+e66*(ol6.thtrl6+thl6.otrl6)+
e66*(tl6.twtrl6+twl6.ttrl6)+g66*(tl6.fotrl6+fol6.ttrl6)+
g66*(twl6.thtrl6+thl6.twtrl6)+i66*(thl6.fotrl6+fol6.thtrl6);
kmat=(k11+k12+k16+k21+k22+k26+k61+k62+k66);
OpenWrite["K.f",PageWidth -> 60,FormatType -> FortranForm]
Write["K.f"," KS2(1,1)=",kmat[[1,1]]]
```

APPENDIX C - SLR Program Guide

The input file for the program is defined as follows. Note that integer values begin with letters i-n, while real (double-precision) values begin with a-h, o-z.

- **Card 1: title**
  - The first line of the program is a title. It is printed on the first line of the output file and may not exceed 133 characters.
- **Card 2: iel, npe, nanal(1),nanal(2),nanal(3),imesh,nprnt,nprint,ncut**
  - Variable **iel** indicates the structure type: 1 for plate or beam, 2 for circular cylindrical shell.
  - Variable **npe** indicates the element type: 4 for a four noded element, 8 for an eight noded element.
  - Variable **nanal(1)** specifies linear (no iteration) or nonliner analysis: 0 for nonliner, 1 for linear, 2 for eigenvalue analysis.
  - Variable **nanal(2)** is used to denote the material type: 0 is used for an arbitrary laminate, 1 is used for isotropic materials, 2 is used for symmetric laminates and 3 is used for sandwich composites.
  - Variable **nanal(3)** is used to indicate SLR (full nonlinear theory) or Von Karman plate/Donnell shell analysis: 0 for SLR, 1 for Von Karman plate/Donnell shell analysis.
  - Variable **imesh** indicates automatic or manual mesh generation. Setting **imesh**=1 (automatic mesh generation) is the only recommended selection.
  - Varable **nprnt** is used to indicate whether or not to print the elasticity arrays: 0 will not print the arrays, 1 will print the arrays. Note, only the initial arrays, prior to failure, will be printed.
  - Variable **nprint** indicates whether or not to print the elemental stiffness matrices: 0 will not print the matrices, 1 will print the matrices.
  - Variable **ncut** defines cutouts in the panel: 0 for no cutouts, "n" indicates "n" cutouts.
- **Card 3:** If **nanal(1)**=2, read **rstep**, which defines the eigenvalue "step". If **nanal(1)**=0, then read **intyp,ninc,imax,ires,tol**
  - Variable **intyp** indicates load or displacement controlled incrementation: 0 for load control, 1 for displacement control.
  - Variable **ninc** specifies the number of load or displacement increments.
  - Variable **imax** indicates the maximum number of iterations performed in a given increment. The program halts when **imax** is reached.
  - Variable **ires** specifies the stiffness matrix update: 0 for every iteration, 1 for every increment.
  - Variable **tol** represents the convergence criteria. If **nanal(1)**=1, then this variable will be skipped.
- **Card 4:** If **nanal(1)**=1, or **nanal(1)**=0 and **intyp**=0 then skip this card. If **nanal(1)**=0 and **intyp**=1, then read **table(ninc)**, which is the table of multipliers for the displacements specified in **Card 3**.
- **Card 5a:** If you choose **imesh**=0, then read **nem,nnm,nx,ny**, if **imesh**=1, then only read **nx** and **ny**.
  - Variable **nem** specifies the number of elements in the mesh.

- Variable **nnm** specifies the number of nodes in the mesh.
- Variable **nx** indicates the number of elemental divisions in the x-direction.
- Variable **ny** indicates the number of elemental divisions in the y-direction.

- **Card 5b**: If **imesh**=0 then read **nod(i,j),x(i),y(i)** where **nod(i,j)** is the ith row of the connectivity matrix, **x(i)** and **y(i)** are the x and y coordinates of node i. If **imesh**=1, then read **dx(i)** and **dy(i)** which are the distances between nodes in the x and y directions respectively.
- **Card 6**: Skip this card if **ncut**=0, otherwise read **icut(ncut)** as the element numbers that need to be deleted. This should equal **ncut**.
- **Card 7: LD,PO**
    - Variable **LD** defines the load type: 0 for no load, 1 for transverse load, 2 for dead weight and 3 for axial loading.
    - Variable **PO** is used to denote whether or not there is distributed loading: 0 for no distributed loading, otherwise the value indicates the intensity of the distributed load. Note, for no distributed loading, choose **LD**=0, **PO**=0.
- **Card 8**: When **LD**=3, read **nedge**, which indicates the number of nodes with inplane loading.
- **Card 8a**: When **LD**=3, read **iedge(nedge)**, which indicates the nodes at which the inplane loading is required.
- **Card 9**: **nbdy**, which specifies the number of nodes where degrees of freedom are specified.
- **Card 9a**: **nbound** This is where the specific degrees of freedom specified in **Card 9** need to be defined. The number of degrees of freedom specified should be equal to **nbdy**. On each card, there should be eight entries. The first entry corresponds to the node number and the next seven correspond to the nodal degrees of freedom, whether or not they are specified. A "1" is used to indicate that the degree of freedom is specified while a "0" is used to represent a free degree of freedom. A node need only be listed if one or more of its degrees of freedom are prescribed. For example, if node 112 has degrees of freedom u, v, and w prescribed, its entry would look like: 112,1,1,1,0,0,0,0.
- **Card 9b**: **vbdy(i)** This vector contains an entry for each of the prescribed displacements from **Cards 9&9a**. The example node, 112, would contribute 3 entries.
- **Card 10**: **nbsf**, which is the number of degrees of freedom having specified loads.
- **Card 10a**: **ibsf(i)** This is an array of **nbsf** degree-of-freedom numbers with prescribed loads.
- **Card 10b**: **vbsf(i)** These are the loads associated with the degrees of freedom specified in **ibsf(i)**. Note that the order of the degree-of-freedom numbers must match the order of the prescribed loads.
- **Card 11**: This card is where material properties are entered. The properties entered will vary with the **nanal(2)** type.
    - For **nanal(2)**=1, then the material is isotropic and the material data entered are **ey,pnu,ht**, where **ey** is Young's modulus, **pnu** is the poisson's ratio and **ht** is the thickness.
    - For **nanal(2)**=0,2 then the material is a composite and the material data entered for the lamina are **e1,e2,g12,pnu12,g13,g23**, where **e1** and **e2** are the modulus along the fiber and matrix directions, **g12, g13, g23** are the shear moduli in the 1-2, 1-3 and 2-3 directions, and **pnu12** is poisson's ratio in the 1-2 plane.
    - For **nanal(2)**=3 then the material is a sandwich composite and the same variables entered for **nanal(2)**=0,2 are entered for the sandwich facesheets only.
- **Card 11a**: Use this card only when **nanal(2)**=3, otherwise skip. Read the core material properties **e1s,e2s,g12s,pnu12s,g13s,g23s**, where **e1s** and **e2s** are the modulus along the fiber

143

and matrix directions, **g12s, g13s, g23s** are the shear moduli in the 1-2, 1-3 and 2-3 directions, and **pnu12s** is poisson's ratio in the 1-2 plane.

- **Card 11b**: Skip this card if nanal(2)=1.
    - If **nanal(2)**=0,2 then read **np,pt**, where **np** is the number of layers and **pt** is the thickness of each layer.
    - If **nanal(2)**=3 the read **np,pt,pts** where **np** is the number of layers in the facesheet, **pt** is the thickness of each facesheet layer and **pts** if the thickness of the core.
- **Card 11c**: Skip this card if **nanal(2)**=1. If **nanal(2)**=0,2,3 then read **the(i)** which is the orientation of the ply lay up. For a sandwich case, it is the orientation of the top and bottom facesheets.
- **Card 12**: Skip this card if **iel**=1 (plate or beam), otherwise read **rad**, or the radius of the shell.
- **Card 13**: **nfor**, or the variable that specifies the number of nodal forces to be calculated at the end of each converged increment.
- **Card 13a**: **ifor(nfor)**, which is an array of **nfor** degree-of-freedom numbers for the force calculations.
- **Card 14: nstress,ifail,icrit**
    - Variable **nstress** specifies the number of elements for which to calculate stresses and strains at the end of each increment.
    - Variable **ifail** is used to specify whether failure criteria will be incorporated into the analysis: 0 for no failure analysis, 1 for failure analysis. If **ifail**=1, then **nstress** is automatically set to the entire number of elements.
    - Variable **icrit** defines the failure criteria to be used in the analysis: 1 for Hashin, 2 for Lee and 3 for maximum stress. Note, if **ifail**=0, or failure analysis will not be accomplished, then the value of **icrit** is irrelevent.
- **Card 14b**: If **ifail**=1 and **nanal(2)**=0,2 then read the allowable strengths **sigfn,sigfs,sigmt,sigmc,sigms,sigdt,sigds**, where the fourth letter f corresponds to fiber strength, m corresponds to matrix strength and d corresponds to delamination strength. The last letter n, c or s refers to tensile, compressive or shear. If **nanal(2)**=3, then these values are the facesheet strengths.
- **Card 14c**: If **ifail**=1 and **nanal(2)**=3, then read the allowable strengths for the core as **sigcr, sig13c,sig23c** where **sigcr** is the transverse direct strength, and **sig13c** and **sig23c** are the transverse shear strengths for the core in the 1-2 and 2-3 directions.

This is the baseline convex shell input deck for the SLR program, with Hashin failure criteria:

Cntr load shell AS4/3501-6, r=152mm(5.98in), t=.804mm(.032in), 12x12 mesh,displ

2,8,0,2,0,1,0,0,0

1,55,50,0,0.001

0.05,.1,.1,0.15,0.15,.2,.2,0.25,0.25,

.3,.3,0.35,0.35,.4,.4,0.45,0.45,.5,

0.55,.6,0.65,.7,0.75,.8,0.85,.9,0.95,1.0,

1.05,1.1,1.15,1.2,1.2,1.25,1.25,1.3,1.3,1.35,

1.35,1.4,1.4,1.45,1.45,1.5,1.5,

1.55,1.55,1.6,1.6,1.65,1.65,1.7,1.7,1.75,1.75

12,12

4.25e-3,4.25e-3,4.25e-3,4.25e-3,4.25e-3,4.25e-3,4.25e-3,4.25e-3,4.25e-3,4.25e-3,4.25e-3,4.25e-3,

4.25e-3,4.25e-3,4.25e-3,4.25e-3,4.25e-3,4.25e-3,4.25e-3,4.25e-3,4.25e-3,4.25e-3,4.25e-3,4.25e-3

4.33e-3,4.33e-3,4.33e-3,4.33e-3,4.33e-3,4.33e-3,4.33e-3,4.33e-3,4.33e-3,4.33e-3,4.33e-3,4.33e-3,

4.33e-3,4.33e-3,4.33e-3,4.33e-3,4.33e-3,4.33e-3,4.33e-3,4.33e-3,4.33e-3,4.33e-3,4.33e-3,4.33e-3

0,0.

51

1,1,1,1,0,0,1,1

2,1,1,0,0,0,0,0

3,1,1,1,0,0,1,1

4,1,1,0,0,0,0,0

5,1,1,1,0,0,1,1

6,1,1,0,0,0,0,0

7,1,1,1,0,0,1,1

8,1,1,0,0,0,0,0

9,1,1,1,0,0,1,1

10,1,1,0,0,0,0,0

11,1,1,1,0,0,1,1

12,1,1,0,0,0,0,0

13,1,1,1,0,0,1,1

14,1,1,0,0,0,0,0

15,1,1,1,0,0,1,1

16,1,1,0,0,0,0,0

17,1,1,1,0,0,1,1

18,1,1,0,0,0,0,0

19,1,1,1,0,0,1,1

20,1,1,0,0,0,0,0

21,1,1,1,0,0,1,1

22,1,1,0,0,0,0,0

23,1,1,1,0,0,1,1

24,1,1,0,0,0,0,0

25,1,1,1,0,0,1,1

241,1,1,1,0,0,0,0

457,1,1,1,0,0,1,1

458,1,1,0,0,0,0,0

459,1,1,1,0,0,1,1

460,1,1,0,0,0,0,0

461,1,1,1,0,0,1,1
462,1,1,0,0,0,0,0
463,1,1,1,0,0,1,1
464,1,1,0,0,0,0,0
465,1,1,1,0,0,1,1
466,1,1,0,0,0,0,0
467,1,1,1,0,0,1,1
468,1,1,0,0,0,0,0
469,1,1,1,0,0,1,1
470,1,1,0,0,0,0,0
471,1,1,1,0,0,1,1
472,1,1,0,0,0,0,0
473,1,1,1,0,0,1,1
474,1,1,0,0,0,0,0
475,1,1,1,0,0,1,1
476,1,1,0,0,0,0,0
477,1,1,1,0,0,1,1
478,1,1,0,0,0,0,0
479,1,1,1,0,0,1,1
480,1,1,0,0,0,0,0
481,1,1,1,0,0,1,1
0.,0.,0.,0.,0.,0.,0.,0.,0.,0.,
0.,0.,0.,0.,0.,0.,0.,0.,0.,0.,
0.,0.,0.,0.,0.,0.,0.,0.,0.,0.,
0.,0.,0.,0.,0.,0.,0.,0.,0.,0.,
0.,0.,0.,0.,0.,0.,0.,0.,0.,0.,
0.,0.,0.,0.,0.,0.,0.,0.,0.,0.,
0.,0.,0.,0.,0.,0.,0.,0.,0.,0.,
0.,0.,0.,0.,0.,0.,0.,0.,0.,0.,
0.,0.,0.,0.,0.,0.,0.,0.,0.,0.,
0.,10.0e-3,0.,0.,0.,0.,0.,0.,0.,0.,
0.,0.,0.,0.,0.,0.,0.,0.,0.,0.,
0.,0.,0.,0.,0.,0.,0.,0.,0.,0.,
0.,0.,0.,0.,0.,0.,0.,0.,0.,0.,
0.,0.,0.,0.,0.,0.,0.,0.,0.,0.,
0.,0.,0.,0.,0.,0.,0.,0.,0.,0.,
0.,0.,0.,0.,0.,0.,0.,0.,0.,0.,
0.,0.,0.,0.,0.,0.,0.,0.,0.,0.,
0.,0.,0.,0.,0.,0.,0.,0.,0.,0.,
0.
0
142.0d9,9.8d9,6.d9,0.24,6.0d9,4.8d9
6,0.134d-3
45.,-45.,90.,90.,-45.,45.
.152
1
903

144,1,1
1500.e6,220.e6,43.8e6,43.8e6,43.8e6,50.e6,86.e6,120.7e6

APPENDIX D - SLR STRESS Subroutine

Included in this appendix is the STRESS subroutine, with the changes incorporating progressive failure analysis.

 SUBROUTINE STRESS (NM,NPE,NDF,IEL,ELXY,RAD,K1,iCRIT,iFLAG,iCNT,iLOAD,NSTRES,SIG13c,SIG23c)
C 21 SEP 92 —-
C..
C THIS SUBROUTINE EVALUATES THE STRESSES AT THE OUTER GAUSS POINTS
C..
C DESCRIPTION OF THE VARIABLES:
C..
C CON(M,N).....IN-PLANE CONSTITUTIVE MATRIX USED IN STRESS
C SUBROUTINE
C CONS(M,N)....IN-PLANE CONSTITUTIVE MATRIX USED IN STRESS
C SUBROUTINE
C D1HRM(M,N)...FIRST DERIVATIVES OF HRM(M,N) WITH RESPECT TO XI
C D2HRM(M,N)...FIRST DERIVATIVES OF HRM(M,N) WITH RESPECT TO ETA
C DD1HRM(M,N)..SECOND DERIVATIVES OF HRM(M,N) WITH RESPECT TO XI
C DD2HRM(M,N)..SECOND DERIVATIVES OF HRM(M,N) WITH RESPECT TO ETA
C D12HRM(M,N)..SECOND MIXED DERIVATIVE OF HRM(M,N)
C DQSF(M,N)....DERIVATIVE OF QSF(M) WITH RESPECT TO XI IF N = 1
C AND WITH RESPECT TO ETA IF N = 2
C DSF(M,N).....DERIVATIVE OF SF(M) WITH RESPECT TO XI IF N = 1
C AND WITH RESPECT TO ETA IF N = 2
C E11..........LINEAR PORTION FOR EPSILON 11 STRAIN
C E12..........LINEAR PORTION FOR EPSILON 12 STRAIN
C E13..........LINEAR PORTION FOR EPSILON 13 STRAIN
C E22..........LINEAR PORTION FOR EPSILON 22 STRAIN
C E23..........LINEAR PORTION FOR EPSILON 23 STRAIN
C ELD(M).......ELEMENT DISPLACEMENT VECTOR
C ELXY(M,N)....Nth COORDINATE OF ELEMENT NODE M (N=1,2)
C ETA..........NATURAL COORDINATE AT A GAUSS POINT FOR AN ELEMENT
C GAUSS(M,N)...ARRAY OF VALUES USED IN GAUSS QUADRATURE
C IEL..........INDICATOR FOR THE ELEMENT TYPE:
C IEL = 1, PLATE ELEMENT
C IEL = 2, CYLINDRICAL SHELL ELEMENT
C IEL = 3, SPHERICAL SHELL ELEMENT
C K1...........CONSTANT FROM KINEMATICS
C NANAL(M).....ANALYSIS PARAMETERS
C NANAL(1) = 0, FOR NONLINEAR ANALYSIS
C = 1, FOR LINEAR ANALYSIS
C = 2, FOR EIGENVALUE ANALYSIS
C NANAL(2) = 0, FOR ARBITRARY LAMINATE
C = 1, FOR ISOTROPIC MATERIAL
C = 2, FOR SYMMETRIC LAMINATE
C NANAL(3) = 0, FOR FULL NONLINEAR SHELL
C ANALYSIS

```fortran
C = 1, FOR VON KARMAN PLATE ANALYSIS
C OR DONNELL SHELL ANALYSIS
C NDF.........DEGREES OF FREEDOM PER CORNER NODES = 7
C NGP.........NUMBER OF GAUSS POINTS USED IN GAUSS QUADRATURE,
C N IMPLIES A NxN GAUSS QUADRATURE
C NL11........NONLINEAR PORTION OF EPSILON 11 STRAIN
C NL12........NONLINEAR PORTION OF EPSILON 12 STRAIN
C NL22........NONLINEAR PORTION OF EPSILON 22 STRAIN
C NP..........NUMBER OF PLIES (LAYERS)
C NPE.........NODES PER ELEMENT, 4 OR 8
C NUM.........NUMBER OF Z VALUES PER PLY (LAYER)
C P1..........CONSTANT (1/RAD) WITH RESPECT TO Y-DIRECTION
C PIN.........CONSTANT USED TO DETERMINE LOAD INTENSITY, BASED
C UPON SF(M) OR QSF(M) DEPENDING UPON NUMBER OF
C NODES PER ELEMENT
C Q(M)........DISPLACEMENT GRADIENT VECTOR
C QSF(M).......QUADRATIC INTERPOLATION FUNCTION FOR NODE M OF
C THE ELEMENT
C RAD.........SHELL RADIUS OF CURVATURE (CYLINDER OR SPHERE)
C SIG11.......COMPUTED STRESS FOR SIGMA 11
C SIG12.......COMPUTED STRESS FOR SIGMA 12
C SIG13.......COMPUTED STRESS FOR SIGMA 13
C SIG22.......COMPUTED STRESS FOR SIGMA 22
C SIG23.......COMPUTED STRESS FOR SIGMA 23
C SF(M).......LINEAR INTERPOLATION FUNCTION FOR NODE M OF THE
C ELEMENT
C XI..........NATURAL COORDINATE AT A GAUSS POINT FOR AN ELEMENT
C ZZ(M,N)......LOCATES Z VALUES, USED IN STRESS SUBROUTINE
C....................................................................
C
 IMPLICIT DOUBLE PRECISION (A-H,O-Z)
 INCLUDE 'disp.cbk'
 INCLUDE 'shap.cbk'
 INCLUDE 'strs.cbk'
 INCLUDE 'elas.cbk'
 INCLUDE 'elas1.cbk'
 INCLUDE 'mat.cbk'
 DOUBLE PRECISION I,J,K,L
 DIMENSION QBAR(3,3),QSBAR(2,2),D(3,3)
 DIMENSION iSIGFT(20,5,200),iSIGMC(20,5,200),iSIGMT(20,5,200)
 DIMENSION iSIGFTc(20,5,200),iSIGMCc(20,5,200),iSIGMTc(20,5,200)
 DIMENSION iSIGC(20,5,200),iSIGD(20,5,200),iSIGS6(20,5,200)
 DIMENSION iSIGS4(20,5,200),iSIGS5(20,5,200),iSIGDc(20,5,200)
 DIMENSION iSIGS4c(20,5,200),iSIGS5c(20,5,200),iSIGS6c(20,5,200)
 EQUIVALENCE(D(1,1),DD(1,1))
 DOUBLE PRECISION K1
 DIMENSION GAUSS(7,7),ELXY(8,2)
```

149

```fortran
      DIMENSION AQ11(5,5),AQ22(5,5),AQ12(5,5),AQ44(5,5),AQ55(5,5)
      DIMENSION AQ66(5,5),UU1(100),UU2(100),UU3(100),UU4(100),UU5(100)
      DIMENSION UG23(100),UG13(100)
C***********************************************************************
C LOAD UP THE GAUSS MATRIX
C***********************************************************************
      DATA GAUSS/0.00000000D0,0.00000000D0,0.00000000D0,0.00000000D0,
     . 0.00000000D0,0.00000000D0,0.00000000D0,
     . -.57735027D0,0.57735027D0,0.00000000D0,0.00000000D0,
     . 0.00000000D0,0.00000000D0,0.00000000D0,
     . -.77459667D0,0.00000000D0,0.77459667D0,0.00000000D0,
     . 0.00000000D0,0.00000000D0,0.00000000D0,
     . -.86113631D0,-.33998104D0,0.33998104D0,0.86113631D0,
     . 0.00000000D0,0.00000000D0,0.00000000D0,
     . -.90617985D0,-.53846931D0,0.00000000D0,0.53846931D0,
     . 0.90617985D0,0.00000000D0,0.00000000D0,
     . -.93246951D0,-.66120939D0,-.23861919D0,0.23861919D0,
     . 0.66120939D0,0.93246951D0,0.00000000D0,
     . -.94910791D0,-.74153119D0,-.40584515D0,0.00000000D0,
     . 0.40584515D0,0.74153119D0,0.94910791D0/
C***********************************************************************
C INITIALIZE THE NGP, P1, AND P2 VARIABLES
C***********************************************************************
C***********************************************************************
C INITIALIZE THE ELASTICITY MATRICES
C***********************************************************************
      iFLAG = iFLAG + 1
      IF (IFAIL .EQ. 0) GOTO 1021
      DO 10 M = 1,3
      DO 11 N = 1,3
      QBAR(M,N) = 0.
      A(M,N) = 0.
      B(M,N) = 0.
      D(M,N) = 0.
      E(M,N) = 0.
      F(M,N) = 0.
      G(M,N) = 0.
      H(M,N) = 0.
      I(M,N) = 0.
      J(M,N) = 0.
      K(M,N) = 0.
      L(M,N) = 0.
      P(M,N) = 0.
      R(M,N) = 0.
      S(M,N) = 0.
 11   T(M,N) = 0.
 10   CONTINUE
```

150

```fortran
      DO 15 M = 1,2
      DO 16 N = 1,2
      QSBAR(M,N) = 0.
      AS(M,N) = 0.
      BS(M,N) = 0.
      DS(M,N) = 0.
      ES(M,N) = 0.
   16 FS(M,N) = 0.
   15 CONTINUE
 1021 CONTINUE
      NGP = 2*NANAL(1)**2 - 5*NANAL(1) + 7
      NGP = 5
      P1 = 0.
      P2 = 0.
      IF (IEL.EQ.2) P1 = 1./RAD
      IF (IEL.EQ.3) P1 = 1./RAD
      IF (IEL.EQ.3) P1 = 1./RAD
C************************************************************************
C CALCULATE THE DISPLACEMENT GRADIENT VECTOR Q(I) FOR THE ELEMENT
C************************************************************************
      WRITE(8,*)' No of Layers=',NP
      IF( NANAL(2) .EQ. 3 )THEN
      NPBY2=NP/2
      NP5=NP+5
      ELSE
      NP5=NP
      ENDIF
C************************************************************************
C INITIALIZE THE FAILURE CRITERIA "FLAGS", i.e., THE FLAGS THAT
C ENSURE ONCE A PLY HAS FAILED , IT REMAINS FAILED. CURRENTLY,
C THE FLAGS CAN HANDLE UP TO 20 LAYERS AND A 14X14 MESH.
C************************************************************************
      IF (iFLAG .EQ. 1)THEN
      DO 17, II = 1,NSTRES
      DO 18, JJ = 1,NP
      DO 19, LL = 1,NGP
      iSIGFT(JJ,LL,II) = 0
      iSIGMC(JJ,LL,II) = 0
      iSIGMT(JJ,LL,II) = 0
      iSIGFTc(JJ,LL,II) = 0
      iSIGMCc(JJ,LL,II) = 0
      iSIGMTc(JJ,LL,II) = 0
      iSIGD(JJ,LL,II) = 0
      iSIGC(JJ,LL,II) = 0
      iSIGS4(JJ,LL,II) = 0
      iSIGS5(JJ,LL,II) = 0
      iSIGS6(JJ,LL,II) = 0
```

```
iSIGS4c(JJ,LL,II) = 0
iSIGS5c(JJ,LL,II) = 0
iSIGS6c(JJ,LL,II) = 0
iSIGDc(JJ,LL,II) = 0
19 CONTINUE
18 CONTINUE
17 CONTINUE
ENDIF
DO 22 JJ=1,NP5
TQ11=0.
TQ22=0.
TQ12=0.
TQ44=0.
TQ55=0.
TG12=0.
DO 40 NI = 1,NGP,NGP-1
DO 40 NJ = 1,NGP,NGP-1
IF( NANAL(2) .EQ. 1 .or. NANAL(2). EQ. 2) THEN
AQ11(NI,NJ)=Q11
AQ12(NI,NJ)=Q12
AQ22(NI,NJ)=Q22
AQ44(NI,NJ)=G23
AQ55(NI,NJ)=G13
AQ66(NI,NJ)=G12
ENDIF
IF(NANAL(2) .EQ. 3)THEN
IF(JJ. LE. NPBY2 .OR. JJ. GT. NPBY2+5)THEN
AQ11(NI,NJ)=Q11
AQ12(NI,NJ)=Q12
AQ22(NI,NJ)=Q22
AQ44(NI,NJ)=G233
AQ55(NI,NJ)=G133
AQ66(NI,NJ)=G12
ELSE
AQ11(NI,NJ)=Q11S
AQ22(NI,NJ)=Q22S
AQ12(NI,NJ)=Q12S
AQ66(NI,NJ)=G12S
AQ44(NI,NJ)=G23S
AQ55(NI,NJ)=G13S
ENDIF
ENDIF
XI = GAUSS(NI,NGP)
ETA = GAUSS(NJ,NGP)
CALL SHAPE (NPE,XI,ETA,ELXY,DET)
CALL DISGRAD (NPE)
X = 0.
```

```
      Y = 0.
      DO 20 II = 1,NPE
      PIN = SF(II)
      IF (NPE.EQ.8) PIN = QSF(II)
      X = X + PIN*ELXY(II,1)
20    Y = Y + PIN*ELXY(II,2)
C************************************************************************
C INITIALIZE THE LINEAR AND NONLINEAR STRAIN VARIABLES
C************************************************************************
      E11 = 0.
      E12 = 0.
      E22 = 0.
      E23 = 0.
      E13 = 0.
      NL11 = 0.
      NL22A = 0.
      NL22B = 0.
      NL22 = 0.
      NL12A = 0.
      NL12B = 0.
      NL12 = 0.
      NUM = 3
      IF (NP5.EQ.1) NUM = 5
      WRITE(8,*)' No of Layers =',NP5
c     DO 24 M = 1,NUM
      m=2
      E11 = Q(2)
     .  + ZZ(M,JJ)*Q(14)
     .  + ZZ(M,JJ)**3*K1*(Q(10)+Q(14))
      E22 = Q(6) - P1*Q(7)
     .  + ZZ(M,JJ)*(Q(18)-P1**2*Q(7))
     .  + ZZ(M,JJ)**2*P1*Q(18)
     .  + ZZ(M,JJ)**3*K1*(Q(11)+Q(18))
     .  + ZZ(M,JJ)**4*P1*K1*(Q(11)+Q(18))
      E12 = Q(3) + Q(5)
     .  + ZZ(M,JJ)*(Q(3)*P1-Q(5)*P1+Q(15)+Q(17))
     .  + ZZ(M,JJ)**2*P1*Q(15)
     .  + ZZ(M,JJ)**3*K1*(2.*Q(12)+Q(15)+Q(17))
     .  + ZZ(M,JJ)**4*P1*K1*(Q(12)+Q(15))
      E23 = Q(9) + Q(16) + ZZ(M,JJ)**2*3.*K1*(Q(9)+Q(16))
      E13 = Q(8) + Q(13) + ZZ(M,JJ)**2*3.*K1*(Q(8)+Q(13))
C************************************************************************
C FOR NONLINEAR ANALYSIS CALCULATE THE NONLINEAR STRAINS
C************************************************************************
      IF(NANAL(1).NE.0) GOTO 270
      NL11 = .5*(Q(2)**2+Q(8)**2+Q(5)**2)+ZZ(M,JJ)*(-Q(5)**2*P1+Q(14)*
     1 Q(2)+Q(5)*Q(17))+ZZ(M,JJ)**2*(Q(5)**2*P1**2/2.-Q(17)*Q(5)*P1+
```

```
2 .5*(Q(14)**2+Q(17)**2))+ZZ(M,JJ)**3*(Q(2)*K1*(Q(10)+Q(14))+
3 Q(5)*K1*(Q(12)+Q(17)))+ZZ(M,JJ)**4*(-Q(5)*K1*P1*(Q(12)+Q(17))+
4 Q(14)*K1*(Q(10)+Q(14))+Q(17)*K1*(Q(12)+Q(17)))+ZZ(M,JJ)**6*
5 K1**2*.5*(Q(10)**2+2*Q(10)*Q(14)+Q(14)**2+Q(12)**2+2*Q(12)*
6 Q(17)+Q(17)**2)
  NL22A = .5*(Q(6)**2+Q(9)**2+Q(3)**2+Q(4)**2*P1**2)-Q(6)*Q(7)*P1+
1 Q(4)*Q(9)*P1+Q(7)**2*.5*P1**2+ZZ(M,JJ)*(Q(3)**2*P1+Q(9)**2*P1+
2 Q(7)**2*P1**3-P1**2*(Q(6)*Q(7)-Q(4)*Q(9))+Q(4)*Q(16)*P1**2+Q(6)*
3 Q(18)+Q(3)*Q(15)-P1*(Q(18)*Q(7)-Q(16)*Q(9)))+ZZ(M,JJ)**2*(2*P1*
4 Q(15)*Q(3)+P1*Q(18)*Q(6)+Q(4)*Q(16)*P1**3-2*P1**2*(Q(18)*Q(7)-
5 Q(16)*Q(9))+.5*P1**2*Q(16)**2+.5*(Q(18)**2+Q(15)**2))+ZZ(M,JJ)**4
6 *(2*K1*P1*Q(3)*(Q(12)+Q(15))+K1*P1*Q(6)*(Q(11)+Q(18))+K1*P1**3
7 *Q(4)*(Q(9)+Q(16))-2*K1*P1**2*Q(7)*(Q(11)+Q(18))+2*K1*P1**2*Q(9)
8 *(Q(9)+Q(16))+K1*Q(18)*(Q(11)+Q(18))+K1*Q(15)*(Q(12)+Q(15))+
9 K1*P1**2*Q(16)*(Q(9)+Q(16)))
  NL22B = ZZ(M,JJ)**3*(P1*(Q(18)**2+Q(15)**2)+Q(16)
1 **2*P1**3+K1*Q(6)*(Q(11)+Q(18))+K1*Q(3)*(Q(12)+Q(15))+Q(4)*K1*
2 P1**2*(Q(9)+Q(16))-K1*P1*(Q(7)*(Q(11)+Q(18))-Q(9)*(Q(9)+Q(16))))+
3 ZZ(M,JJ)**5*2*K1*(P1*(Q(18)*(Q(11)+Q(18))+P1*Q(15)*(Q(12)+Q(15))+
4 P1**3*Q(16)*(Q(9)+Q(16))))+ZZ(M,JJ)**6*K1**2*.5*(Q(11)**2+2*Q(11)
5 *Q(18)+Q(18)**2+Q(12)**2+2*Q(12)*Q(15)+Q(15)**2+P1**2*(Q(9)**2+
6 2*Q(9)*Q(16)+Q(16)**2))+ZZ(M,JJ)**7*K1**2*(P1*(Q(11)+Q(18))**2+
7 P1*(Q(12)+Q(15))**2+P1**3*(Q(9)+Q(16))**2)
  NL22 = NL22A + NL22B
  NL12A = Q(2)*Q(3)+Q(5)*Q(6)+Q(8)*Q(9)+P1*(-Q(5)*Q(7)+Q(4)*Q(8))+
1 ZZ(M,JJ)*(P1*(Q(2)*Q(3)-Q(5)*Q(6)+Q(8)*Q(9))+Q(2)*Q(15)+Q(3)*
2 Q(14)+Q(5)*Q(18)+Q(6)*Q(17)+P1*(-Q(7)*Q(17)+Q(8)*Q(16)))+
3 ZZ(M,JJ)**2*(Q(14)*Q(15)+Q(17)*Q(18)+P1*(Q(15)*Q(2)+Q(14)*Q(3))+
4 P1**2*(-Q(7)*Q(17)+Q(8)*Q(16)))+ZZ(M,JJ)**3*(K1*Q(3)*
5 (Q(10)+Q(14))+K1*Q(2)*(Q(12)+Q(15))+K1*Q(5)*(Q(18)+Q(11))+
6 K1*Q(6)*(Q(12)+Q(17))-K1*P1*Q(7)*(Q(12)+Q(17))+K1*P1*Q(8)*(Q(9)+
7 Q(16))+P1*(Q(14)*Q(15)+Q(17)*Q(18)))
  NL12B = ZZ(M,JJ)**4*(K1*P1*Q(3)*(Q(10)+Q(14))-K1*P1**2*
8 (Q(7)*(Q(12)+Q(17))-Q(8)*(Q(9)+Q(16)))+K1*(Q(14)*(Q(12)+Q(15))+
9 Q(15)*(Q(10)+Q(14))+Q(17)*(Q(11)+Q(18))+Q(18)*(Q(12)+Q(17)))+
1 K1*P1*Q(2)*(Q(12)+Q(15)))+ZZ(M,JJ)**5*K1*P1*(Q(14)*(Q(12)+Q(15))+
2 Q(15)*(Q(10)+Q(14))+Q(17)*(Q(11)+Q(18))+
3 Q(18)*(Q(12)+Q(17)))+ZZ(M,JJ)**6*K1**2*((Q(10)+Q(14))*(Q(12)
4 +Q(15))+(Q(12)+Q(17))*(Q(11)+Q(18)))+ZZ(M,JJ)**7*P1*K1**2*
5 ((Q(10)+Q(14))*(Q(12)+Q(15))*(Q(12)+Q(17))*(Q(11)+Q(18)))
  NL12 = NL12A + NL12B
  E11 = E11 + NL11
  E22 = E22 + NL22
  E12 = E12 + NL12
C*********************************************************************
C CALCULATE THE STRESSES
C*********************************************************************
```

```
270 SIG11 = CON(1,JJ)*E11 + CON(2,JJ)*E22 + CON(3,JJ)*E12
    SIG22 = CON(2,JJ)*E11 + CON(4,JJ)*E22 + CON(5,JJ)*E12
    SIG12 = CON(3,JJ)*E11 + CON(5,JJ)*E22 + CON(6,JJ)*E12
    SIG23 = CONS(1,JJ)*E23 + CONS(2,JJ)*E13
    SIG13 = CONS(2,JJ)*E23 + CONS(3,JJ)*E13
C*********************************************************************
C TRANSFORM THE STRESSES INTO THE MATERIAL AXIS SYSTEM
C*********************************************************************
    SIG1 = SIG11*(COS(RTHE(JJ)))**2+SIG22*(SIN(RTHE(JJ)))**2+
   1 2*SIG12*COS(RTHE(JJ))*SIN(RTHE(JJ))
    SIG2 = SIG11*(SIN(RTHE(JJ)))**2+SIG22*(COS(RTHE(JJ)))**2-
   1 2*SIG12*SIN(RTHE(JJ))*COS(RTHE(JJ))
    SIG6 = -SIG11*COS(RTHE(JJ))*SIN(RTHE(JJ))+SIG12*
   * (COS((RTHE(JJ)))**2-(SIN(RTHE(JJ)))**2)+
   * SIG22*(SIN(RTHE(JJ))*COS(RTHE(JJ)))
    SIG4 = -SIG13*SIN(RTHE(JJ))+SIG23*COS(RTHE(JJ))
    SIG5 = SIG13*COS(RTHE(JJ))+SIG23*SIN(RTHE(JJ))
24  WRITE (8,250) ZZ(M,JJ),X,Y,SIG1,SIG2,SIG6,SIG4,SIG5
c 24 continue
    WRITE(8,*)' '
250 FORMAT (5X,10E12.4)
    IF(IFAIL. EQ. 0)GOTO 22
CCCCCCCCCCCCCCCCCCCCCCCCCCCCCCCCCCCCCCCCCCCCCCCCCCCCCCCCCCCCCCCCCCCCCC
C C
C iCRIT = 1 FOR HASHIN FAILURE THEORY C
C iCRIT = 2 FOR LEE FAILURE CRITERIA C
C iCRIT = 3 FOR MAXIMUM STRESS FAILURE THEORY C
C C
CCCCCCCCCCCCCCCCCCCCCCCCCCCCCCCCCCCCCCCCCCCCCCCCCCCCCCCCCCCCCCCCCCCCCC
    IF(iCRIT .EQ. 1) THEN
C Hashin Criteria for Isotropic or Composite Laminate
    IF( NANAL(2) .EQ. 1 .or. NANAL(2). EQ. 2) THEN
    FFHA=(SIG1/SIGFT)**2+(SIG6**2+SIG5**2)/(SIGFS**2)
    FFMT1=(SIG2/SIGMT)**2+(SIG6**2+SIG5**2)/(SIGFS**2)
    FFMT2=(SIG4/SIGMS)**2
    FFMT=FFMT1+FFMT2
    FFMC1=(SIG2/SIGMC)*(((SIGMC/(SIGMS*2.))**2)-1.)
    FFMC2=((SIG2/SIGMS)**2)*0.25
    FFMC3=(SIG4/SIGMS)**2
    FFMC4=(SIG6**2+SIG5**2)/(SIGFS**2)
    FFMC=FFMC1+FFMC2+FFMC3+FFMC4
    FFDC=(SIG5**2+SIG4**2)/SIGDS**2
    IF(FFHA .GE. 1 .or. iSIGFT(JJ,NI,iCNT) .EQ. 1) THEN
    iSIGFT(JJ,NI,iCNT) = 1
    AQ11(NI,NJ)=0.0025*AQ11(NI,NJ)
    AQ12(NI,NJ)=0.0025*AQ12(NI,NJ)
    AQ55(NI,NJ)=0.0025*AQ55(NI,NJ)
```

155

```
AQ66(NI,NJ)=0.0025*AQ66(NI,NJ)
WRITE(8,*)' FIBER FAILURE FOR', JJ, 'LAYER',FFHA
ENDIF
IF(SIG2 .GT. 0.) THEN
IF(FFMT .GE. 1 .or. iSIGMT(JJ,NI,iCNT) .EQ. 1) THEN
iSIGMT(JJ,NI,iCNT) = 1
AQ22(NI,NJ)=0.0025*AQ22(NI,NJ)
AQ12(NI,NJ)=0.0025*AQ12(NI,NJ)
AQ44(NI,NJ)=0.0025*AQ44(NI,NJ)
AQ66(NI,NJ)=0.0025*AQ66(NI,NJ)
WRITE(8,*)' MATRIX FAILURE DUE TO TENSION FOR', JJ, 'LAYER',FFMT
ENDIF
ELSE
IF(FFMC .GE. 1 .or. iSIGMT(JJ,NI,iCNT) .EQ. 1) THEN
iSIGMT(JJ,NI,iCNT) = 1
AQ22(NI,NJ)=0.0025*AQ22(NI,NJ)
AQ12(NI,NJ)=0.0025*AQ12(NI,NJ)
AQ44(NI,NJ)=0.0025*AQ44(NI,NJ)
AQ66(NI,NJ)=0.0025*AQ66(NI,NJ)
WRITE(8,*)' MATRIX FAILURE DUE TO COMP. ', JJ, 'LAYER',FFMC
ENDIF
ENDIF
IF(FFDC .GE. 1 .or. iSIGD(JJ,NI,iCNT) .EQ. 1) THEN
iSIGD(JJ,NI,iCNT) = 1
AQ44(NI,NJ)=0.0025*AQ44(NI,NJ)
AQ55(NI,NJ)=0.0025*AQ55(NI,NJ)
WRITE(8,*)' FAILURE DUE TO DELAMINATION FOR', JJ, 'LAYER',FFDC
ENDIF
ENDIF
C Hashin Criteria for Sandwich Facesheets
IF( NANAL(2) .EQ. 3 ) THEN
IF(JJ. LE. NPBY2 .OR. JJ. GT. NPBY2+5)THEN
FFHA=(SIG1/SIGFT)**2+(SIG6**2+SIG5**2)/(SIGFS**2)
FFMT1=(SIG2/SIGMT)**2+(SIG6**2+SIG5**2)/(SIGFS**2)
FFMT2=(SIG4/SIGMS)**2
FFMT=FFMT1+FFMT2
FFMC1=(SIG2/SIGMC)*(((SIGMC/(SIGMS*2.))**2)-1.)
FFMC2=((SIG2/SIGMS)**2)*0.25
FFMC3=(SIG4/SIGMS)**2
FFMC4=(SIG6**2+SIG5**2)/(SIGFS**2)
FFMC=FFMC1+FFMC2+FFMC3+FFMC4
FFDC=(SIG5**2+SIG4**2)/SIGDS**2
IF(FFHA .GE. 1 .or. iSIGFT(JJ,NI,iCNT) .EQ. 1) THEN
iSIGFT(JJ,NI,iCNT) = 1
AQ11(NI,NJ)=0.0025*AQ11(NI,NJ)
AQ12(NI,NJ)=0.0025*AQ12(NI,NJ)
AQ55(NI,NJ)=0.0025*AQ55(NI,NJ)
```

156

```fortran
AQ66(NI,NJ)=0.0025*AQ66(NI,NJ)
WRITE(8,*)' FIBER FAILURE FOR', JJ, 'LAYER'
ENDIF
IF(SIG2 .GT. 0.) THEN
IF(FFMT .GE. 1 .or. iSIGMT(JJ,NI,iCNT) .EQ. 1) THEN
iSIGMT(JJ,NI,iCNT) = 1
AQ22(NI,NJ)=0.0025*AQ22(NI,NJ)
AQ12(NI,NJ)=0.0025*AQ12(NI,NJ)
AQ44(NI,NJ)=0.0025*AQ44(NI,NJ)
AQ66(NI,NJ)=0.0025*AQ66(NI,NJ)
WRITE(8,*)' MATRIX FAILURE DUE TO TENSION FOR', JJ, 'LAYER'
ENDIF
ELSE
IF(FFMC .GE. 1 .or. iSIGMT(JJ,NI,iCNT) .EQ. 1) THEN
iSIGMT(JJ,NI,iCNT) = 1
AQ22(NI,NJ)=0.0025*AQ22(NI,NJ)
AQ12(NI,NJ)=0.0025*AQ12(NI,NJ)
AQ44(NI,NJ)=0.0025*AQ44(NI,NJ)
AQ66(NI,NJ)=0.0025*AQ66(NI,NJ)
WRITE(8,*)' MATRIX FAILURE DUE TO COMP FOR', JJ, 'LAYER'
ENDIF
ENDIF
IF(FFDC .GE. 1 .or. iSIGD(JJ,NI,iCNT) .EQ. 1) THEN
iSIGD(JJ,NI,iCNT) = 1
AQ44(NI,NJ)=0.0025*AQ44(NI,NJ)
AQ55(NI,NJ)=0.0025*AQ55(NI,NJ)
WRITE(8,*)' FAILURE DUE TO DELAMINATION FOR', JJ, 'LAYER'
ENDIF
ELSE
C Hashin Criteria for the Core
FFDCc=(SIG5**2+SIG4**2)/((SIG13c+SIG23c)/2.)**2
IF(FFDCc .GE. 1 .or. iSIGDc(JJ,NI,iCNT) .EQ. 1) THEN
iSIGDc(JJ,NI,iCNT) = 1
AQ11(NI,NJ)=0.0025*AQ11(NI,NJ)
AQ22(NI,NJ)=0.0025*AQ22(NI,NJ)
AQ12(NI,NJ)=0.0025*AQ12(NI,NJ)
AQ66(NI,NJ)=0.0025*AQ66(NI,NJ)
AQ44(NI,NJ)=0.0025*AQ44(NI,NJ)
AQ55(NI,NJ)=0.0025*AQ55(NI,NJ)
WRITE(8,*)' CORE FAILURE', JJ, 'LAYER'
ENDIF
ENDIF
ENDIF
ENDIF
IF(iCRIT .EQ. 2) THEN
C Lee Criteria for Isotropic or Composite Laminate
IF( NANAL(2) .EQ. 1 .or. NANAL(2). EQ. 2) THEN
```

157

```
FFMT=(SIG6**2+SIG4**2)**0.5
FFMC=(SIG6**2+SIG4**2)**0.5
FFDC=(SIG5**2+SIG4**2)**0.5
FFFT=(SIG6**2+SIG5**2)**0.5
IF(FFFT .GE. SIGFS .or. iSIGFT(JJ,NI,iCNT) .EQ. 1) THEN
iSIGFT(JJ,NI,iCNT) = 1
AQ11(NI,NJ)=0.0025*AQ11(NI,NJ)
AQ12(NI,NJ)=0.0025*AQ12(NI,NJ)
AQ55(NI,NJ)=0.0025*AQ55(NI,NJ)
AQ66(NI,NJ)=0.0025*AQ66(NI,NJ)
WRITE(8,*)' FIBER FAILURE FOR', JJ, 'LAYER',FFHA
ENDIF
IF(FFMT .GE. SIGMS .or. iSIGMT(JJ,NI,iCNT) .EQ. 1) THEN
iSIGMT(JJ,NI,iCNT) = 1
AQ22(NI,NJ)=0.0025*AQ22(NI,NJ)
AQ12(NI,NJ)=0.0025*AQ12(NI,NJ)
AQ44(NI,NJ)=0.0025*AQ44(NI,NJ)
AQ66(NI,NJ)=0.0025*AQ66(NI,NJ)
WRITE(8,*)' MATRIX FAILURE DUE TO TENSION FOR', JJ, 'LAYER',FFMT
ENDIF
IF(FFMC .GE. SIGMS .or. iSIGMC(JJ,NI,iCNT) .EQ. 1) THEN
iSIGMC(JJ,NI,iCNT) = 1
AQ22(NI,NJ)=0.0025*AQ22(NI,NJ)
AQ12(NI,NJ)=0.0025*AQ12(NI,NJ)
AQ44(NI,NJ)=0.0025*AQ44(NI,NJ)
AQ66(NI,NJ)=0.0025*AQ66(NI,NJ)
WRITE(8,*)' MATRIX FAILURE DUE TO COMP. ', JJ, 'LAYER',FFMC
ENDIF
IF(FFDC .GE. SIGDS .or. iSIGD(JJ,NI,iCNT) .EQ. 1) THEN
iSIGD(JJ,NI,iCNT) = 1
AQ44(NI,NJ)=0.0025*AQ44(NI,NJ)
AQ55(NI,NJ)=0.0025*AQ55(NI,NJ)
WRITE(8,*)' FAILURE DUE TO DELAMINATION FOR', JJ, 'LAYER',FFDC
ENDIF
ENDIF
C Lee Criteria for Sandwich Facesheets
IF( NANAL(2) .EQ. 3 ) THEN
IF(JJ. LE. NPBY2 .OR. JJ. GT. NPBY2+5)THEN
FFMT=(SIG6**2+SIG4**2)**0.5
FFMC=(SIG6**2+SIG4**2)**0.5
FFDC=(SIG5**2+SIG4**2)**0.5
FFFT=(SIG6**2+SIG5**2)**0.5
IF(FFFT .GE. SIGFS .or. iSIGFT(JJ,NI,iCNT) .EQ. 1) THEN
iSIGFT(JJ,NI,iCNT) = 1
AQ11(NI,NJ)=0.0025*AQ11(NI,NJ)
AQ12(NI,NJ)=0.0025*AQ12(NI,NJ)
AQ55(NI,NJ)=0.0025*AQ55(NI,NJ)
```

158

```fortran
      AQ66(NI,NJ)=0.0025*AQ66(NI,NJ)
      WRITE(8,*)' FIBER FAILURE FOR', JJ, 'LAYER',FFHA
      ENDIF
      IF(FFMT .GE. SIGMS .or. iSIGMT(JJ,NI,iCNT) .EQ. 1) THEN
      iSIGMT(JJ,NI,iCNT) = 1
      AQ22(NI,NJ)=0.0025*AQ22(NI,NJ)
      AQ12(NI,NJ)=0.0025*AQ12(NI,NJ)
      AQ44(NI,NJ)=0.0025*AQ44(NI,NJ)
      AQ66(NI,NJ)=0.0025*AQ66(NI,NJ)
      WRITE(8,*)' MATRIX FAILURE DUE TO TENSION FOR', JJ, 'LAYER',FFMT
      ENDIF
      IF(FFMC .GE. SIGMS .or. iSIGMC(JJ,NI,iCNT) .EQ. 1) THEN
      iSIGMC(JJ,NI,iCNT) = 1
      AQ22(NI,NJ)=0.0025*AQ22(NI,NJ)
      AQ12(NI,NJ)=0.0025*AQ12(NI,NJ)
      AQ44(NI,NJ)=0.0025*AQ44(NI,NJ)
      AQ66(NI,NJ)=0.0025*AQ66(NI,NJ)
      WRITE(8,*)' MATRIX FAILURE DUE TO COMP. ', JJ, 'LAYER',FFMC
      ENDIF
      IF(FFDC .GE. SIGDS .or. iSIGD(JJ,NI,iCNT) .EQ. 1) THEN
      iSIGD(JJ,NI,iCNT) = 1
      AQ44(NI,NJ)=0.0025*AQ44(NI,NJ)
      AQ55(NI,NJ)=0.0025*AQ55(NI,NJ)
      WRITE(8,*)' FAILURE DUE TO DELAMINATION FOR', JJ, 'LAYER'
      ENDIF
      ELSE
C Lee Criteria for Sandwich Core
      FFDCc=(SIG5**2+SIG4**2)/((SIG13c+SIG23c)/2.)**2
      IF(FFDCc .GE. 1 .or. iSIGDc(JJ,NI,iCNT) .EQ. 1) THEN
      iSIGDc(JJ,NI,iCNT) = 1
      AQ11(NI,NJ)=0.0025*AQ11(NI,NJ)
      AQ22(NI,NJ)=0.0025*AQ22(NI,NJ)
      AQ12(NI,NJ)=0.0025*AQ12(NI,NJ)
      AQ66(NI,NJ)=0.0025*AQ66(NI,NJ)
      AQ44(NI,NJ)=0.0025*AQ44(NI,NJ)
      AQ55(NI,NJ)=0.0025*AQ55(NI,NJ)
      WRITE(8,*)' CORE FAILURE', JJ, 'LAYER'
      ENDIF
      ENDIF
      ENDIF
      ENDIF
      IF(iCRIT .EQ. 3) THEN
C Maximum Stress Failure Criteria for Isotropic and Composite Laminates
      IF( NANAL(2) .EQ. 1 .or. NANAL(2). EQ. 2) THEN
      IF(ABS(SIG5) .GE. SIGDS .or. iSIGS5(JJ,NI,iCNT) .EQ. 1) THEN
      iSIGS5(JJ,NI,iCNT) = 1
      AQ55(NI,NJ)=0.0025*AQ55(NI,NJ)
```

159

```
WRITE(8,*)' 13 DELAMINATION FOR', JJ, 'LAYER',FFHA
ENDIF
IF(ABS(SIG4) .GE. SIGDS .or. iSIGS4(JJ,NI,iCNT) .EQ. 1) THEN
iSIGS4(JJ,NI,iCNT) = 1
AQ44(NI,NJ)=0.0025*AQ44(NI,NJ)
WRITE(8,*)' 23 DELAMINATION FOR', JJ, 'LAYER',FFHA
ENDIF
IF(SIG1 .GE. SIGFT .or. iSIGFT(JJ,NI,iCNT) .EQ. 1) THEN
iSIGFT(JJ,NI,iCNT) = 1
AQ11(NI,NJ)=0.0025*AQ11(NI,NJ)
AQ12(NI,NJ)=0.0025*AQ12(NI,NJ)
AQ55(NI,NJ)=0.0025*AQ55(NI,NJ)
AQ66(NI,NJ)=0.0025*AQ66(NI,NJ)
WRITE(8,*)' FIBER FAILURE FOR', JJ, 'LAYER',FFHA
ENDIF
IF(SIG2 .GT. 0.) THEN
IF(SIG2 .GE. SIGMT .or. iSIGMT(JJ,NI,iCNT) .EQ. 1) THEN
iSIGMT(JJ,NI,iCNT) = 1
AQ22(NI,NJ)=0.0025*AQ22(NI,NJ)
AQ12(NI,NJ)=0.0025*AQ12(NI,NJ)
AQ44(NI,NJ)=0.0025*AQ44(NI,NJ)
AQ66(NI,NJ)=0.0025*AQ66(NI,NJ)
WRITE(8,*)' MATRIX FAILURE DUE TO TENSION FOR', JJ, 'LAYER',FFMT
ENDIF
ELSE
IF(ABS(SIG2) .GE. SIGMC .or. iSIGMT(JJ,NI,iCNT) .EQ. 1) THEN
iSIGMT(JJ,NI,iCNT) = 1
AQ22(NI,NJ)=0.0025*AQ22(NI,NJ)
AQ12(NI,NJ)=0.0025*AQ12(NI,NJ)
AQ44(NI,NJ)=0.0025*AQ44(NI,NJ)
AQ66(NI,NJ)=0.0025*AQ66(NI,NJ)
WRITE(8,*)' MATRIX FAILURE DUE TO COMP. ', JJ, 'LAYER',FFMC
ENDIF
ENDIF
ENDIF
C Maximum Stress Failure Criteria for Sandwich Facesheets
IF( NANAL(2) .EQ. 3 ) THEN
IF(JJ. LE. NPBY2 .OR. JJ. GT. NPBY2+5)THEN
FFHA=SIG11
FFMT=SIG22
FFMC=SIG22
IF(ABS(SIG5) .GE. SIGDS .or. iSIGS5(JJ,NI,iCNT) .EQ. 1) THEN
iSIGS5(JJ,NI,iCNT) = 1
AQ55(NI,NJ)=0.0025*AQ55(NI,NJ)
WRITE(8,*)' 13 DELAMINATION FOR', JJ, 'LAYER',FFHA
ENDIF
IF(ABS(SIG4) .GE. SIGDS .or. iSIGS4(JJ,NI,iCNT) .EQ. 1) THEN
```

160

```fortran
iSIGS4(JJ,NI,iCNT) = 1
AQ44(NI,NJ)=0.0025*AQ44(NI,NJ)
WRITE(8,*)' 23 DELAMINATION FOR', JJ, 'LAYER',FFHA
ENDIF
IF(SIG1 .GE. SIGFT .or. iSIGFT(JJ,NI,iCNT) .EQ. 1) THEN
iSIGFT(JJ,NI,iCNT) = 1
AQ11(NI,NJ)=0.0025*AQ11(NI,NJ)
AQ12(NI,NJ)=0.0025*AQ12(NI,NJ)
AQ55(NI,NJ)=0.0025*AQ55(NI,NJ)
AQ66(NI,NJ)=0.0025*AQ66(NI,NJ)
WRITE(8,*)' FIBER FAILURE FOR', JJ, 'LAYER',FFHA
ENDIF
IF(SIG2 .GT. 0.) THEN
IF(SIG2 .GE. SIGMT .or. iSIGMT(JJ,NI,iCNT) .EQ. 1) THEN
iSIGMT(JJ,NI,iCNT) = 1
AQ22(NI,NJ)=0.0025*AQ22(NI,NJ)
AQ12(NI,NJ)=0.0025*AQ12(NI,NJ)
AQ44(NI,NJ)=0.0025*AQ44(NI,NJ)
AQ66(NI,NJ)=0.0025*AQ66(NI,NJ)
WRITE(8,*)' MATRIX FAILURE DUE TO TENSION FOR', JJ, 'LAYER',FFMT
ENDIF
ELSE
IF(ABS(SIG2) .GE. SIGMC .or. iSIGMT(JJ,NI,iCNT) .EQ. 1) THEN
iSIGMT(JJ,NI,iCNT) = 1
AQ22(NI,NJ)=0.0025*AQ22(NI,NJ)
AQ12(NI,NJ)=0.0025*AQ12(NI,NJ)
AQ44(NI,NJ)=0.0025*AQ44(NI,NJ)
AQ66(NI,NJ)=0.0025*AQ66(NI,NJ)
WRITE(8,*)' MATRIX FAILURE DUE TO COMP. ', JJ, 'LAYER',FFMC
ENDIF
ENDIF
ELSE
C Maximum Stress Failure Criteria for Sandwich Core
IF(ABS(SIG5) .GE. SIG13c .or. iSIGS5c(JJ,NI,iCNT) .EQ. 1) THEN
iSIGS5c(JJ,NI,iCNT) = 1
AQ55(NI,NJ)=0.0025*AQ55(NI,NJ)
AQ11(NI,NJ)=0.0025*AQ11(NI,NJ)
AQ22(NI,NJ)=0.0025*AQ22(NI,NJ)
AQ12(NI,NJ)=0.0025*AQ12(NI,NJ)
AQ66(NI,NJ)=0.0025*AQ66(NI,NJ)
WRITE(8,*)' 13 CORE FAILURE FOR', JJ, 'LAYER',SIG13c
ENDIF
IF(ABS(SIG4) .GE. SIG23c .or. iSIGS4c(JJ,NI,iCNT) .EQ. 1) THEN
iSIGS4c(JJ,NI,iCNT) = 1
AQ44(NI,NJ)=0.0025*AQ44(NI,NJ)
AQ11(NI,NJ)=0.0025*AQ11(NI,NJ)
AQ22(NI,NJ)=0.0025*AQ22(NI,NJ)
```

```fortran
      AQ12(NI,NJ)=0.0025*AQ12(NI,NJ)
      AQ66(NI,NJ)=0.0025*AQ66(NI,NJ)
      WRITE(8,*)' 23 CORE FAILURE FOR', JJ, 'LAYER',FFHA
      ENDIF
      ENDIF
      ENDIF
      ENDIF
      TQ11=TQ11+AQ11(NI,NJ)/4.
      TQ22=TQ22+AQ22(NI,NJ)/4.
      TQ12=TQ12+AQ12(NI,NJ)/4.
      TQ44=TQ44+AQ44(NI,NJ)/4.
      TQ55=TQ55+AQ55(NI,NJ)/4.
      TG12=TG12+AQ66(NI,NJ)/4.
C*********************************************************************
C CALCULATE INVARIANTS
C*********************************************************************
      UU1(JJ) = (3.*TQ11+3.*TQ22+2.*TQ12+4.*TG12)/8.
      UU2(JJ) = (TQ11-TQ22)/2.
      UU3(JJ) = (TQ11+TQ22-2.*TQ12-4.*TG12)/8.
      UU4(JJ) = (TQ11+TQ22+6.*TQ12-4.*TG12)/8.
      UU5(JJ) = (TQ11+TQ22-2.*TQ12+4.*TG12)/8.
      UG13(JJ)=TQ44
      UG23(JJ)=TQ55
40    CONTINUE
22    CONTINUE
      IF(IFAIL. EQ.0)RETURN
      DO 50 KK = 1,NP5
      ZL=ZL1(KK)
      ZU=ZU1(KK)
      IF(NANAL(2) .EQ. 3) THEN
      IF(KK .LE. NPBY2 .OR. KK .GT. NPBY2+5)THEN
      G13=G133
      G23=G233
      ELSE
      G13=G13S
      G23=G23S
      ENDIF
      ENDIF
      QBAR(1,1) = UU1(KK) + UU2(KK)*DCOS(2.*RTHE(KK)) +UU3(KK)*DCOS(4.*RTHE(KK))
      QBAR(1,2) = UU4(KK) - UU3(KK)*DCOS(4.*RTHE(KK))
      QBAR(2,2) = UU1(KK) - UU2(KK)*DCOS(2.*RTHE(KK))+UU3(KK)*DCOS(4.*RTHE(KK))
      QBAR(1,3) = .5*UU2(KK)*DSIN(2.*RTHE(KK)) +UU3(KK)*DSIN(4.*RTHE(KK))
      QBAR(2,3) = .5*UU2(KK)*DSIN(2.*RTHE(KK)) -UU3(KK)*DSIN(4.*RTHE(KK))
      QBAR(3,3) = UU5(KK) - UU3(KK)*DCOS(4.*RTHE(KK))
      QBAR(2,1) = QBAR(1,2)
      QBAR(3,1) = QBAR(1,3)
      QBAR(3,2) = QBAR(2,3)
```

```fortran
      QSBAR(1,1) = G23*DCOS(RTHE(KK))**2. + G13*DSIN(RTHE(KK))**2.
      QSBAR(2,2) = G13*DCOS(RTHE(KK))**2. + G23*DSIN(RTHE(KK))**2.
      QSBAR(1,2) = -(G23-G13)*DCOS(RTHE(KK))*DSIN(RTHE(KK))
      QSBAR(2,1) = QSBAR(1,2)
C**********************************************************************
C FORM MATRICES CON,CONS,ZZ FOR STRESS SUBROUTINE
C**********************************************************************
      CON(1,KK) = QBAR(1,1)
      CON(2,KK) = QBAR(1,2)
      CON(3,KK) = QBAR(1,3)
      CON(4,KK) = QBAR(2,2)
      CON(5,KK) = QBAR(2,3)
      CON(6,KK) = QBAR(3,3)
      CONS(1,KK) = QSBAR(1,1)
      CONS(2,KK) = QSBAR(1,2)
      CONS(3,KK) = QSBAR(2,2)
      DO 51 M = 1,3
      DO 52 N = 1,3
      A(M,N) = A(M,N) + QBAR(M,N)*(ZL- ZU)
      D(M,N) = D(M,N) + QBAR(M,N)*(ZL**3-ZU**3)/3.
      F(M,N) = F(M,N) + QBAR(M,N)*(ZL**5-ZU**5)/5.
      H(M,N) = H(M,N) + QBAR(M,N)*(ZL**7-ZU**7)/7.
      J(M,N) = J(M,N) + QBAR(M,N)*(ZL**9-ZU**9)/9.
      IF (NANAL(1).EQ.1) GOTO 240
      L(M,N) = L(M,N) + QBAR(M,N)*(ZL**11-ZU**11)/11.
      IF (NANAL(1).EQ.2) GOTO 240
      R(M,N) = R(M,N) + QBAR(M,N)*(ZL**13-ZU**13)/13.
      T(M,N) = T(M,N) + QBAR(M,N)*(ZL**15-ZU**15)/15.
  240 B(M,N) = B(M,N) + QBAR(M,N)*(ZL**2-ZU**2)/2.
      E(M,N) = E(M,N) + QBAR(M,N)*(ZL**4-ZU**4)/4.
      G(M,N) = G(M,N) + QBAR(M,N)*(ZL**6-ZU**6)/6.
      I(M,N) = I(M,N) + QBAR(M,N)*(ZL**8-ZU**8)/8.
      IF (NANAL(1).EQ.1) GOTO 52
      K(M,N) = K(M,N) + QBAR(M,N)*(ZL**10-ZU**10)/10.
      P(M,N) = P(M,N) + QBAR(M,N)*(ZL**12-ZU**12)/12.
      IF (NANAL(1).EQ.2) GOTO 52
      S(M,N) = S(M,N) + QBAR(M,N)*(ZL**14-ZU**14)/14.
   52 CONTINUE
   51 CONTINUE
      DO 60 M = 1,2
      DO 61 N = 1,2
      AS(M,N) = AS(M,N) + QSBAR(M,N)*(ZL-ZU)
      BS(M,N) = BS(M,N) + QSBAR(M,N)*(ZL**2-ZU**2)/2.
      DS(M,N) = DS(M,N) + QSBAR(M,N)*(ZL**3-ZU**3)/3.
      ES(M,N) = ES(M,N) + QSBAR(M,N)*(ZL**4-ZU**4)/4.
   61 FS(M,N) = FS(M,N) + QSBAR(M,N)*(ZL**5-ZU**5)/5.
   60 CONTINUE
```

163

```
  50 CONTINUE
C***********************************************************************
C SET TO ZERO THOSE ENTRIES DUE TO ROUNDOFF ERROR
C***********************************************************************
  29 DO 85 M = 1,3
  DO 86 N = 1,3
  IF (DABS(A(1,1)).GT.DABS(A(M,N)*1.D08)) A(M,N) = 0.
  IF (DABS(B(1,1)).GT.DABS(B(M,N)*1.D08)) B(M,N) = 0.
  IF (DABS(D(1,1)).GT.DABS(D(M,N)*1.D08)) D(M,N) = 0.
  IF (DABS(E(1,1)).GT.DABS(E(M,N)*1.D08)) E(M,N) = 0.
  IF (DABS(F(1,1)).GT.DABS(F(M,N)*1.D08)) F(M,N) = 0.
  IF (DABS(G(1,1)).GT.DABS(G(M,N)*1.D08)) G(M,N) = 0.
  IF (DABS(H(1,1)).GT.DABS(H(M,N)*1.D08)) H(M,N) = 0.
  IF (DABS(I(1,1)).GT.DABS(I(M,N)*1.D08)) I(M,N) = 0.
  IF (DABS(J(1,1)).GT.DABS(J(M,N)*1.D08)) J(M,N) = 0.
  IF (DABS(K(1,1)).GT.DABS(K(M,N)*1.D08)) K(M,N) = 0.
  IF (DABS(L(1,1)).GT.DABS(L(M,N)*1.D08)) L(M,N) = 0.
  IF (DABS(P(1,1)).GT.DABS(P(M,N)*1.D08)) P(M,N) = 0.
  IF (DABS(R(1,1)).GT.DABS(R(M,N)*1.D08)) R(M,N) = 0.
  IF (DABS(S(1,1)).GT.DABS(S(M,N)*1.D08)) S(M,N) = 0.
  IF (DABS(T(1,1)).GT.DABS(T(M,N)*1.D08)) T(M,N) = 0.
  86 CONTINUE
  85 CONTINUE
  DO 90 M = 1,2
  DO 91 N = 1,2
  IF (DABS(AS(1,1)).GT.DABS(AS(M,N)*1.D08)) AS(M,N) = 0.
  IF (DABS(BS(1,1)).GT.DABS(BS(M,N)*1.D08)) BS(M,N) = 0.
  IF (DABS(DS(1,1)).GT.DABS(DS(M,N)*1.D08)) DS(M,N) = 0.
  IF (DABS(ES(1,1)).GT.DABS(ES(M,N)*1.D08)) ES(M,N) = 0.
  IF (DABS(FS(1,1)).GT.DABS(FS(M,N)*1.D08)) FS(M,N) = 0.
  91 CONTINUE
  90 CONTINUE
  write(8,*)'ae=',a(2,2),'de=',d(2,2),'as=',as(2,2)
  IF(NPRNT.EQ.0) GOTO 1212
  1212 continue
  aa11(nm)=a(1,1)
  aa12(nm)=a(1,2)
  aa16(nm)=a(1,3)
  aa22(nm)=a(2,2)
  aa26(nm)=a(2,3)
  aa66(nm)=a(3,3)
  ba11(nm)=b(1,1)
  ba12(nm)=b(1,2)
  ba16(nm)=b(1,3)
  ba22(nm)=b(2,2)
  ba26(nm)=b(2,3)
  ba66(nm)=b(3,3)
```

164

```
da11(nm)=d(1,1)
da12(nm)=d(1,2)
da16(nm)=d(1,3)
da22(nm)=d(2,2)
da26(nm)=d(2,3)
da66(nm)=d(3,3)
ea11(nm)=e(1,1)
ea12(nm)=e(1,2)
ea16(nm)=e(1,3)
ea22(nm)=e(2,2)
ea26(nm)=e(2,3)
ea66(nm)=e(3,3)
fa11(nm)=f(1,1)
fa12(nm)=f(1,2)
fa16(nm)=f(1,3)
fa22(nm)=f(2,2)
fa26(nm)=f(2,3)
fa66(nm)=f(3,3)
ga11(nm)=g(1,1)
ga12(nm)=g(1,2)
ga16(nm)=g(1,3)
ga22(nm)=g(2,2)
ga26(nm)=g(2,3)
ga66(nm)=g(3,3)
ha11(nm)=h(1,1)
ha12(nm)=h(1,2)
ha16(nm)=h(1,3)
ha22(nm)=h(2,2)
ha26(nm)=h(2,3)
ha66(nm)=h(3,3)
ai11(nm)=i(1,1)
ai12(nm)=i(1,2)
ai16(nm)=i(1,3)
ai22(nm)=i(2,2)
ai26(nm)=i(2,3)
ai66(nm)=i(3,3)
aj11(nm)=j(1,1)
aj12(nm)=j(1,2)
aj16(nm)=j(1,3)
aj22(nm)=j(2,2)
aj26(nm)=j(2,3)
aj66(nm)=j(3,3)
ak11(nm)=k(1,1)
ak12(nm)=k(1,2)
ak16(nm)=k(1,3)
ak22(nm)=k(2,2)
ak26(nm)=k(2,3)
```

```
ak66(nm)=k(3,3)
al11(nm)=l(1,1)
al12(nm)=l(1,2)
al16(nm)=l(1,3)
al22(nm)=l(2,2)
al26(nm)=l(2,3)
al66(nm)=l(3,3)
ap11(nm)=p(1,1)
ap12(nm)=p(1,2)
ap16(nm)=p(1,3)
ap22(nm)=p(2,2)
ap26(nm)=p(2,3)
ap66(nm)=p(3,3)
ar11(nm)=r(1,1)
ar12(nm)=r(1,2)
ar16(nm)=r(1,3)
ar22(nm)=r(2,2)
ar26(nm)=r(2,3)
ar66(nm)=r(3,3)
as11(nm)=s(1,1)
as12(nm)=s(1,2)
as16(nm)=s(1,3)
as22(nm)=s(2,2)
as26(nm)=s(2,3)
as66(nm)=s(3,3)
at11(nm)=t(1,1)
at12(nm)=t(1,2)
at16(nm)=t(1,3)
at22(nm)=t(2,2)
at26(nm)=t(2,3)
at66(nm)=t(3,3)
aas11(nm)=as(1,1)
aas12(nm)=as(1,2)
aas22(nm)=as(2,2)
bas11(nm)=bs(1,1)
bas12(nm)=bs(1,2)
bas22(nm)=bs(2,2)
das11(nm)=ds(1,1)
das12(nm)=ds(1,2)
das22(nm)=ds(2,2)
eas11(nm)=es(1,1)
eas12(nm)=es(1,2)
eas22(nm)=es(2,2)
fas11(nm)=fs(1,1)
fas12(nm)=fs(1,2)
fas22(nm)=fs(2,2)
RETURN
```

END

Bibliography

[1] Abu-Farsakh, G. A. and Abdel-Jawad, Y. A. "A new failure criterion for nonlinear composite materials," *Journal of Composites Technology & Research*, 16: 138-145 (April 1994).

[2] Bailey, Ronald, H. "THE AIR WAR IN EUROPE," in *WORLD WAR II*. Alexandria VA: Time-Life Books, 1979.

[3] Cook, Robert D. and others. *Concepts and Applications of Finite Element Analysis* (Third Edition). New York: John Wiley & Sons, 1989.

[4] Cron, Steven M. *Improvement of End Boundary Conditions for Off-Axis Tension Specimen Use*. MS thesis, AFIT/GAE/AA/85D-3. School of Engineering, Air Force Institute of Technology (AU), Wright-Patterson AFB OH, December 1985 (AD-A164321).

[5] Cron, S. M., A. N. Palazotto, and R. S. Sandhu. "A failure criterion evaluation for composite materials," *Composite Materials: Testing and Design* (Ninth Volume), ASTM STP 1059, S. P. Garbo, Ed., American Society for Testing and Materials, Philadelphia, 1990, pp. 494-507.

[6] Daniel, Isaac M. and Ori Ishai. *Engineering Mechanics of Composite Materials*. New York: Oxford University Press, 1994.

[7] Daniels, J. A., A. N. Palazotto, and R. S. Sandhu. "Failure characteristics in thermoplastic composite laminates due to an eccentric circular discontinuity," *AIAA Journal*, 29: 830-837 (May 1991).

[8] Daniels, John A. *A Study of Failure Characteristics in Thermoplastic Composite Laminates Due to an Eccentric Circular Discontinuity*. MS thesis, AFIT/GAE/ENY/89D-06. School of Engineering, Air Force Institute of Technology (AU), Wright-Patterson AFB OH, December 1989 (AD-A216226).

[9] Eason T. G. and O. O. Ochoa. "Modeling progressive damage in composites: a shear deformable element for ABAQUS$^{\circledR}$," *Composite Structures*, 34: (1996).

[10] Eckold, G. C., "Failure criteria for use in the design environment," *Composites Science & Technology*, 58: 1095-1105 (1998).

[11] Fisher, James M. *A Study of Failure Characteristics in a Thermoplastic Composite Material at High Temperature*. MS thesis, AFIT/GAE/AA/88D-15. School of Engineering, Air Force Institute of Technology (AU), Wright-Patterson AFB OH, December 1988 (AD-A203015).

[12] Gummadi, L. N. B. and A. N. Palazotto. "Progressive failure analysis of composite cylindrical shells considering large rotations," *Composites*, 6: 547-563 (1998).

[13] Gummadi, L. N. B. and A. N. Palazotto. "Progressive failure analysis of laminated beams and arches undergoing large rotations," *Mechanics of Composite Materials and Structures*, 6: 69-93 (1999).

[14]   Hashin, Zvi. "Failure criteria for unidirectional fiber composites," *Journal of Applied Mechanics*, 47: 329-334 (1980).

[15]   Herup, Eric J. *Low-Velocity Impact on Composite Sandwich Plates*. Air Force Institute of Technology (AU), Wright-Patterson AFB OH, July 1996 (ADA324254).

[16]   Herup, Eric J. "Low-velocity impact damage initiation in graphite/epoxy/nomex honeycomb-sandwich plates." *Composites Science and Technology*, 57: 1581-1598 (1997).

[17]   Hwang, W. C. and C. T. Sun. "Failure analysis of laminated composites by using iterative three-dimensional finite element method," *Computers & Structures*, 33: 41-47 (1989).

[18]   Kim, Y. W. and C. S. Hong. "Progressive failure model for the analysis of laminated composites based on finite element approach," *Journal of Reinforced Plastics and Composites*, 11: 1078-1092 (1992).

[19]   Kim, Seng Jo and Joon Seok Hwang. "Progressive failure analysis of pin-loaded laminated composites using penalty finite element method," *AIAA Journal*, 36: 75-80 (1998).

[20]   Kim, Youngchan, Julio F. Davalos, and Ever J. Barbero. "Progressive failure analysis of laminated composite beams," *Journal of Composite Materials*, 30: 536- (1996).

[21]   Lee, James D. "Three dimensional finite element analysis of damage accumulation in composite laminate," *Computers & Structures*, 15: 335-350 (1982).

[22]   Martin, Robert J. *A Study of Failure Characteristics in Thermoplastic Composite Material*. MS thesis, AFIT/GA/AA/88M-2. School of Engineering, Air Force Institute of Technology (AU), Wright-Patterson AFB OH, March 1988 (AD-A190613).

[23]   Martin, R. J., R. S. Sandhu, and A. N. Palazotto. "Experimental and analytical comparisons of failure in thermoplastic composite laminates," *Experimental Mechanics*, 37: 53-65 (March 1994).

[24]   Minguet, Pierre and John Dugundji. "Experiments and analysis for composite blades under large deflections part I: static behavior," *AIAA Journal*, 28: 1573-1577 (September 1990).

[25]   Moas, Eduardo and O. Hayden Griffin, Jr. "Progressive failure analysis of laminated composite structures," *AIAA paper*, No. 97-1186, 2246-2256 (1997).

[26]   Nahas, Mahmoud, N., "Survey of failure and post-failure theories of laminated fiber-reinforced composites," *Journal of Composites Technology & Research*, 8: 138-153 (1986).

[27]   Palazotto, Anthony N. and Scott T. Dennis. *Nonlinear Analysis of Shell Structures*. Washington DC: American Institute of Aeronautics and Astronautics, Inc., 1992.

[28]   Perry, R., A. N. Palazotto, and R. S. Sandhu. "Impact response of graphite/epoxy cylindrical panels," *AIAA Journal*, 30: 1827-1832 (July 1992).

[29]   R. S. Sandhu, R. L. Gallo, and G. P. Sendeckyj. "Initiation and accumulation of damage in composite laminates," *Composite Materials: Testing and Design (Sixth Conference)*, ASTM STP 787, I.M. Daniel, Ed., American Society for Testing and Materials, 1982, pp. 163-182.

[30]   Reddy, J. N. and A. K. Pandey. "A first-ply failure analysis of composite laminates," *Computers & Structures*, 25: 371-393 (1987).

[31]   Reddy, Y. S. N. and J. N. Reddy. "Linear and non-linear failure analysis of composite laminates with transverse shear," *Composites Science and Technology*, 44: 227-255 (1992).

[32]   Reddy, Y. S. N., C. M. Dakshina Moorthy, and J. N. Reddy, "Non-linear progressive failure analysis of laminated composite plates," *International Journal of non-linear mechanics*, 30: 629-649 (1995).

[33]   Richardson, Terry. Composites: *A DESIGN GUIDE*. Aberdeen SD: Industrial Press Inc., 1987.

[34]   Rotem, Assa and Zvi Hashin. "Failure modes of angle ply laminates," *Journal of Composite Materials*, 9: 191-206 (April 1975).

[35]   Rowlands, Robert E. "Strength (failure) theories and their experimental correlation," *Handbook of Composites - Vol 3 - Failure Mechanics of Composites*, Ed. Sih, G.C. and Skudra, A.M., Elsevier, Amsterdam. 1985.

[36]   Saada, Adel S. *Elasticity: Theory and Applications* (Second Edition). Florida: Krieger Publishing Company, 1993.

[37]   Sandhu, R. S. *Ultimate Strength Analysis of Symmetric Laminates*. Technical Report AFFDL-TR-73-137, AD 779927, Air Force Flight Dynamics Lab, Wright-Patterson AFB, OH, February 1974.

[38]   Sleight, David W., Norman F. Knight, and John T. Wang. "Evaluation of a progressive failure analysis methodology for laminated composite structures," *AIAA paper*, No. 97-1187, 2257-2272 (1997).

[39]   Strong, Brent A. *Fundamentals of Composites Manufacturing: Materials, Methods & Applications*. Dearborn MI: Society of Manufacturing Engineers, 1989.

[40]   Tan, Seng C. "A progressive failure model for composite laminates containing openings," *Journal of Composite Materials*, 25: 556-577 (May 1991).

[41]   Tan, Seng C. and Jose Perez. "Progressive failure of laminated composites with a hole under compressive loading," *Journal of Reinforced Plastics and Composites*, 12: 1043-1057 (October 1993).

[42]   Tolson, S. and N. Zabaras. "Finite element analysis of progressive failure in laminated composite plates," *Computers & Structures*, 38: 361-376 (1991).

[43]   Tsai, Stephen W. "A survey of macroscopic failure criteria for composite materials,"

Journal of Reinforced Plastics and Composites, 13: 40-62 (January 1984).

[44]   Wardle, Brian L. and Paul A. Lagace. "Behavior of composite shells under transverse impact and quasi-static loading," *AIAA Journal*, 36: 1065-1073 (June 1998).

[45]   Wham, Benjamin, II. *An Investigation of Graphite PEEK Composite Under Compression With a Centrally Located Circular Discontinuity*. MS thesis, AFIT/GA/93M-01. School of Engineering, Air Force Institute of Technology (AU), Wright-Patterson AFB OH, March 1993 (AAJ-6651).

[46]   Xue, David Y. and Michael F. Card. "Prediction of laminate damage processes using combined micro-mechanics, fracture mechanics and statistics approach," *AIAA paper*, No. 97-1188, 2273-2283 (1997).

[47]   Yeh, Hsien-Yang and Robert Chun-Yen Lee. "Simple analysis of the Yeh-Stratton failure criterion on composite materials," *Engineering Fracture Mechanics*, 51: 37-49 (1995).

Vita

Stephen Michael Spottswood was born on 3 September 1972 in Patuxent River, Maryland. He attended 9th grade at Edna Karr Jr. High School, New Orleans, Lousiana, 10th grade at Carlisle High School, Carlisle, Pennsylvania, and graduated from Hatboro-Horsham High School, Horsham, Pennsylvania, 1990. Michael obtained a Bachelor of Science degree in Mechanical Engineering from the University of New Hampshire and was commissioned through their ROTC program in 1995. His first assignment after commissioning was as a developmental engineer in the Space and Special Systems Directorate, Robins AFB, Georgia, performing a myriad of engineering tasks in the support of aircraft launch and release equipment. In 1997, Michael was sent to the Air Force Institute of Technology, to pursue a Master of Science degree in Aeronautical Engineering. Upon completion of the AFIT program, Michael will be assigned to the Air Vehicles Directorate, Structures Divison, Air Force Research Lab, Wright-Patterson AFB.

Michael is married to the former Rachel Neri of Broadalbin, New York. They have one child, Sidney Morgan (1). Michael is the son of Stephen and Marion Spottswood of Orford, New Hampshire.

Permanent Address: R.R.1 Box 193A

Orford, NH 03777

REPORT DOCUMENTATION PAGE	*Form Approved* *OMB No. 0704-0188*

Public reporting burden for this collection of information is estimated to average 1 hour per response, including the time for reviewing instructions, searching existing data sources, gathering and maintaining the data needed, and completing and reviewing the collection of information. Send comments regarding this burden estimate or any other aspect of this collection of information, including suggestions for reducing this burden, to Washington Headquarters Services, Directorate for Information Operations and Reports, 1215 Jefferson Davis Highway, Suite 1204, Arlington, VA 22202-4302, and to the Office of Management and Budget, Paperwork Reduction Project (0704-0188), Washington, DC 20503.

1. AGENCY USE ONLY *(Leave blank)*	2. REPORT DATE March 1999	3. REPORT TYPE AND DATES COVERED Master's Thesis	
4. TITLE AND SUBTITLE PROGRESSIVE FAILURE ANALYSIS OF COMPOSITE PANELS			**5. FUNDING NUMBERS**
6. AUTHOR(S) Stephen M. Spottswood, Lieutenant, USAF			
7. PERFORMING ORGANIZATION NAME(S) AND ADDRESS(ES) Air Force Institute of Technology, 2950 P Street, WPAFB OH 45433-7765			**8. PERFORMING ORGANIZATION REPORT NUMBER** AFIT/GAE/ENY/99M-08
9. SPONSORING/MONITORING AGENCY NAME(S) AND ADDRESS(ES) Dr. Steven Walker AFOSR/NA 801 North Randolph Street, Room 732 Arlington, VA 22203-1997			**10. SPONSORING/MONITORING AGENCY REPORT NUMBER**
11. SUPPLEMENTARY NOTES Dr. Anthony N. Palazotto			
12a. DISTRIBUTION AVAILABILITY STATEMENT Distribution Unlimited			**12b. DISTRIBUTION CODE**

13. ABSTRACT *(Maximum 200 words)*

The objective of this research was to determine the physical response, including material failure, of a curved composite panel designed to resist transverse loading. The cause of the material failure, in the form of delamination, fiber and/or matrix failure, was determined through various criterion based on non-linear movement using a finite element analysis technique. Data generated both with and without the addition of progressive failure criteria, was compared with previously published experimental data, noting where the theory diverges from the experimental results. The inclusion of various failure criterion, to include maximum stress, Lee, and Hashin, provided a more realistic representation of the total physical response of the shell. Once an approximate range of accurate physical representation was realized, progressive failure of composite sandwich shells under transverse loading were examined. Results of the analytic comparison with the published experimental data indicate that the SLR theory overpredicts the stiffness of the various shells for both the cases considering and not considering failure criteria. Furthermore, matrix failure patterns predicted by all three criterion were similar to the experimental results. Core failures predicted in the composite sandwich analysis were similar between the failure criterion.

14. SUBJECT TERMS Failure, Composite Structures, Finite Element Analysis, Sandwich Panels			15. NUMBER OF PAGES 188
			16. PRICE CODE
17. SECURITY CLASSIFICATION OF REPORT Unclassified	18. SECURITY CLASSIFICATION OF THIS PAGE Unclassified	19. SECURITY CLASSIFICATION OF ABSTRACT Unclassified	20. LIMITATION OF ABSTRACT UL

Standard Form 298 (Rev. 2-89) (EG)
Prescribed by ANSI Std. 239.18
Designed using Perform Pro, WHS/DIOR, Oct 94